

بِسْمِ اللَّهِ الرَّحْمَنِ الرَّحِيمِ



ISLAMIC UNIVERSITY OF TECHNOLOGY
DHAKA, BANGLADESH
ORGANISATION OF ISLAMIC COOPERATION



**Effect of Tool Geometry on Chip Morphology and Cutting
Parameters in Turning Process by FEM Analysis**

B.SC. ENGINEERING (MECHANICAL) THESIS

AUTHORED BY

RAHNUM TAHIA MEEM

STUDENT ID: 160011034

SUPERVISED BY

PROF. DR. MD. ANAYET ULLAH PATWARI

HEAD, DEPARTMENT OF MECHANICAL & PRODUCTION ENGINEERING (MPE)

ISLAMIC UNIVERSITY OF TECHNOLOGY

BOARD BAZAR, GAZIPUR

DHAKA, BANGLADESH.

**DEPARTMENT OF MECHANICAL AND PRODUCTION
ENGINEERING (MPE)**

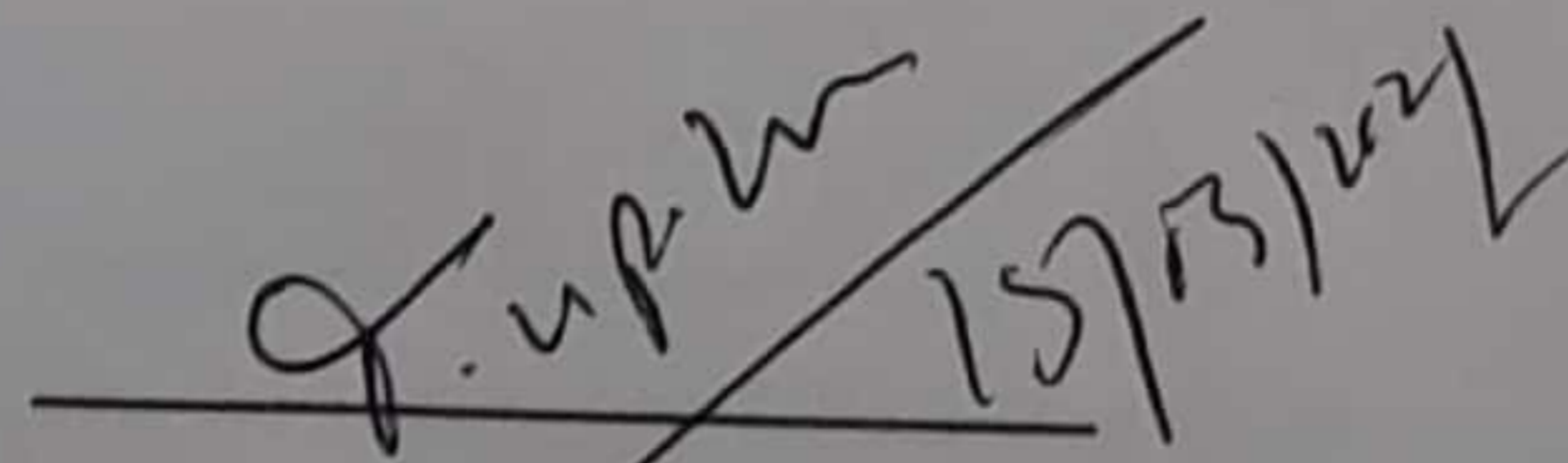
ISLAMIC UNIVERSITY OF TECHNOLOGY (IUT)

MARCH 2021

RESEARCH CERTIFICATION

The thesis title “**Effect of Tool Geometry on Chip Morphology and Cutting Parameters in Turning Process by FEM Analysis**” submitted by **Rahnum Tahia Meem (160011034)** has been accepted as satisfactory in partial fulfillment of the requirement for the Degree of Bachelor of Science in Mechanical Engineering on March 2021.

Signature of the Supervisor

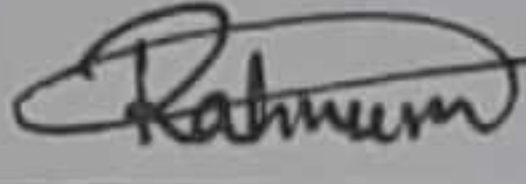


Prof. Dr. Md. Anayet Ullah Patwari
Head, Department of Mechanical & Production Engineering (MPE)
Islamic University of Technology
Board Bazar, Gazipur
Dhaka, Bangladesh.

CANDIDATE'S DECLARATION

It is hereby declared that this thesis or any part of it has not been submitted elsewhere for the award of any degree or professional qualification.

Signature of the Candidates

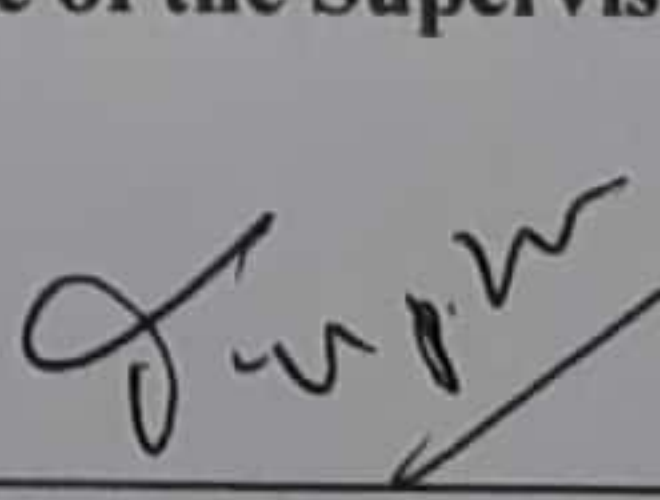
 15-09-21

Rahnum Tahia Meem

Student ID: 160011034

Department of Mechanical and Production Engineering (MPE)
Islamic University of Technology (IUT), OIC
Board Bazar, Gazipur
Dhaka, Bangladesh

Signature of the Supervisor

 15/03/2021

Prof. Dr. Md. Anayet Ullah Patwari
Head, Department of Mechanical & Production Engineering (MPE)
Islamic University of Technology
Board Bazar, Gazipur
Dhaka, Bangladesh.

DEDICATION

I would like to dedicate this thesis to my beloved parents and my honorable thesis supervisor Prof. Dr. Md. Anayet Ullah Patwari.

DECLARATION

I hereby declare that, except where specific reference is made to work of others, the contents of this dissertation are original and have not been submitted in whole or in part for consideration for any other degree or qualification in this, or any other university. This dissertation is our work and contains nothing which is the outcome of work done in collaboration with others, except as specified in texts and Acknowledgements. This dissertation contains fewer than 13,000 words including appendices, bibliography, footnotes, tables, and has fewer than 60 figures.

ACKNOWLEDGEMENT

The author expresses gratefulness to the Almighty Allah (SWT) for his blessings, which enabled to complete this thesis successfully.

The author expresses gratitude to her supervisor Professor, Dr. Md. Anayet Ullah Patwari, Head, Department of Mechanical & Production Engineering (MPE), Islamic University of Technology (IUT) for his continuous guidance, helpful suggestions and supervision at all stages of this thesis work.

The author expresses gratefulness to Professor, Dr. Mohammad Ahsan Habib for his valuable guidance and encouragement. The author is highly indebted to him for guidance about the Engineering Simulation Software Third Wave AdvantEdge and highly complements his knowledge and expertise in the field of Finite Element Analysis.

The author is indebted to her fellow classmates Mr. A.N.M Nihaj Uddin Shan and Mr. Mokid Mohammad Shelley Serajee for supporting throughout the work. The author expresses her deepest gratitude.

The author conveys gratefulness to her parents for their financial and mental support in perusing the Bachelor's degree in Mechanical Engineering at all times. Without their guidance, it would not have been possible.

ABSTRACT

The purpose of this study is to analyze various parameters like temperature, pressure, maximum shear stress, von mises stress, cutting force, feed force, heat rate etc while keeping two tool parameters constant. In this research the main objective is to determine the fashion of chip formation due to variation of rake angle, relief angle and cutting edge radius. The total analysis was done using an Engineering simulation software that is dedicated for machining simulation called Third Wave AdvantEdge. In this simulation software various boundary conditions can be set before performing the simulation. In this study, all simulation was done in 2D interface. Firstly relief angle and cutting edge radius were kept constant to observe the impact on temperature, pressure, shear stress, von mises stress, cutting force, feed force, etc for variable rake angles. From this study, it is deduced that chip thickness gets decreased when rake angle, relief angle or cutting edge radius is increased. The change in thickness is sharper on relief angle compared to cutting edge radius and rake angle

TABLE OF CONTENTS

ACKNOWLEDGEMENT	i
ABSTRACT	ii
LIST OF FIGURES.....	vi
LIST OF TABLES	xii
CHAPTER 1 INTRODUCTION	1
1.1 Introduction	1
1.2 Simulation Materials	3
1.3 Objectives.....	3
1.4 Research organization	4
CHAPTER 2 LITERATURE REVIEW	6
CHAPTER 3 METHODOLOGY.....	10
2.1 Finite Element Input Parameters	11
2.2 Simulation Steps.....	16
CHAPTER 4 RESULTS AND DISCUSSION	25
3.1 Effects of rake angle.....	25
3.1.1 Cutting forces and feed forces.....	25
3.1.2 Temperature and pressure	26
3.1.3 Maximum shear stress and von mises stress	30
3.1.4 Heat rate	33

3.1.5 Plastic strain and plastic strain rate	34
3.1.6 Cutting power and maximum cutting temperature.....	36
3.2 Effect of relief angle.....	37
3.2.1 Cutting forces and feed forces.....	37
3.2.2 Temperature and pressure	38
3.2.3 Maximum shear stress and von mises stress	42
3.2.4 Heat rate	45
3.2.5 Plastic strain and plastic strain rate	46
3.2.6 Cutting power and maximum cutting temperature.....	48
3.3 Effect of cutting edge radius	49
3.3.1 Cutting forces and feed forces.....	49
3.3.2 Temperature and pressure	50
3.3.3 Maximum shear stress and von mises stress	54
3.3.4 Heat rate	57
3.3.5 Plastic strain and plastic strain rate	58
3.3.6 Cutting power and maximum cutting temperature.....	60
3.4 Chip formation on three different parameters	61
3.4.1 Effect of chip thickness on variation of rake angle.....	61
3.4.2 Effect of chip thickness on variation of relief angle	62
3.4.3 Effect of chip thickness on variation of cutting edge radius	63
CHAPTER 5 CONCLUSION	65

REFERENCES.....66

LIST OF FIGURES

Figure 1 Software input parameters (image taken from the software AdvantEdge)	13
Figure 2 Example of mesh (72,000 nodes) used in simulations. The cutting speed was 1000m/min, feed was 0.14mm/rev and depth of cut was 2 mm.	14
Figure 3 Opening new project	16
Figure 4 Naming the project	16
Figure 5 Displaying project	17
Figure 6 Inputting data of workpiece	17
Figure 7 Selecting material of workpiece	18
Figure 8 Inputting data of tool	18
Figure 9 Selecting material of tool	19
Figure 10 Inputting data of process parameters	19
Figure 11 Saving the project	20
Figure 12 Inputting max. number of nodes	20
Figure 13 Submitting simulation	21
Figure 14 Distribution of temperature	21
Figure 15 Selecting contour	22
Figure 16 Distribution of pressure	22
Figure 17 Selecting maximum shear stress	23
Figure 18 Distribution of maximum shear stress	23
Figure 19 Measuring Distance	24
Figure 20 Distribution of cutting and feed forces with the variation of rake angle for Cemented carbide-General tool	26

Figure 21 Distribution of temperature with the variation of rake angle for cemented carbide-General tool	27
Figure 22 Distribution of temperature in the workpiece, tool(cemented carbide-General) and chip at the 150 m/min simulation when rake angle is 15° (image at 5 mm length of cut)	28
Figure 23 Distribution of pressure with the variation of rake angle for cemented carbide-General tool	29
Figure 24 Distribution of pressure in the workpiece, tool(cemented carbide-General) and chip at the 150 m/min simulation when rake angle is 6° (image at 5 mm length of cut)	30
Figure 25 Distribution of maximum shear stress with the variation of rake angle for cemented carbide-General tool	31
Figure 26 Distribution of maximum shear stress in the workpiece, tool(cemented carbide-General) and chip at the 150 m/min simulation when rake angle is 15° (image at 5 mm length of cut)	32
Figure 27 Distribution of von mises stress in the workpiece, tool(cemented carbide-General) and chip at the 150 m/min simulation when rake angle is 3° (image at 5 mm length of cut)	33
Figure 28 Distribution of heat rate in the workpiece, tool(cemented carbide-General) and chip at the 150 m/min simulation when rake angle is 15° (image at 5 mm length of cut)	34
Figure 29 Distribution of plastic strain in the workpiece, tool(cemented carbide-General) and chip at the 150 m/min simulation when rake angle is 9° (image at 5 mm length of cut)	35

Figure 30 Distribution of plastic strain rate in the workpiece, tool(cemented carbide-General) and chip at the 150 m/min simulation when rake angle is 9° (image at 5 mm length of cut)	36
Figure 31 Cutting power and maximum cutting temperature along the time in the machining of the cemented carbide-General with a cutting speed of 150 m/min at the rake angle of 3° and a depth of cut of 2 mm	37
Figure 32 Distribution of cutting and feed forces with the variation of relief angle for Cemented carbide-General tool	38
Figure 33 Distribution of temperature with the variation of relief angle for Cemented carbide-General tool	39
Figure 34 Distribution of temperature in the workpiece, tool(cemented carbide-General) and chip at the 150 m/min simulation when relief angle is 19° (image at 5 mm length of cut)	40
Figure 35 Distribution of pressure with the variation of relief angle for Cemented carbide-General tool	41
Figure 36 Distribution of pressure in the workpiece, tool(cemented carbide-General) and chip at the 150 m/min simulation when relief angle is 13° (image at 5 mm length of cut)	42
Figure 37 Distribution of maximum shear stress with the variation of relief angle for Cemented carbide-General tool	43
Figure 38 Distribution of maximum shear stress in the workpiece, tool(cemented carbide-General) and chip at the 150 m/min simulation when relief angle is 19° (image at 5 mm length of cut)	44

Figure 39 Distribution of von mises stress in the workpiece, tool(cemented carbide-General) and chip at the 150 m/min simulation when relief angle is 19° (image at 5 mm length of cut)	45
Figure 40 Distribution of heat rate in the workpiece, tool(cemented carbide-General) and chip at the 150 m/min simulation when relief angle is 16° (image at 5 mm length of cut)	46
Figure 41 Distribution of plastic strain in the workpiece, tool(cemented carbide-General) and chip at the 150 m/min simulation when relief angle is 10° (image at 5 mm length of cut)	47
Figure 42 Distribution of plastic strain rate in the workpiece, tool(cemented carbide-General) and chip at the 150 m/min simulation when relief angle is 7° (image at 5 mm length of cut)	48
Figure 43 Cutting power and maximum cutting temperature along the time in the machining of the cemented carbide-General with a cutting speed of 150 m/min at the relief angle of 13° and a depth of cut of 2 mm	49
Figure 44 Distribution of cutting and feed forces with the variation of cutting edge radii for Cemented carbide-General tool	50
Figure 45 Distribution of temperature with the variation of cutting edge radii for Cemented carbide-General tool	51
Figure 46 Distribution of temperature in the workpiece, tool(cemented carbide-General) and chip at the 150 m/min when cutting edge radius is 0.08 mm (image at 5 mm length of cut)	52
Figure 47 Distribution of pressure with the variation of cutting edge radii for Cemented carbide-General tool	53

Figure 48 Distribution of pressure in the workpiece, tool(cemented carbide-General) and chip at the 150 m/min when cutting edge radius is 0.10 mm (image at 5 mm length of cut)	54
Figure 49 Distribution of maximum shear stress with the variation of cutting edge radii for Cemented carbide-General tool	55
Figure 50 Distribution of maximum shear stress in the workpiece, tool(cemented carbide-General) and chip at the 150 m/min when cutting edge radius is 0.10 mm (image at 5 mm length of cut)	56
Figure 51 Distribution of von mises stress in the workpiece, tool(cemented carbide-General) and chip at the 150 m/min when cutting edge radius is 0.10 mm (image at 5 mm length of cut)	57
Figure 52 Distribution of heat rate in the workpiece, tool(cemented carbide-General) and chip at the 150 m/min when cutting edge radius is 0.08 mm (image at 5 mm length of cut)	58
Figure 53 Distribution of heat rate in the workpiece, tool(cemented carbide-General) and chip at the 150 m/min when cutting edge radius is 0.08 mm (image at 5 mm length of cut)	59
Figure 54 Distribution of plastic strain rate in the workpiece, tool(cemented carbide-General) and chip at the 150 m/min when cutting edge radius is 0.04 mm (image at 5 mm length of cut)	60
Figure 55 Cutting power and maximum cutting temperature along the time in the machining of the cemented carbide-General with a cutting speed of 150 m/min at the cutting edge radius of 0.06 mm and a depth of cut of 2 mm	61

Figure 56 Distribution of chip thickness with the variation of rake angles for Cemented carbide-General tool	62
Figure 57 Distribution of chip thickness with the variation of rake angles for Cemented carbide-General tool	63
Figure 58 Distribution of chip thickness with the variation of cutting edge radii for Cemented carbide-General tool	64

LIST OF TABLES

Table 2-1 FEM of machining of steel (AISI 1020) input parameters	11
Table 2-2 Chemical composition and mechanical properties of the Steel (AISI 1020).	14

CHAPTER 1

INTRODUCTION

1.1 Introduction

In industry, cutting is the most familiar process of manufacturing. For simulating the metal cutting process, FEM has introduced one of the leading models. Fatigue failure, frictional interaction, thermo-mechanical coupling, and chip and burr structural features are all part of the cutting processes, which is a dynamic process that consists of natural processes. The ability to simulate mechanical and thermal activity instead of using experimentation of both the tool and material is a major benefit of using numerical simulation. This is how, without going back to time and money, we can maximize our productivity and lower our costs. Numerical processing applications are now widely used and therefore are a valuable method to study chip movement in machining and obtaining knowledge that is hard to obtain experimentally[1][2]. Nevertheless, the precision of the obtained results of the finite element method is mostly determined by the accuracy of the input values. So, it is critical to consider how the input data influences the Finite Element Methods analysis prediction. To understand how the chip flow works in machining, the FEM method is very useful[3].

FEM-based simulations are very essential in the case of predicting how the chip formation forms, computing plastic strain rate, stress rate, von mises stress, shear stress rate, temperature, heat rate and pressure distribution on cutting edge. For the chip and machined work surface, FEM simulation is also highly required. Machining covers a

huge collection of designing manufacturing processes where removing material from the workpiece is the main concern. We know some machining process named Turning, Boring, Shaping, Milling, Drilling, Sawing, Broaching, and grinding. Turning is a process where using a cutting tool, cylindrical forms can be generated. Milling is a surface-generation technique that involves scraping a defined number of samples from a workpiece. Drilling is the process of making circular holes in objects. Shaping extracts substrate from objects using a single-point instrument assisted by a roller that acts in accordance the devive against by the machined surface in a linear movement. Internal spinning to create internal forms is known as boring. Broaching is a procedure that involves moving or dragging a drill bit with several circumferential sharp edges via a gap or over a layer to extract substance by lateral cutting. Sawing is the method of cutting a metal with different geometry power system. Lastly, the grinding method is a subtractive manufacturing technique in which expected to vary strip metal from workpiece in tiny pieces or fragments[4][5]. Some of the researchers work on taking different parameters. In advanced manufacturing technology, high-speed machining has become the most essential aspects. Once, there have been some difficulties in machining difficult metals[6]. But nowadays, using high-speed machining is continuously increasing. So, it provides us higher productivity and also a better quality of surface[7][8].

Models are mainly two types. Orthogonal is a model for two forces and another one, oblique, which is three forced models. From an understanding view point, the orthogonal model is much easier to simulate than the oblique model. To know about the basic mechanics of machining processes, the orthogonal model is very helpful[4]. In a

model of orthogonal cutting, tip of cutting tool is vertical to the associated model of tool and workpiece in its direction. Feed works together with the movement of tool and workpiece, allows forming chips.

1.2 Simulation Materials

Nowadays, aeronautical and automotive have expanded widely. Thus the aim of this field is to manufacture lighter goods. There are so many tools and one of them is cemented carbide-General which doesnot wear easily, resisting even extreme heat. Cemented carbide is used for as a medium of cutting and it's a strong material. The reason behind choosing this tool is high hardness, high strength and high rigidity. It offers a stronger finish and makes it possible to work faster.. It gives a finer finish which makes it possible to work faster. In my research, I have simulated in 2D. As workpiece, AISI 1020 steel has been used. AISI 1020 has low hardenability properties and is a low tensile carbon steel with a brinell hardness of 119-235, and a tensile strength of 410-790 MPa and also it has high machinability, high ductility and high weldability.

1.3 Objectives

The prime goal of my study is to analysis the effect of tool geometry like temperature, pressure, maximum shear stress, plastic strain, and heat and strain rate on cutting parameters, to predict the tool life and the quality of machining of various cutting radius, rake angles and relief angles. Also compute the change of tool temperature and power with respect to time. Another main objective of this work is to determine the chip thickness during chip formation.

1.4 Research organization

This study begins with an introduction that provides background information on the effect of tool geometry while forming chip by FEM analysis. FEM-based simulations are very essential in the case of predicting how the chip formation forms. Using numerical simulation maximizes productivity and lowers the cost. There are so many processing methods. The one that is taken is Turning process. The materials used for the tool and workpiece are cemented carbide-General and AISI 1020 steel. After that, the main objective of this study is discussed.

In chapter 2, a detailed literature review of previous studies is briefly discussed. Some of the researchers have worked on different coated materials and some of them have worked on chip formation. Some researchers have used different types of methods named Lagrangian, ABAQUS, etc. Some of the researchers' main concerns are the tool life of the material that has been used.

Chapter 3 presents a brief discussion on how the software named Third Wave AdvantEdge is used. The simulation steps and the parameters are discussed as well. The steps of performing simulation are shown. Firstly, define the workpiece dimension and material, secondly define tool dimension and material, then set up process parameters like the number of nodes, mesh type, etc and finally set up simulation options and run the simulation.

The results and discussions are described in chapter 4. For taking different parameters like temperature, pressure, maximum shear and von mises stress, plastic strain and strain rate, etc and also taking one varying cutting parameter when others two are kept

constant, what are the changes occurring are described. This means if the temperature is decreasing or increasing or the pressure is increasing or decreasing etc.

After the result and discussion part, a summary of the findings are given in Chapter 5.

CHAPTER 2

LITERATURE REVIEW

Athulan and Joel[9] have shown three different simulations named Deform, ABAQUS and AdvantEdge where they have described the robustness for the performance of machining simulations. The article provides a comparative study of three locally available finite element analysis software packages. The complexity of the workpieces flow stress can be ignored with the use of models called Lagrangian while there is a fundamental template for work metal that is experimentally obtained from temperature deformation and high strain rate testing. The FEM simulation system used in the orthogonal cutting phase can be an absolute and workable review as long as the work material's flow stress behavior is well established which is stated by Ozel[10]. Also, Sartkulvanich and Altan express that friction coefficient, flow stress and tool-chip interface of the workpiece are the most essential input values for a mathematical simulation. This mathematical illustration was presumed to signify the workpiece flow stress[3]. Some of the researchers have worked on different optimal cutting conditions. The Johnson-Cook material model is used in this analysis to simulate cutting force and tool temperature when doing high-speed machining using ABAQUS explicit software. It was decided that raising the cutting tool rake angle above its optimal value had a negative effect on tool efficiency and increased cutting temperature[11].

A method is described by Bouzid[12] where models are used for cutting forces, roughness and tool life. To spin AISI 4340, four different types of commonly produced inserts were used. 3 CVD-coated plates and one composite tool were being

investigated. The procedure limitations throughout the work were also the engine power and the maximal rotational speeds. The technique entails describing the feed in connection to the hardness, which is affected by the cutting conditions. There have some restrictions named machine control and maximum spindle speed. Agrahari et. al.[13] researched on validation of virtual cutting forces obtained from a finite element based program in dry turning of Aluminum 7075 alloy. This study has revealed an ability to use Deform 3D to verify other machining responses such as residual tension, tool wear and chip morphology, as well as to compare findings obtained with other FEA-based software. In one research paper, for turning processes, a 3D model and software were built. Mechanical power, friction and heat transfer coefficient at the tool-chip interface can be calculated by using this software. A distinction was also made between the experimental and numerical results for the cutting power, temperature and thrust force[14].

Some of the researchers have worked on different optimal cutting conditions. Like in turning, our main criteria are to get the maximum rate of production. Using FEM models, Altan et. al.[15] analyzed the role of cutting tool edge planning on chip shape, cutting forces and process variables. The prediction made in this study was for tool rake face, while the material flow around the edge was defined by the position of the stagnation point. Strenkowski et. al.[16] worked on an Eulerian finite element method where orthogonal cutting has discussed. The model is exceptionally useful because it does not depend on any knowledge on empirical cutting. Therefore, without its demand for additional cutting experiments, the instrument forces and temperatures, rate of stress and strain field in the chip and workpiece can be calculated. Good correlation is

observed on the basis of tool intensity and mean temperature scale through the tool-chip embrasure.

A metal cutting process habitually implicates massive deformation and rate of strain. This cutting process therefore should be viewed as a combined thermo-mechanical process[17]. Strenkowski and Carroll[18] described a new modified Lagrangian configuration for the conditions of the plane strain. It involves friction across the surface of the rake as well as a simpler convective heating method. Metal distortion and slithering friction resolve in heat, which can have an impact on distortion and residual stress. Chip morphology, workpiece surface finish and tool life are also affected by temperature[19].

Bouzakis et. al.[20] worked on the possibility of improving the tensile properties of cemented carbide by micro-blasting. A FEM-based assessment is used to ascertain the bearing capacity pre and post micro-blasting. The micro-blasting induced covering topomorphy was measured and associated with surface roughness and films conductivity. The cutting qualities of inserts wrapped with micro-blasted films were researched and explained using a material removal FEM simulation. The acquired results show an increase in surface finish through micro-blasting of composites preserved on substances with acceptable tightness properties.

Another researcher Tugrul Ozel[21] analyzed FE modeling studies on turning in 3D with basic and varying edge layout PcBN additives. On uniform and variable edge micro geometry tools, 3D finite element modeling is used to determine chip formation, loads, pressures, strains, and tool wear. Experiments are used to contrast projected formations and tool wear. These findings discovered that varying edge readiness inserts

outpace uniform sharpened and uniform landside honed shaped slots. The results show that specific micro-geometry inserts outperform uniform equivalents for wider scope whenever the flexible edge is similarity for a given cutting parameters.

Albert[22] analyzed the rake angle effects in orthogonal metal cutting. In this analysis, a plane strain finite element approach is developed and applied to model orthogonal low carbon steel metal cutting with chip forming. Under the same cutting conditions and friction limitations, steady state continuous chip forming when cutting with a particular rake angle could not be accomplished. Numerical and experimental studies are conducted by Outeiro et. al.[23] to evaluate the impacts of geometrical parameters, cutting scheme specifications and tool coating on residual stress in the chamfered surfaces of AISI 316L. They found that whenever the cutting speed, edge radius and chip thickness which is uncut increase, the residual stresses increase. Replacing the uncoated tool to coated tool also increases residual stress. Increasing tool rake angle also increases residual stress.

Nowadays diamond materials are commonly used in manufacture of mirror-like layers of non-ferrous materials like aluminum or copper. However, aluminum machining with conventional cutting tools decreases tool life. It has an inauspicious impact on material and edge consistency due to the creation of built-in surfaces and burrs. Burrs is harmful mostly during tooling because they strike the sharp edge of the tool which cause groove tear[7]. Grzesik et. al.[24] worked on different coated materials where the applicability of various simulation models was explored in order to obtain a FE solution of cutting forces, acceptable temperatures and cutting resources. The effects of different thermal simulations were then equivalent to cutting temperature measurements.

CHPATER 3

METHODOLOGY

Third Wave AdvantEdge is a dedicated platform to simulate various machining processes like turning, drilling, milling both in 2D and 3D configurations Advantedge by manipulating a number of parameters that could affect the formation of chips while machining. It is a versatile tool. It allows users to evaluate machining parameters and tool and workpiece settings that can minimize cutting temperature and pressure and components distortions. AdvantEdge contains three major components treated as a single program package[25].

1. The **Simulation Configuration** interface helps users to change up the complete simulation, plus tool geometry description, machining parameters and material circumstances.
2. The **AdvantEdge Engine** measures all configuration inputs.
3. The **Results Viewfinder** helps users to capture all simulation results required, including input forces, stable status results and instrument temperature etc.

Machining has already programmed systems, including milling and turning for 2-dimensional and 3-dimensional machining operations. In order to enhance simulation performance, the software uses advanced meshing. Although the operator cannot customize the optimizer controls. Advantedge is strong software which allows quick machining due to its easy and simple operation. AdvantEdge has many aircraft alloys and designs with several aerospace metals. New materials are reasonably easy to determine and consumers can join the structure of the metal with various versions[9].

2.1 Finite Element Input Parameters

At Table 1[2], the input parameters are shown. As workpiece, AISI 1020 steel has been used. AISI 1020 has low hardenability properties and is a low tensile carbon steel with a brinell hardness of 119-235, and a tensile strength of 410-790 MPa and also it has high machinability, high ductility and high weldability. As cutting tool, we have used Cemented Carbide – General. The reason behind choosing this tool is high hardness, high strength and high rigidity. It offers a stronger finish and makes it possible to work faster. For cemented carbide cutting tool, we have performed a number of simulations by changing the Rake angle, Relief angle and cutting edge radius. Rake angle is a parameter used in various cutting and machining processes describing the angle of the cutting face relative to the workpiece. The angle between the part of the flanks of a cutting tool below the cutting edge and a plane perpendicular to the base is known as Relief angle. To prevent catastrophic failure of tool tip, a tiny rounding or small radius is provided there which is known as Cutting edge radius or nose radius. While changing the rake angle, the other two parameters were kept constant. The rake angles, cutting edge radius and relief angle we have taken are 3°, 6°, 9°, 12°, 15°; 0.02mm, 0.04mm, 0.06mm, 0.08mm, 0.10mm and 7°, 10°, 13°, 16°, 19° respectively.

Table 2-1 FEM of machining of steel (AISI 1020) input parameters

<i>Workpiece</i>	
Workpiece length, L	5 mm
Workpiece height, h	2 mm
Workpiece material	AISI 1020
<i>Tool</i>	

Rake angle, a	3°,6°,9°,12°,15°
Rake face length, q	2 mm
Relief angle, b	7°,10°,13°,16°,19°
Relief face length, p	2 mm
Cutting edge radius, r	(0.02,0.04,0.06,0.08,0.10) mm
Material	Cemented carbide-General
<i>Process</i>	
Depth of cut, d	2 mm
Length of cut, l	5 mm
Feed, f	0.15 mm/rev
Cutting speed, V	150 m/min
Initial Temperature, T_o	20°C
<i>Coolant</i>	
Heat transfer co-efficient	9933 W/m ² ·k
Density	981 kg/m ³
Temperature	20°C
Area option	Immersed
<i>Simulation</i>	
Maximum number of nodes	72,000
Maximum element size	0.1 mm
Minimum element size	0.02 mm
Mesh Refine	2
Mesh coarse	6

Number of Threads	1
-------------------	---

Here, fig. 1 is given for a clearer understanding of the interaction between these inputs[19]. Our main concern is the length of cut, depth of cut, rake angle, relief angle, and cutting edge radius.

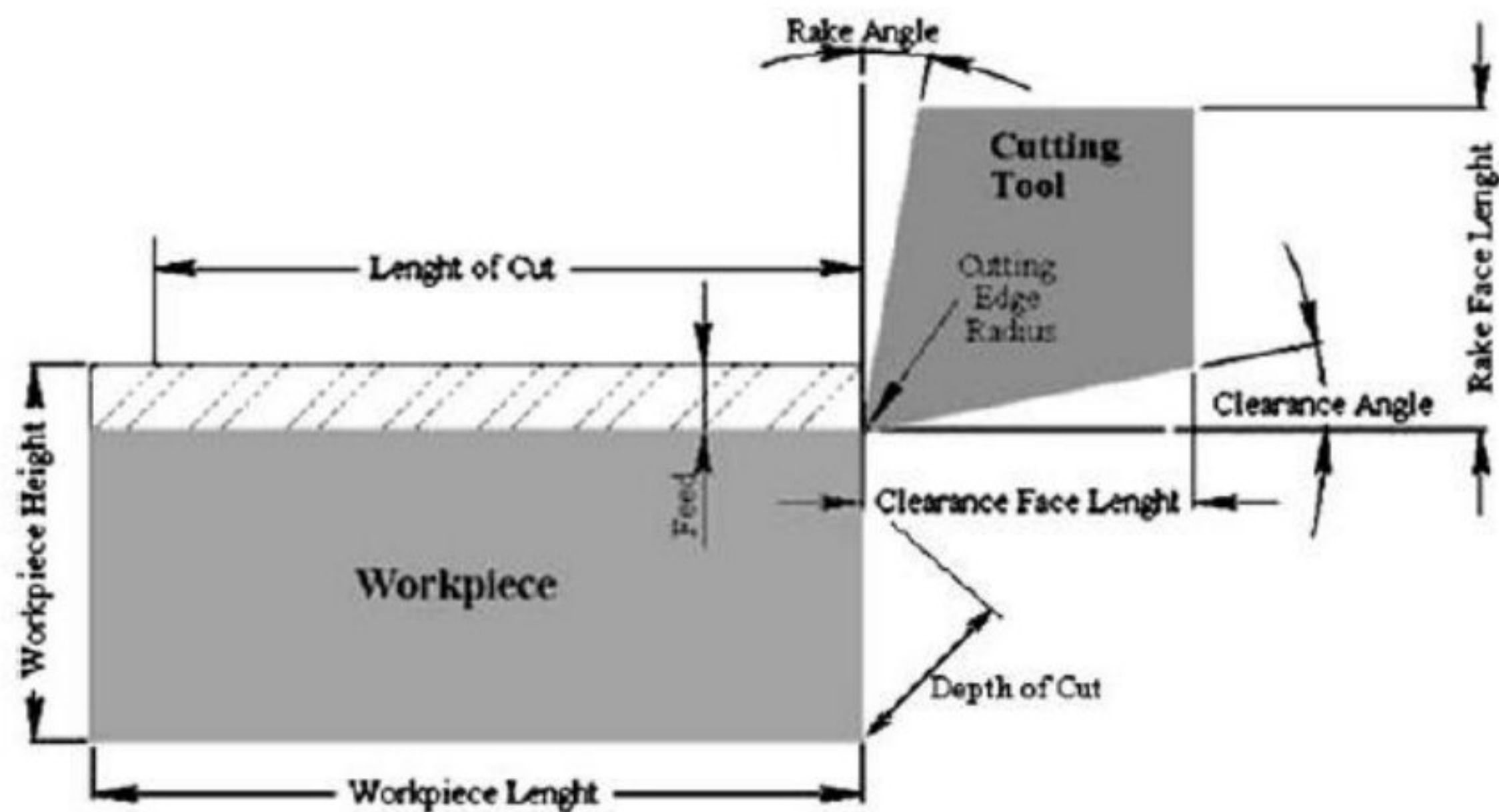


Figure 1 Software input parameters (image taken from the software AdvantEdge)

The example of mesh is shown in fig. 2 where the cutting speed is 1000 m/min, feed rate is 0.14 mm/rev and depth of cut is 2 mm.

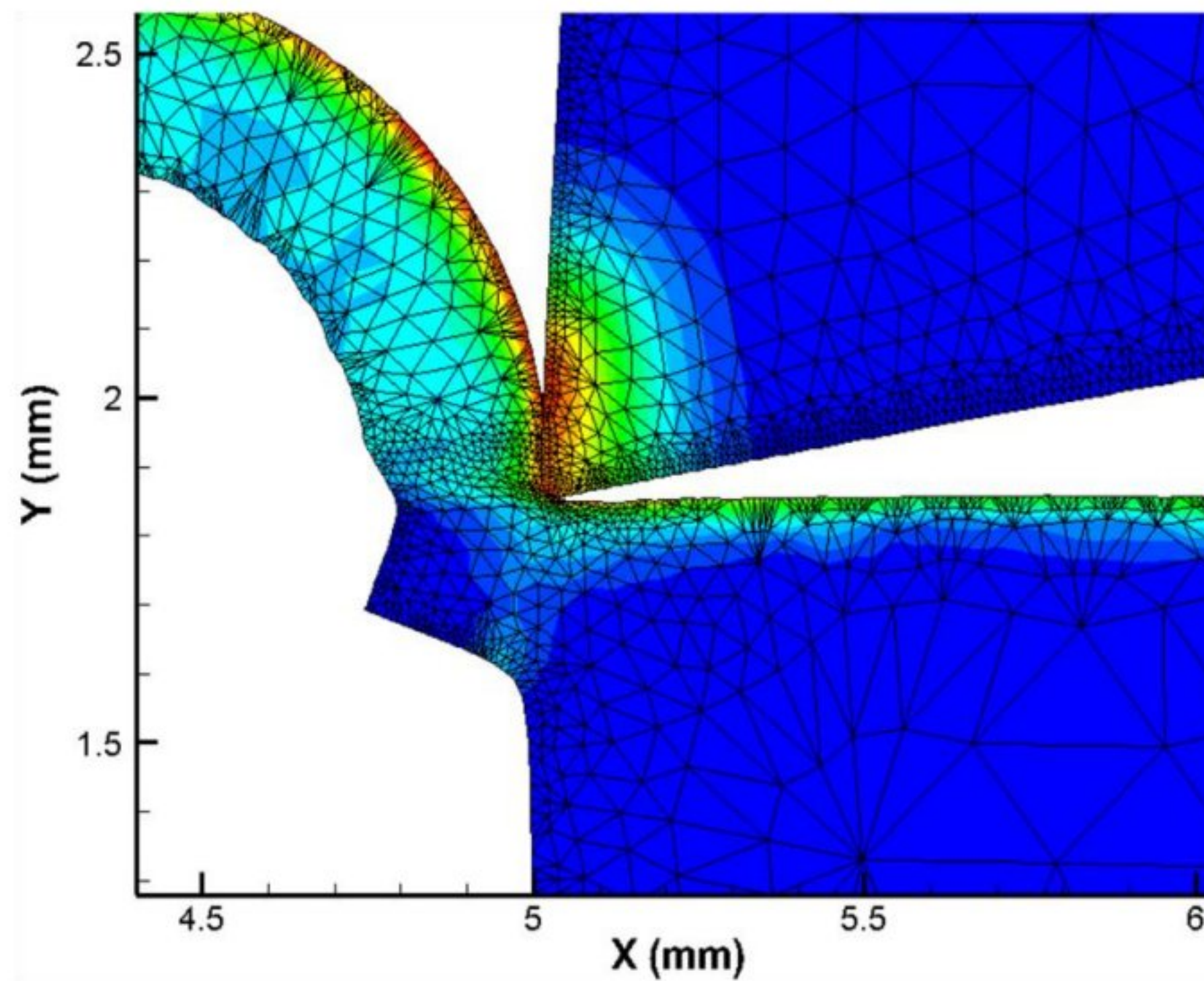


Figure 2 Example of mesh (72,000 nodes) used in simulations. The cutting speed was 1000m/min, feed was 0.14mm/rev and depth of cut was 2 mm.

Table 2[2] shows the chemical composition and mechanical properties of AISI 1020. The AISI 1020 steel has a chemical composition of Iron, Manganese, Sulphur, Phosphorous and Carbon. It has an ultimate tensile strength of 395 MPa and Brinell hardness of 111 with a Shear modulus of 80 GPa. These are some of the mechanical properties.

Table 2-2 Chemical composition and mechanical properties of the Steel (AISI 1020)

<i>Chemical composition (%)</i>	
Fe	99.08 - 99.53
Mn	0.30 - 0.60
S	≤ 0.050
P	≤ 0.040

C	0.17 - 0.230
<i>Mechanical properties</i>	
Tensile strength, yield	295 MPa
Tensile strength, ultimate	395 MPa
Modulus of Elasticity	200 GPa
Izod impact	125 J
Shear modulus	80.0 GPa
Elongation at break	36.5%
Hardness, Brinell (HB)	111
Density	7.87 g/cc
Bulk Modulus	140 GPa
Poisson's Ratio	0.290
Reduction of Area	66.0%

2.2 Simulation Steps

Open a new project in Third Wave AdvantEdge as shown in fig. 3.

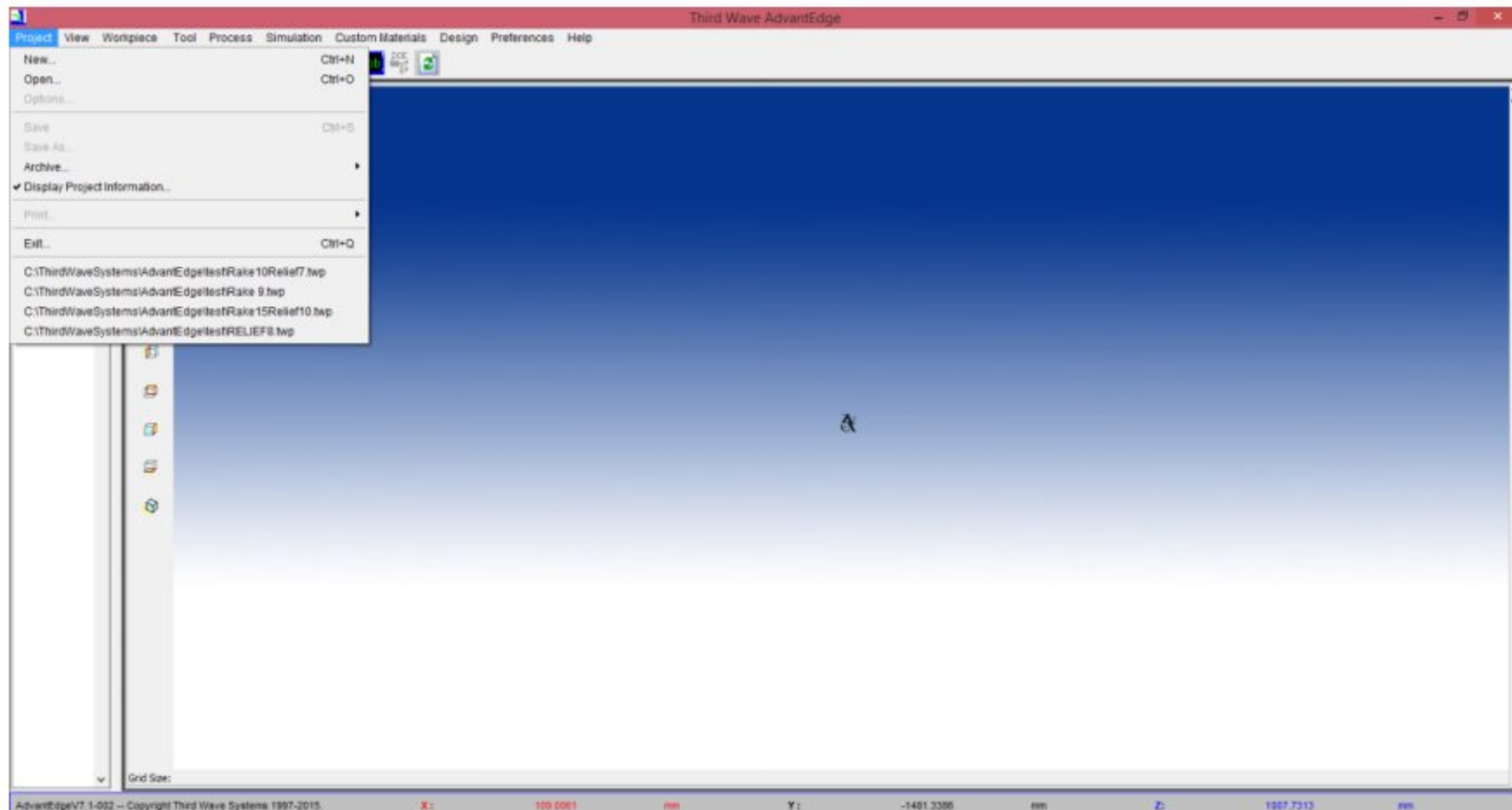


Figure 3 Opening new project

Input the name of the project as shown in fig. 4. The process type was chosen as turning.

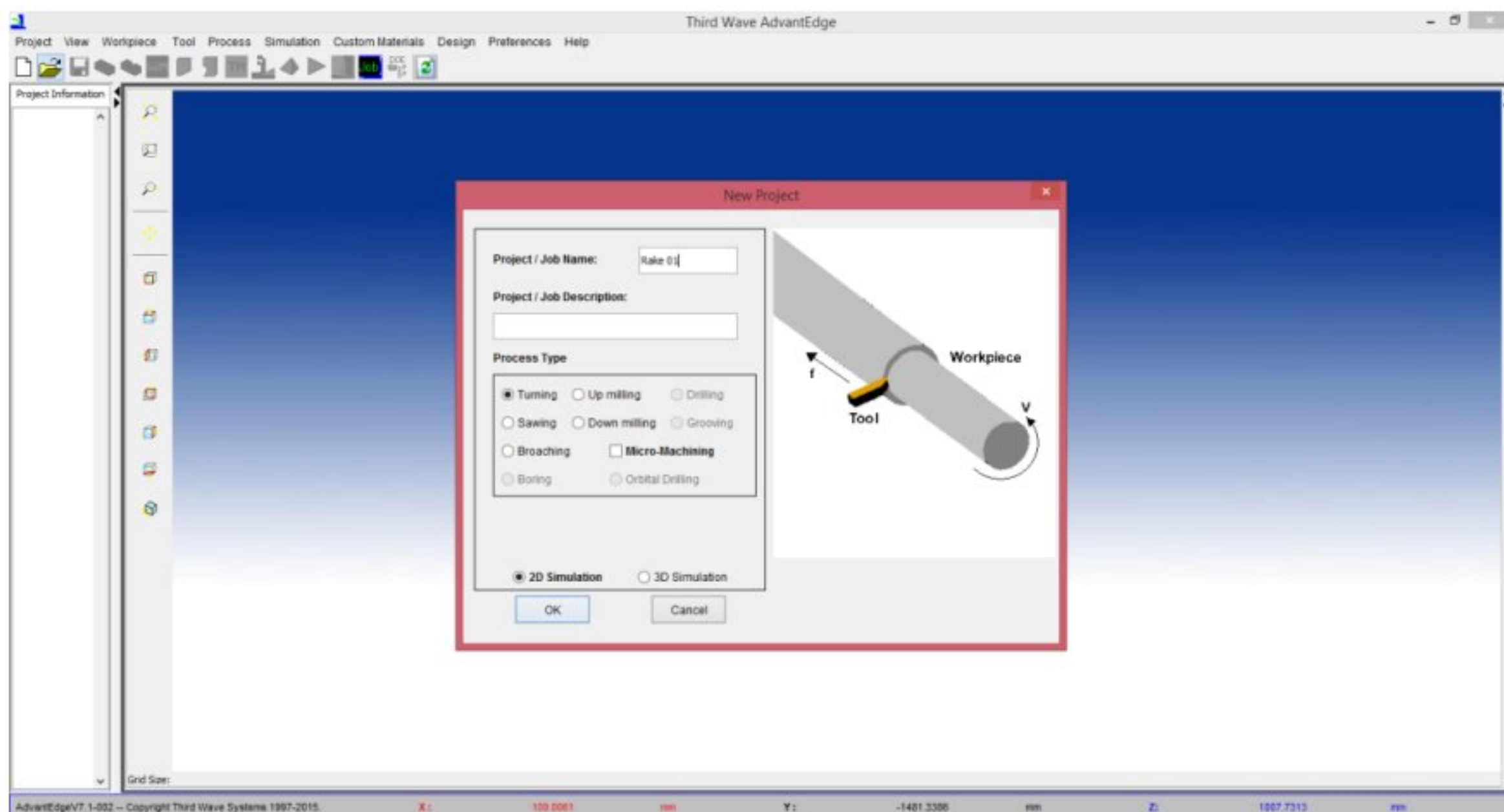


Figure 4 Naming the project

The display window shows the following as fig. 5. The left panel shows the project information.

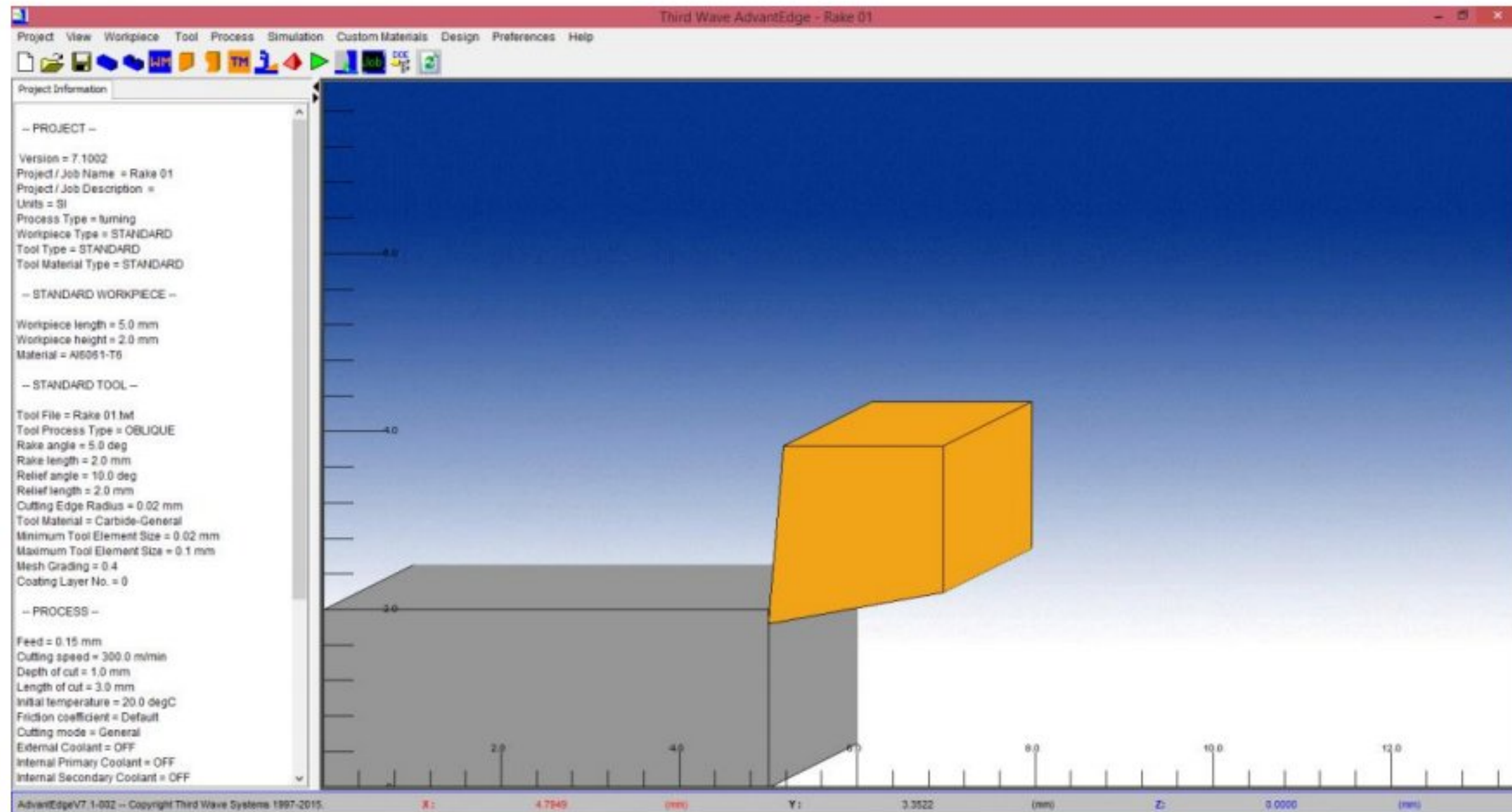


Figure 5 Displaying project

Fig. 6 shows the created workpiece and necessary data input. The height of the workpiece was 2 mm and length is 5 mm.

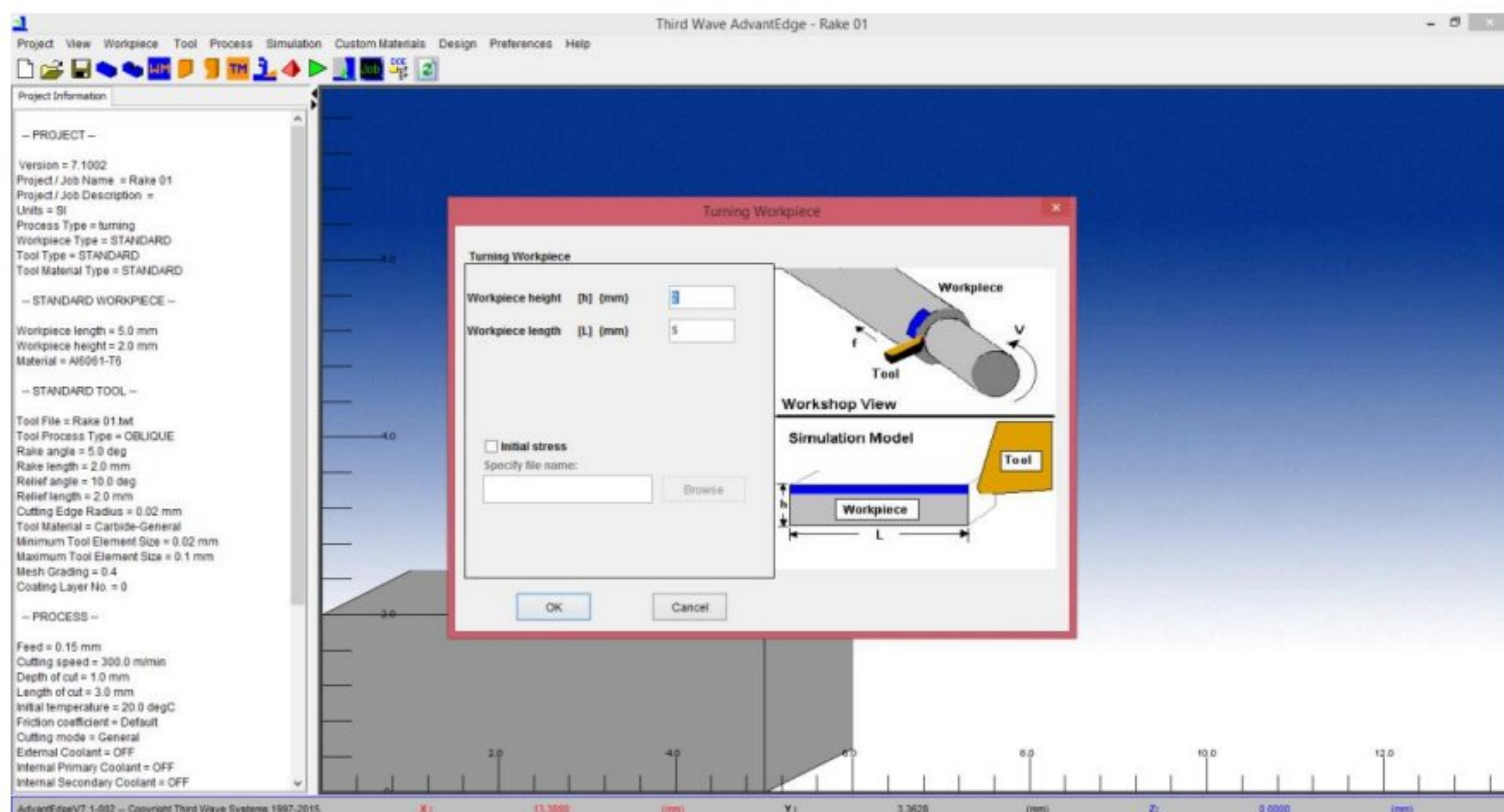


Figure 6 Inputting data of workpiece

From workpiece tab, the appropriate workpiece material was selected according to standard grade as shown in fig. 7. The material was AISI 1020 steel.

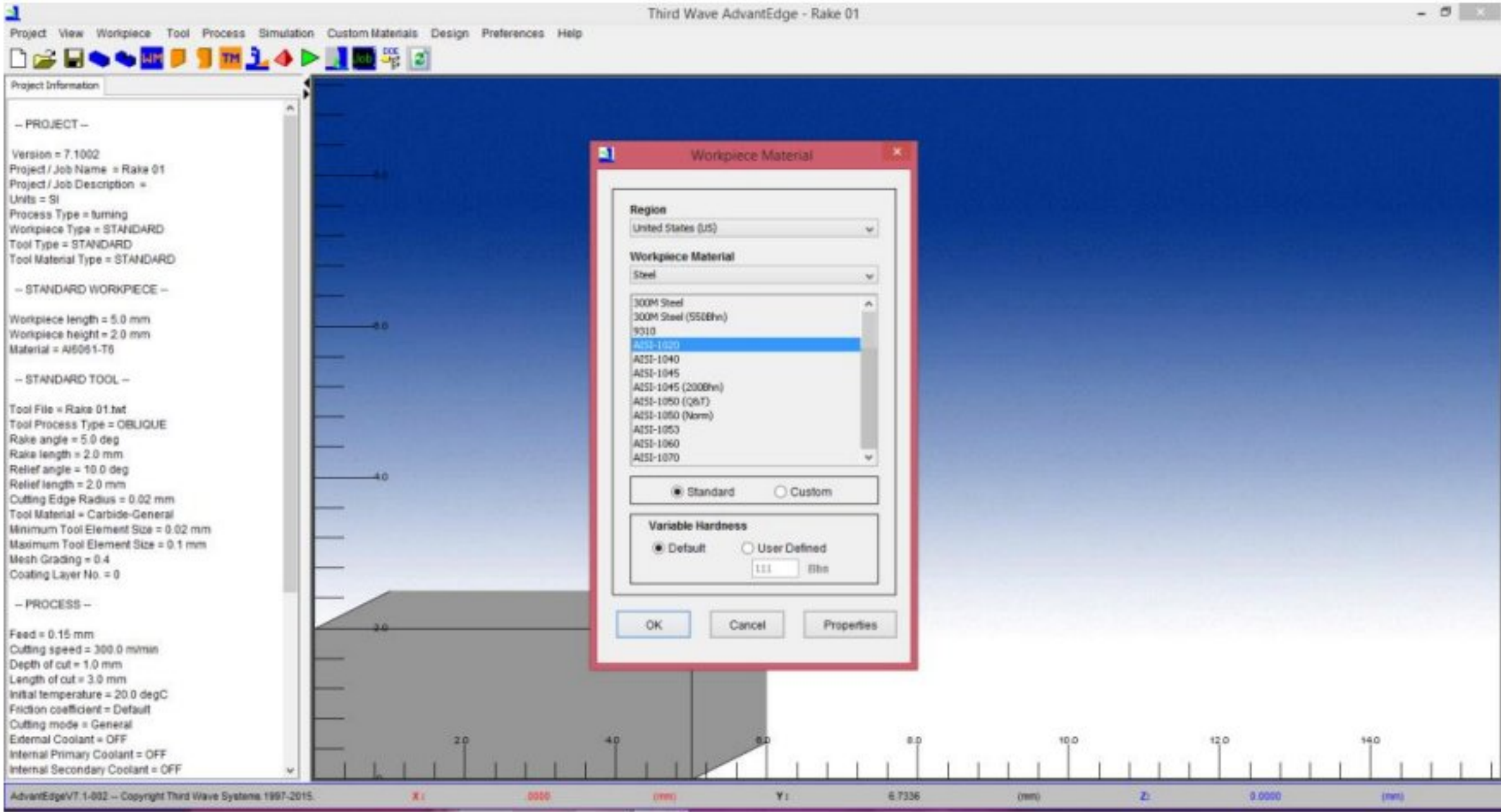


Figure 7 Selecting material of workpiece

Fig. 8 shows the created tool and necessary data input. The rake angle, relief angle and cutting edge radius was taken 3°, 7° and 0.02 mm.

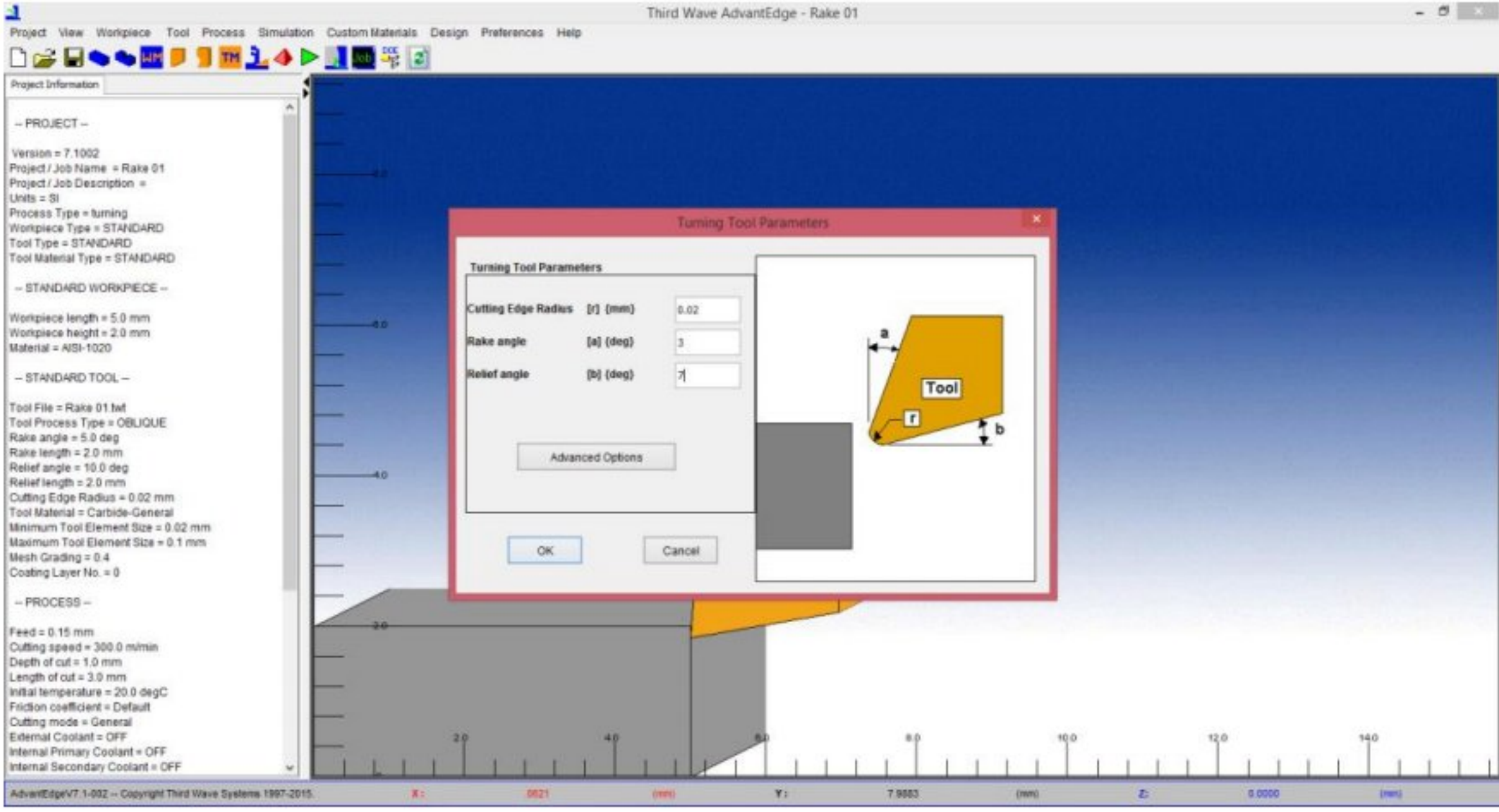


Figure 8 Inputting data of tool

From tool tab, the appropriate workpiece material was selected according to standard grade as shown in fig. 9. The tool material was cemented carbide-General.

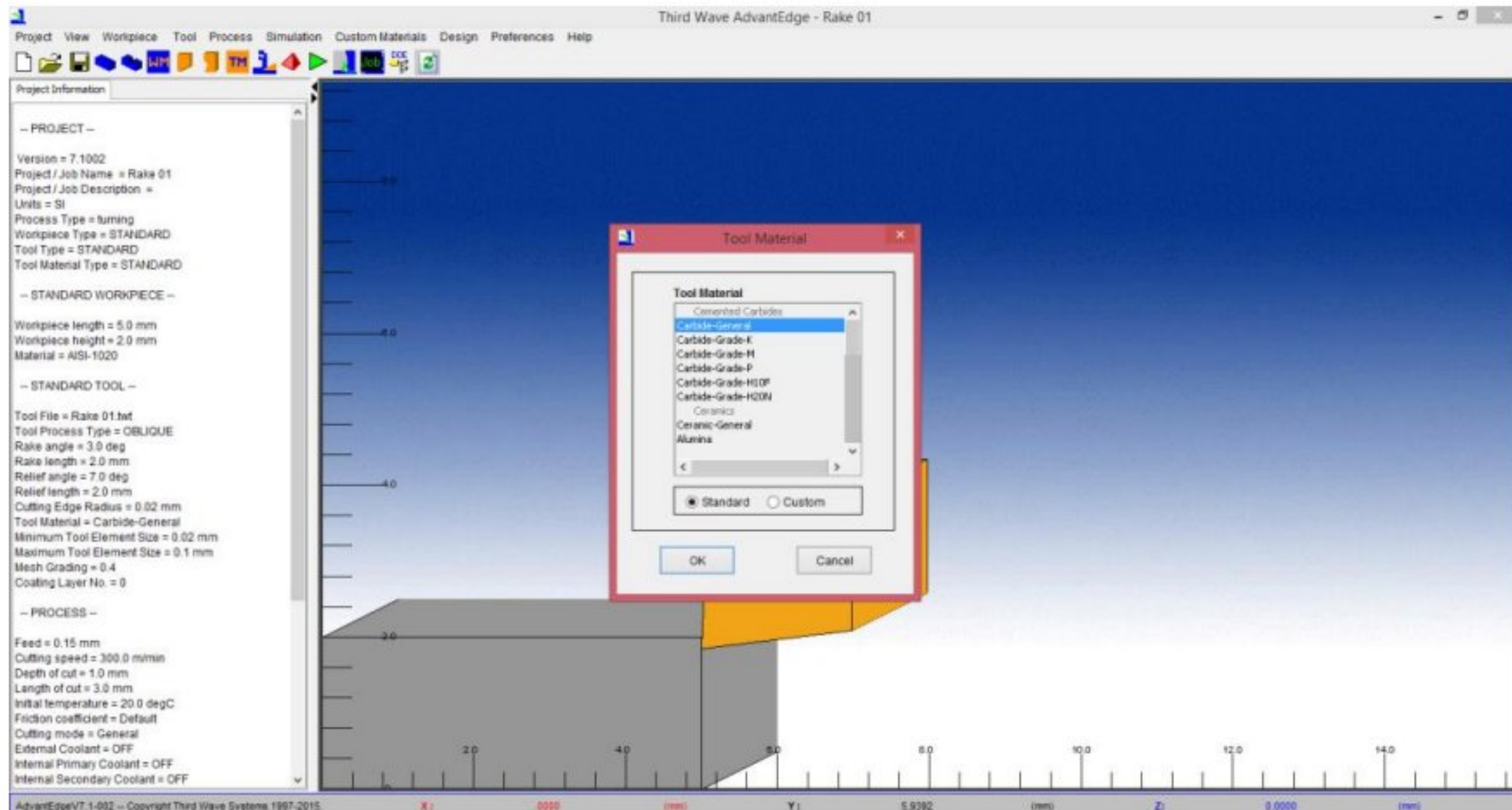


Figure 9 Selecting material of tool

The process parameters of turning is shown in fig. 10 where the feed rate, depth of cut, length of cut, cutting speed and initial temperature was inputted.

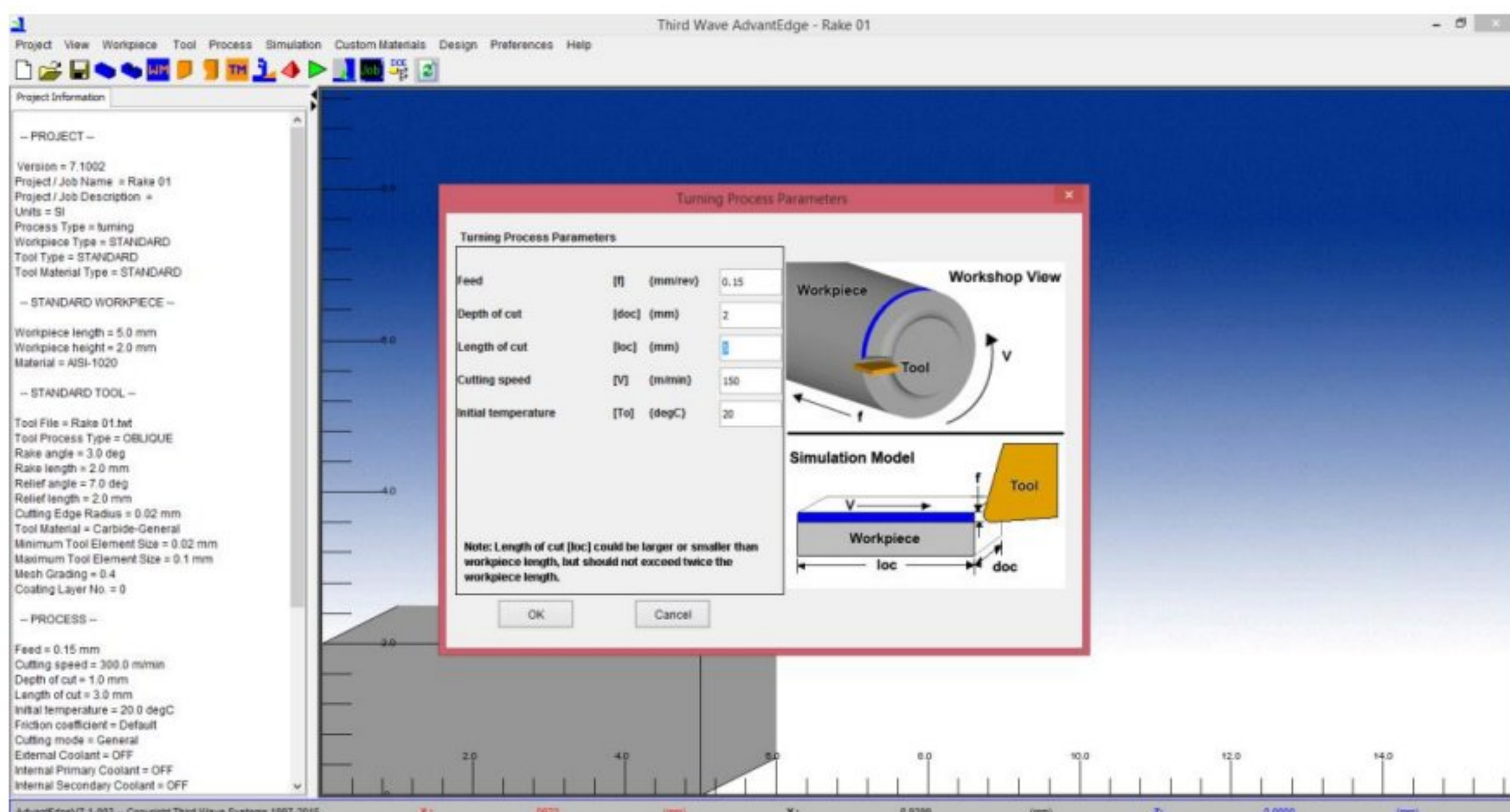


Figure 10 Inputting data of process parameters

After process parameters, the file was saved which is shown in fig. 11.

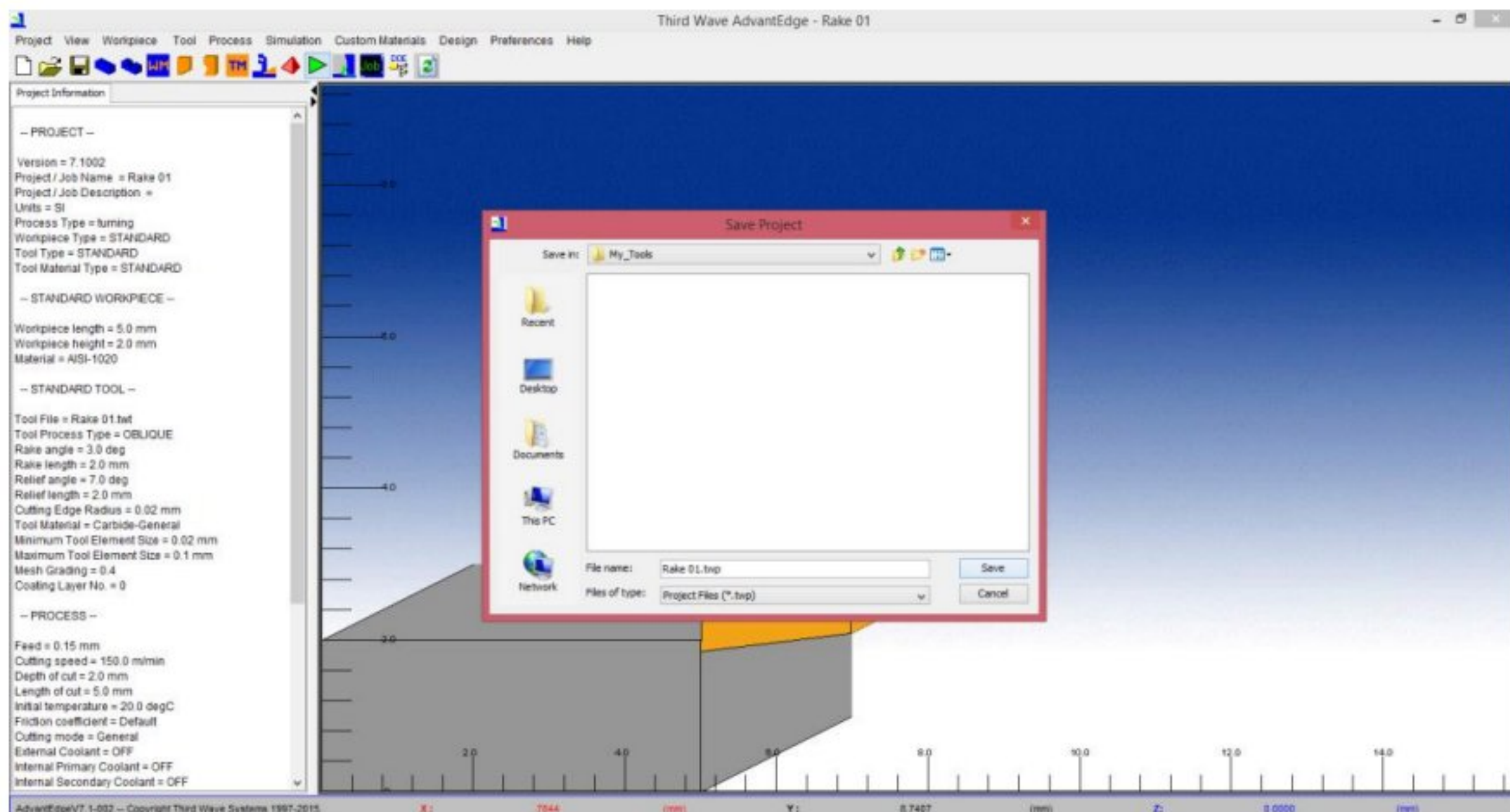


Figure 11 Saving the project

Fig. 12 shows the simulation options. It was taken as general and number of nodes are 72000.

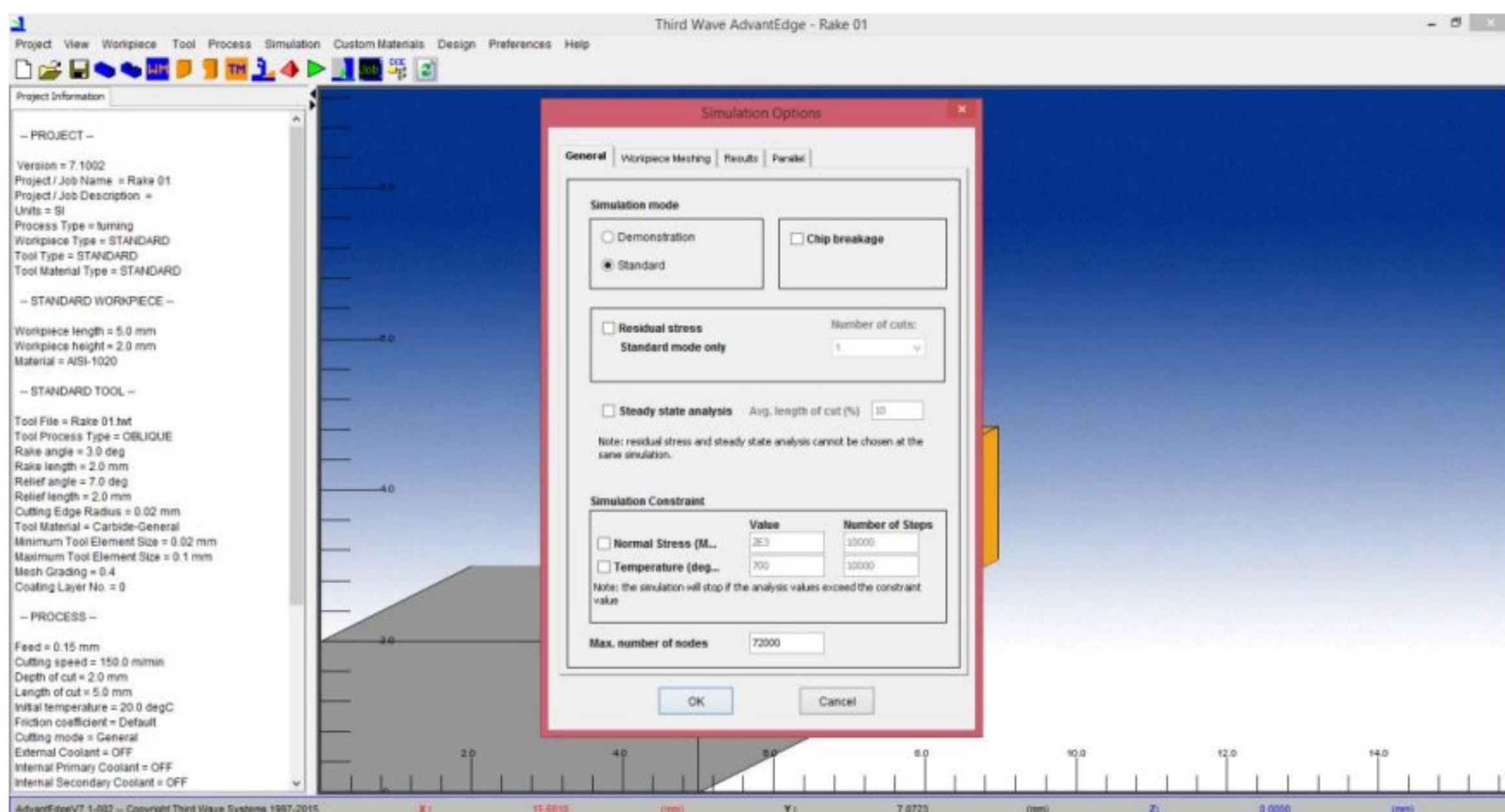


Figure 12 Inputting max. number of nodes

Fig. 13 shows how to submit the simulation. It has to be in mind to choose the simulation as a new job.

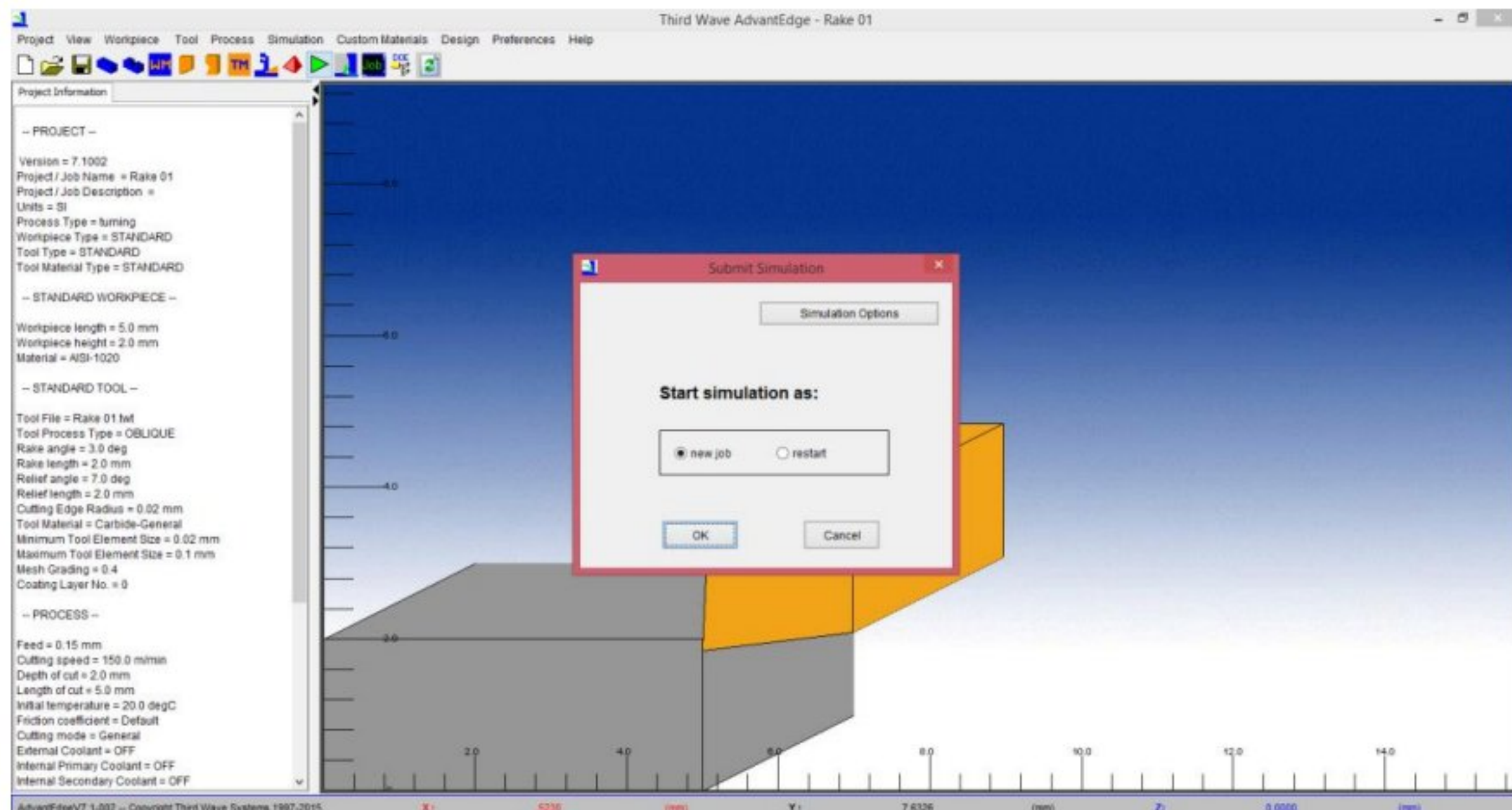


Figure 13 Submitting simulation

A new software will open named tecplot where it shows all the results like temperature, pressure, maximum shear stress, plastic strain rate, cutting and feed force and so on.

Fig. 14 shows the temperature distribution.

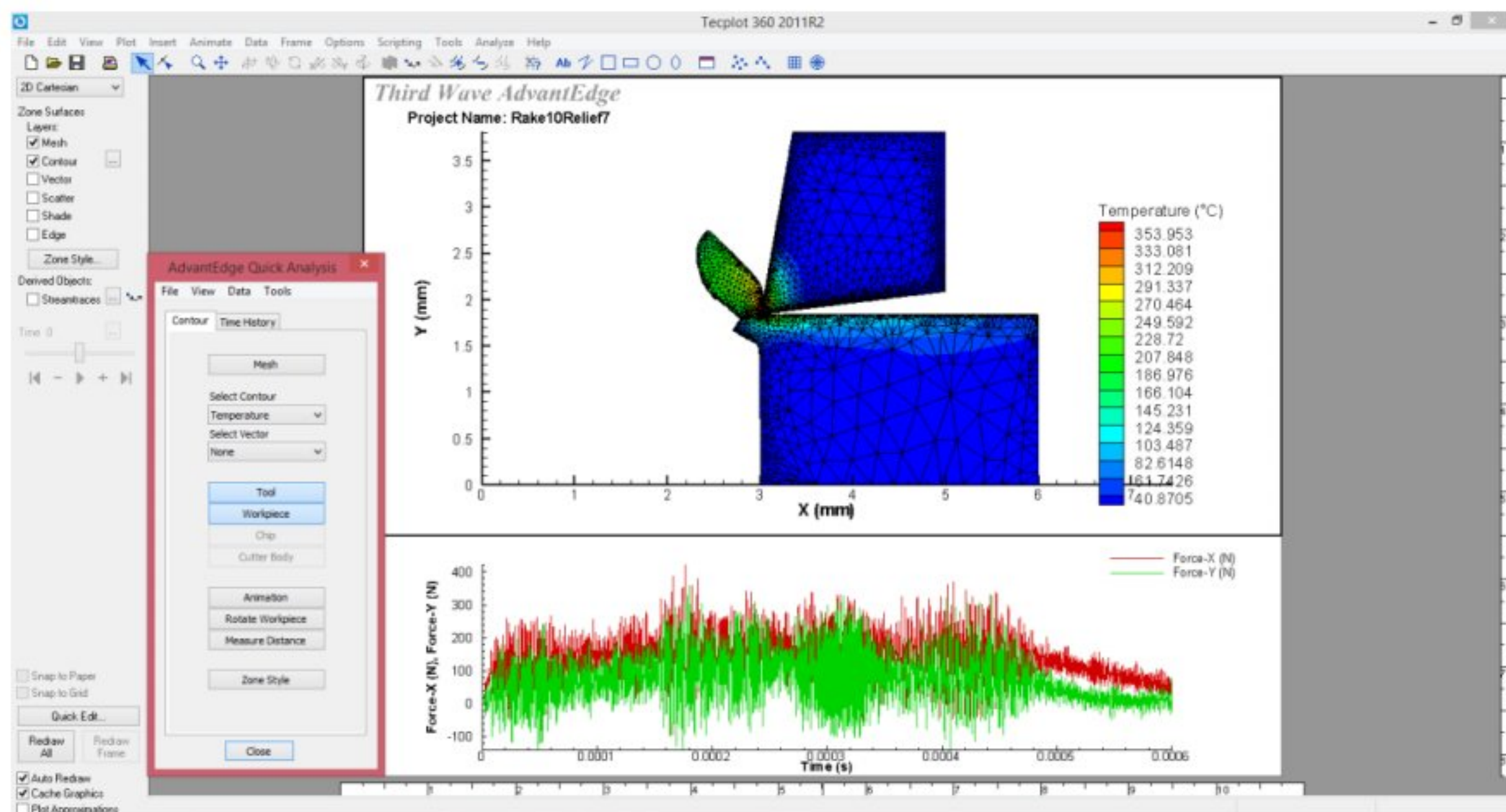


Figure 14 Distribution of temperature

From AdvantEdge quick analysis, after selecting contour, all the parameters distribution can be seen as shown in fig. 15.

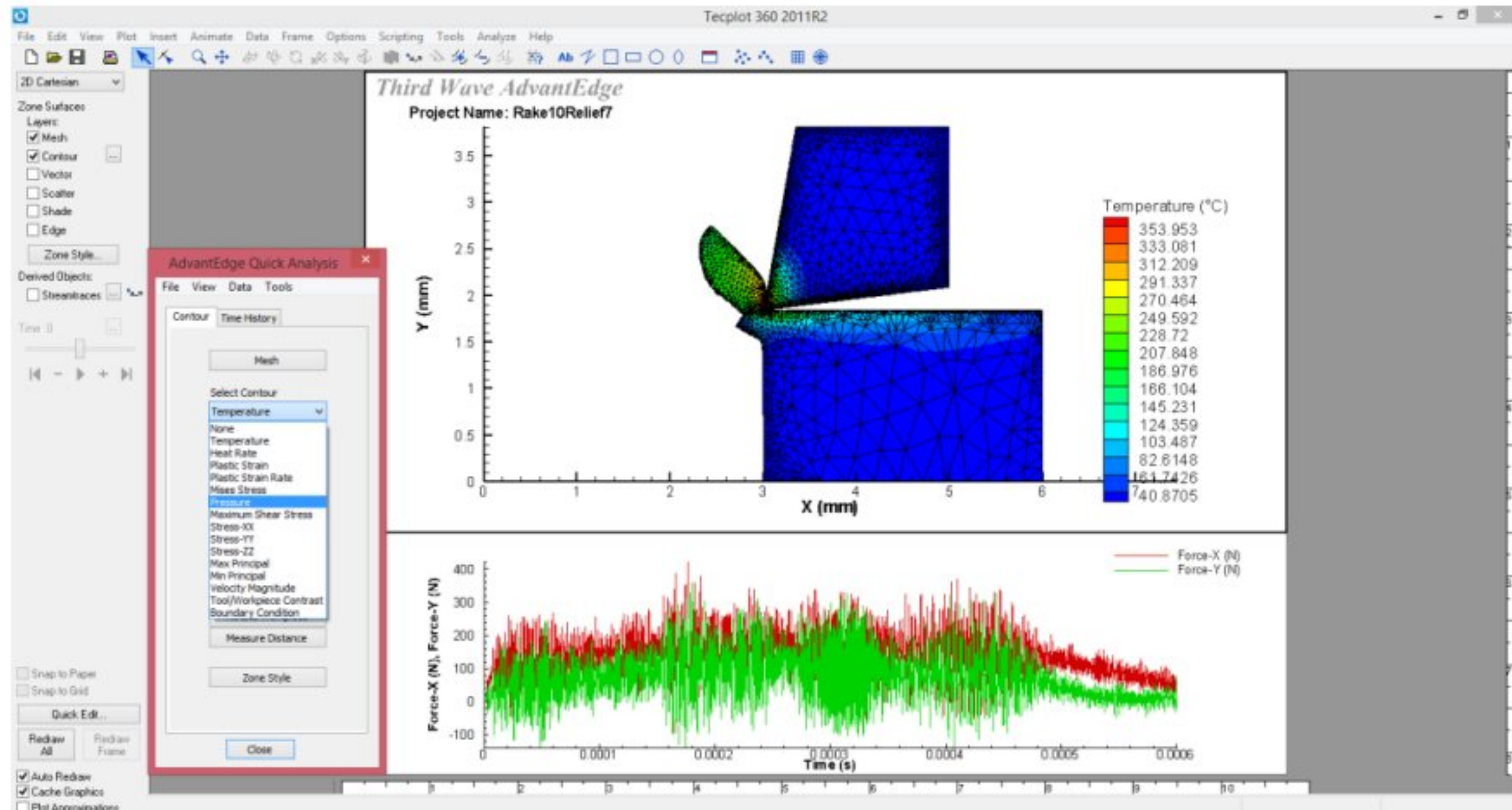


Figure 15 Selecting contour

Like as fig. 14, fig. 16 shows the distribution of pressure throughout the cut.

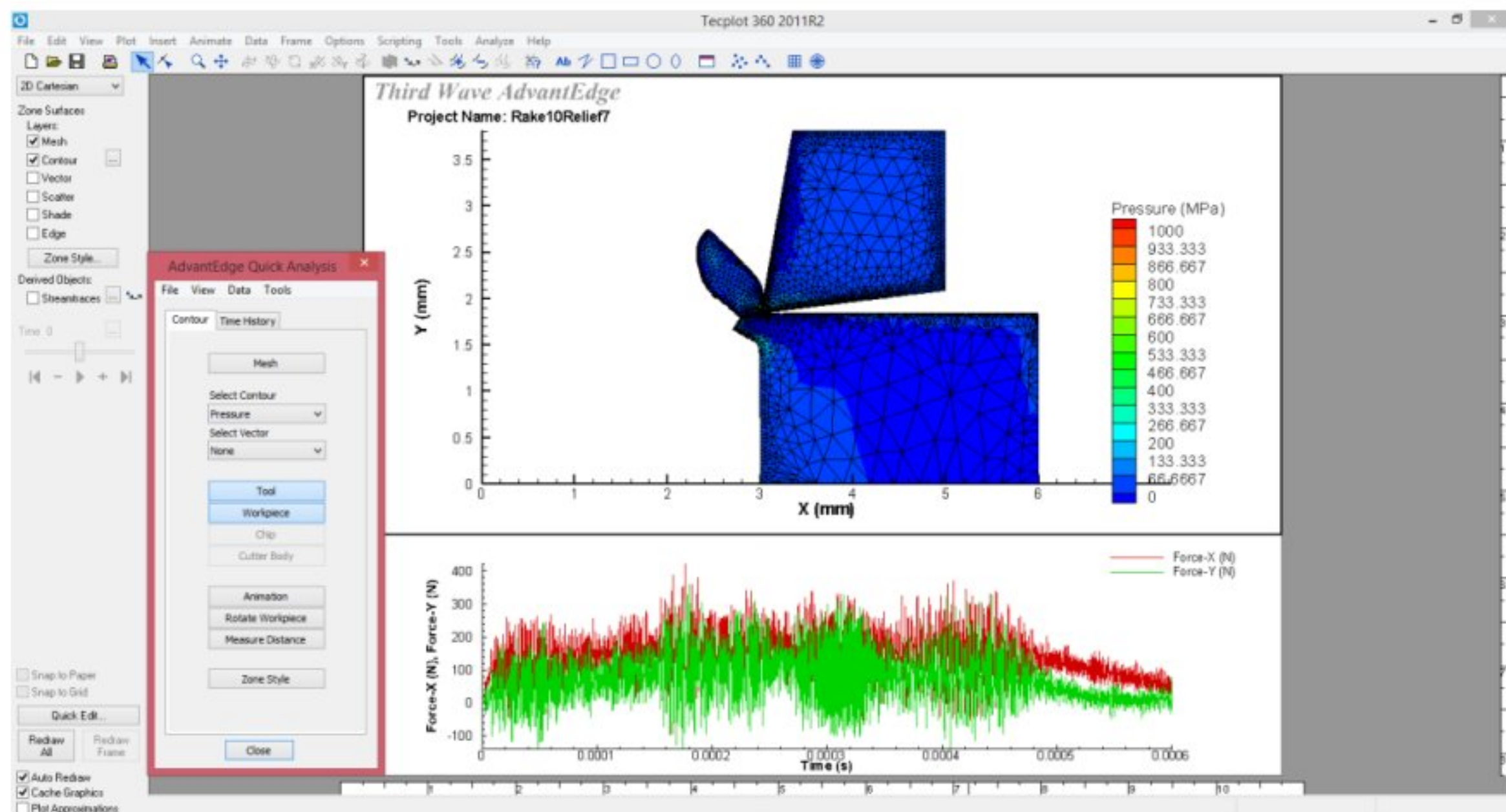


Figure 16 Distribution of pressure

Maximum shear stress was selected as contour from AdvantEdge quick analysis tab as shown in fig. 17.

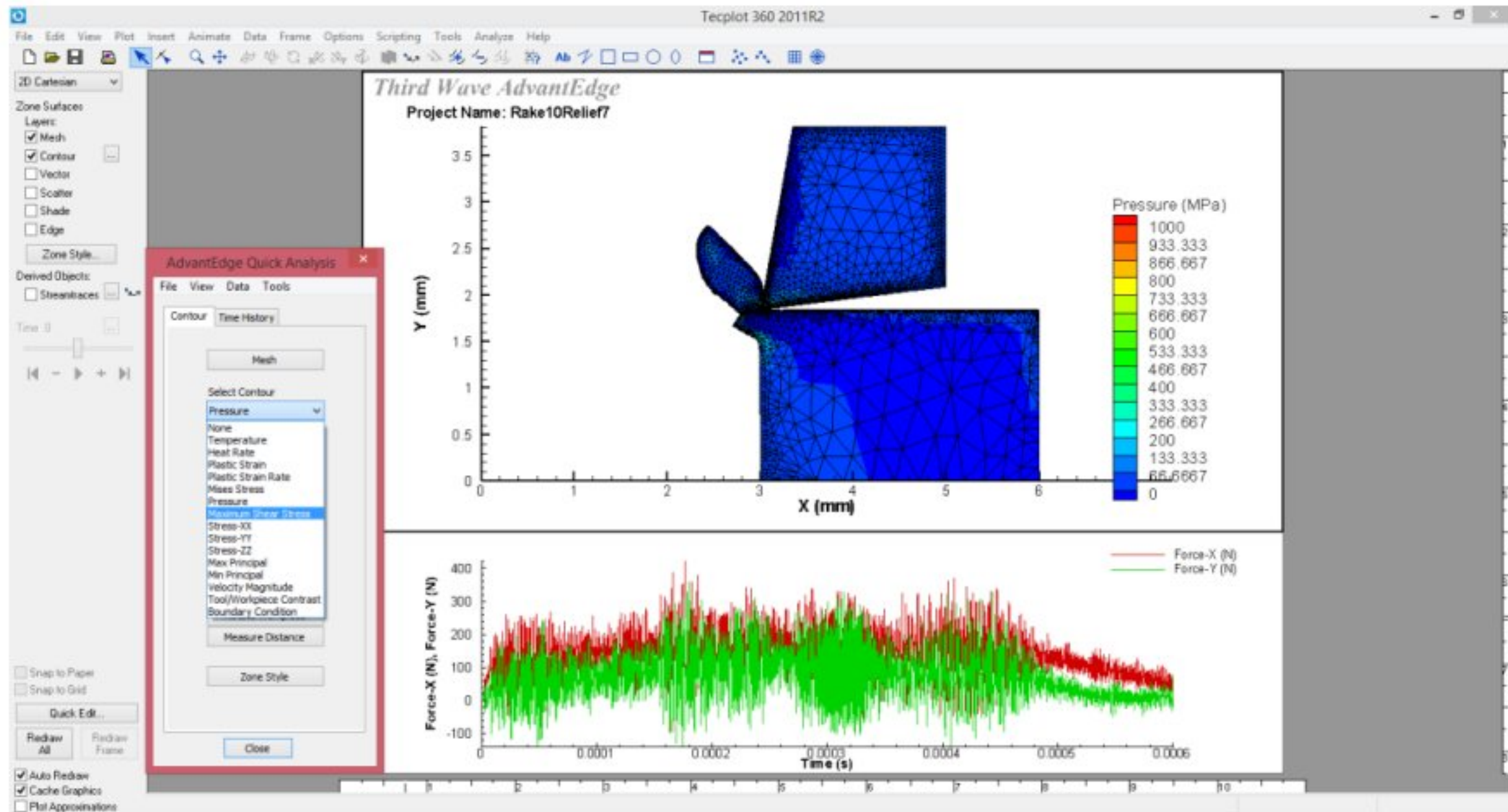


Figure 17 Selecting maximum shear stress

Fig. 18 shows the distribution of maximum shear stress.

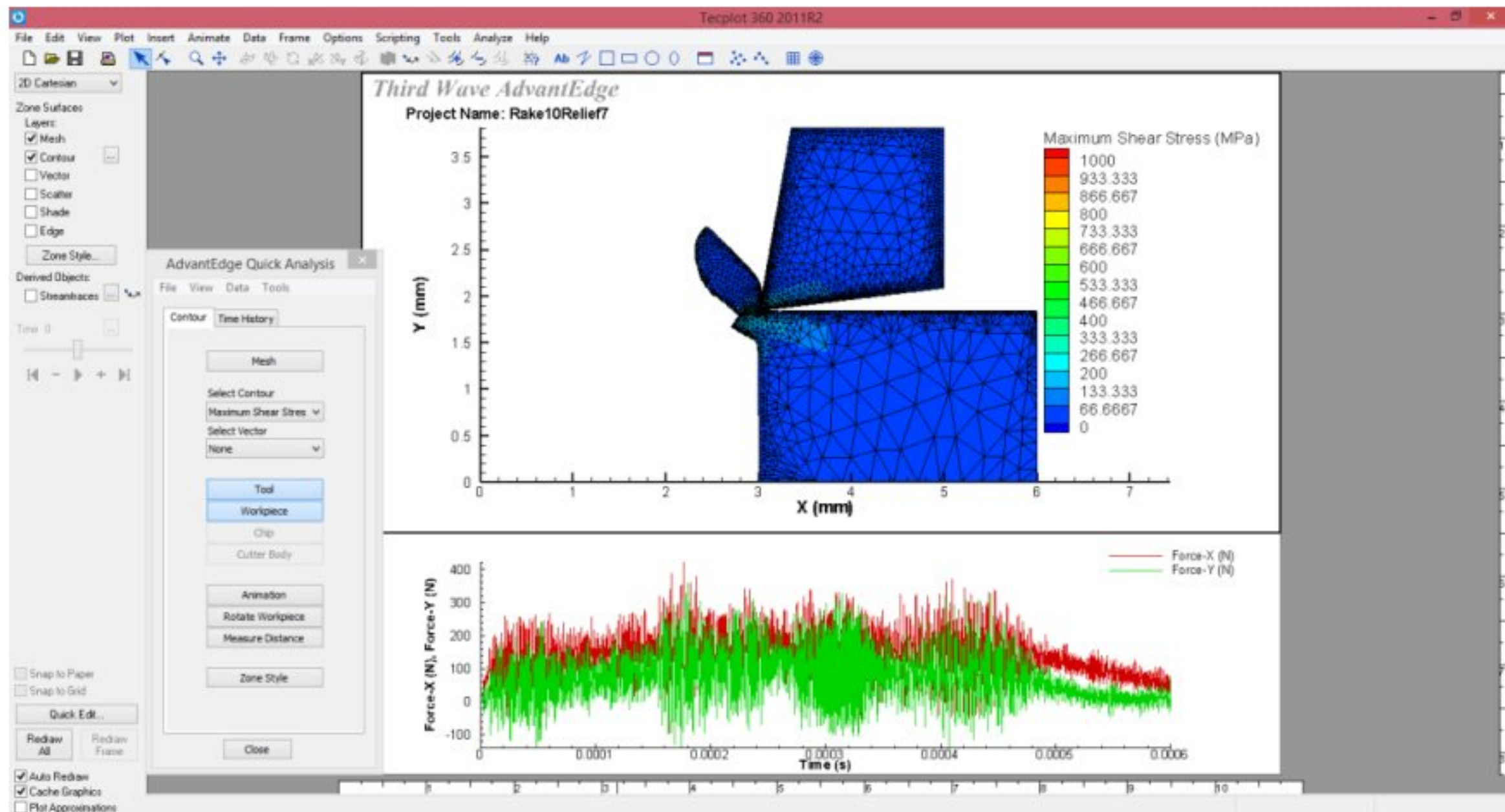


Figure 18 Distribution of maximum shear stress

In AdvantEdge quick analysis bar, there is an option named measure distance where by selecting two points the results can be seen. From fig. 19, it is clearly visible that the chip thickness can be measured.

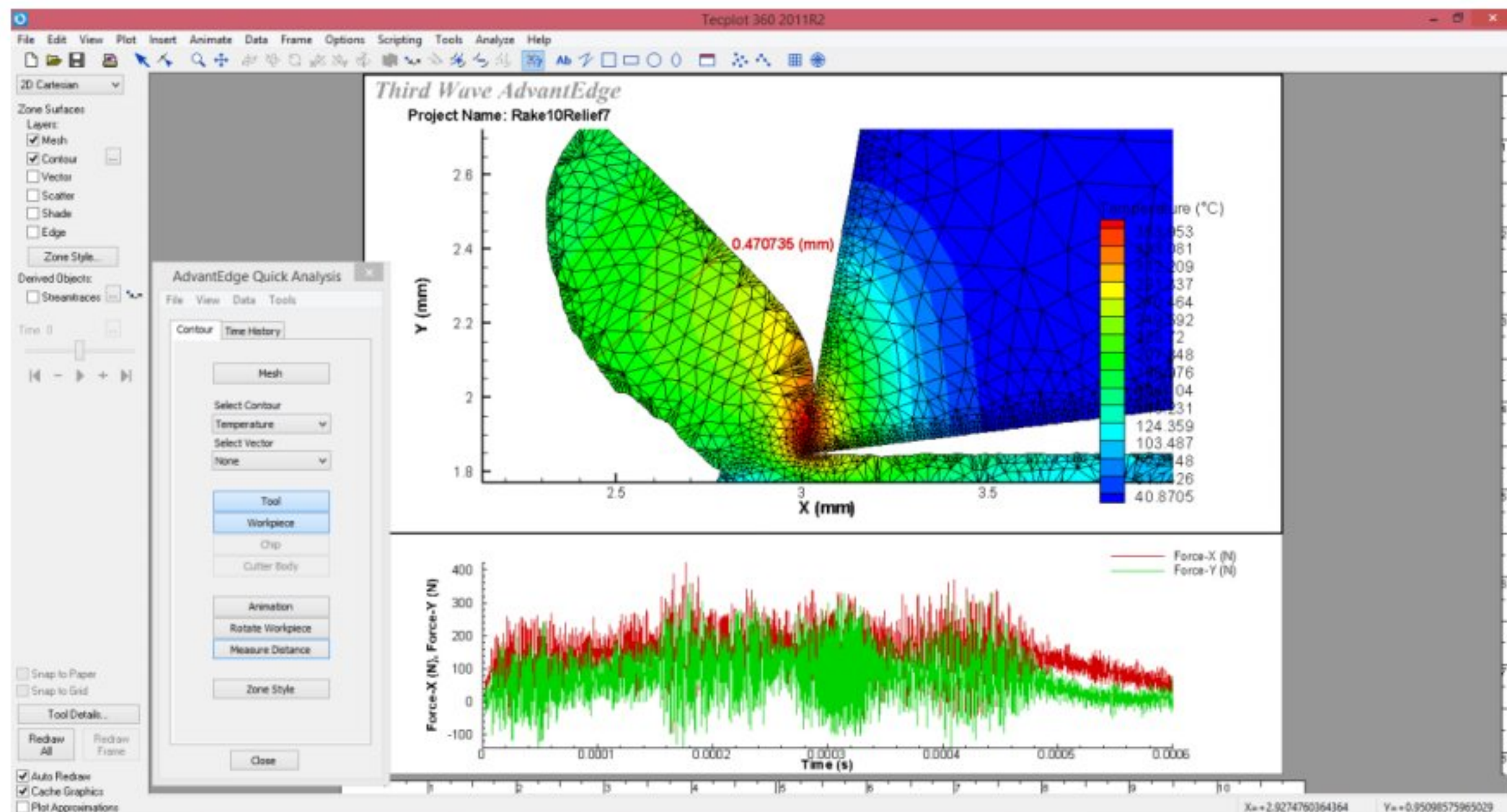


Figure 19 Measuring Distance

CHAPTER 4

RESULTS AND DISCUSSION

3.1 Effects of rake angle

Here, we have taken the relief angle and cutting edge radius as constant and changed the values of rake angle for five times like 3° , 6° , 9° , 12° and 15° where for different angles the heat rate, temperature, pressure, maximum shear stress, von mises stress, plastic strain and strain rate varies. Some of the changes are shown in graphs and a brief discussion is given below.

3.1.1 Cutting forces and feed forces

In Fig. 20, the evolution of the cutting forces and feed forces along with the variance in rake angle for cemented carbide-General is showed. The simulation was carried out in 2D. After observing, it can be said that increasing the rake angle decreases the cutting force and feed force as well. For example, at a cutting speed of 150 m/min, the cutting force for the cemented carbide-General is 648 N and the feed force is 310 N when rake angle is taken 3° and others two parameters keep constant. For rake angle of 6° , 9° , 12° and 15° , the cutting forces are 620 N, 580 N, 554 N and 540 N and feed forces are 260 N, 227 N, 182 N and 161 N respectively.

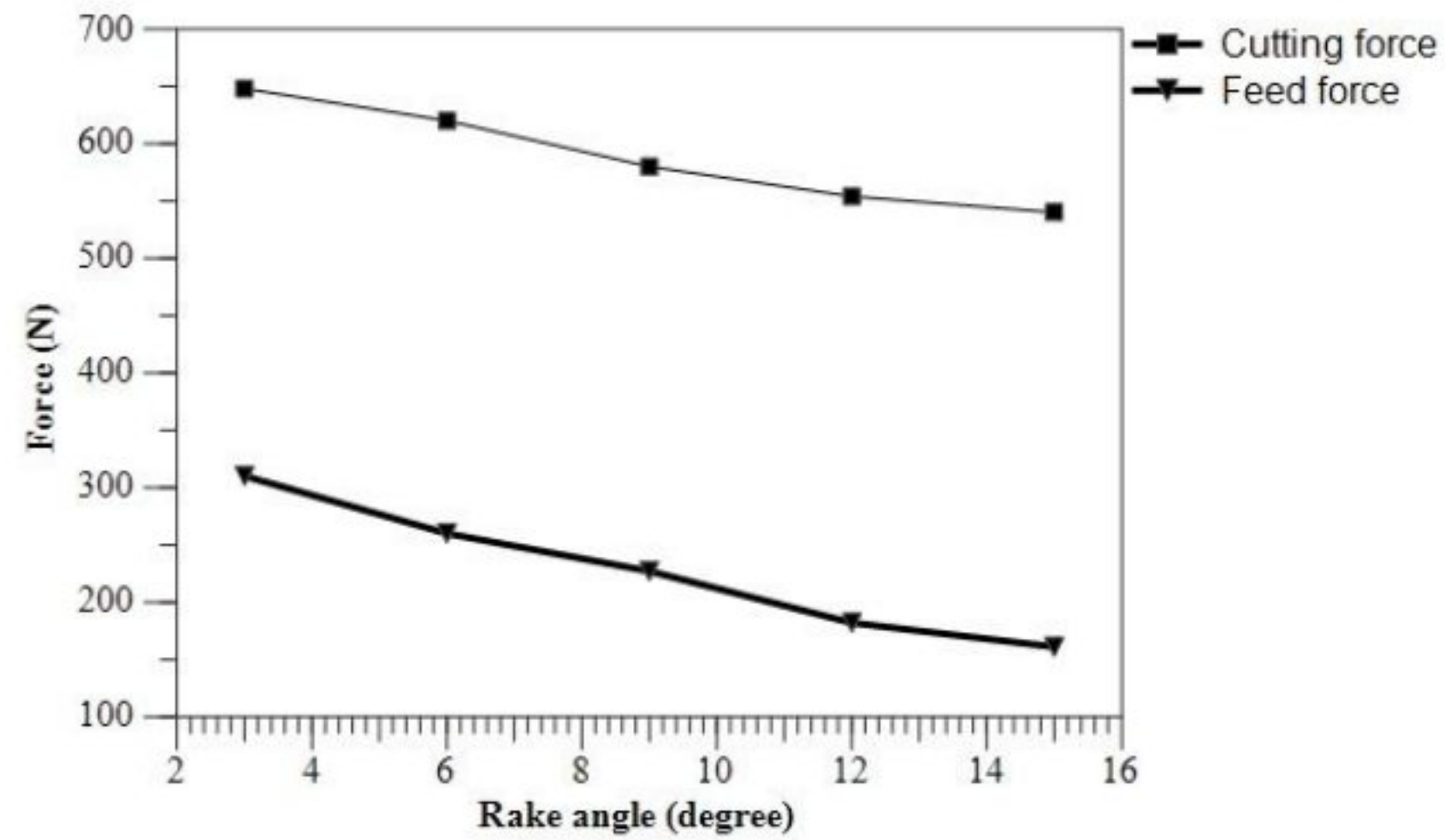


Figure 20 Distribution of cutting and feed forces with the variation of rake angle for Cemented carbide-General tool

3.1.2 Temperature and pressure

In Fig. 21, the evolution of the temperature with the varying rake angle for cemented carbide is presented. It can be seen that increasing the value of rake angle gives us decreasing of temperature. For example, at a cutting speed of 150 m/min, with the increment of rake angle by 3°, temperature decreases. Temperature decreases quite significantly after 12° where the value of the temperature is 428.915°C. This pattern is repeated throughout the progression of the rake angle. The temperature continued to low until the end of the length of cut and at 15°, the temperature is 419.367°C.

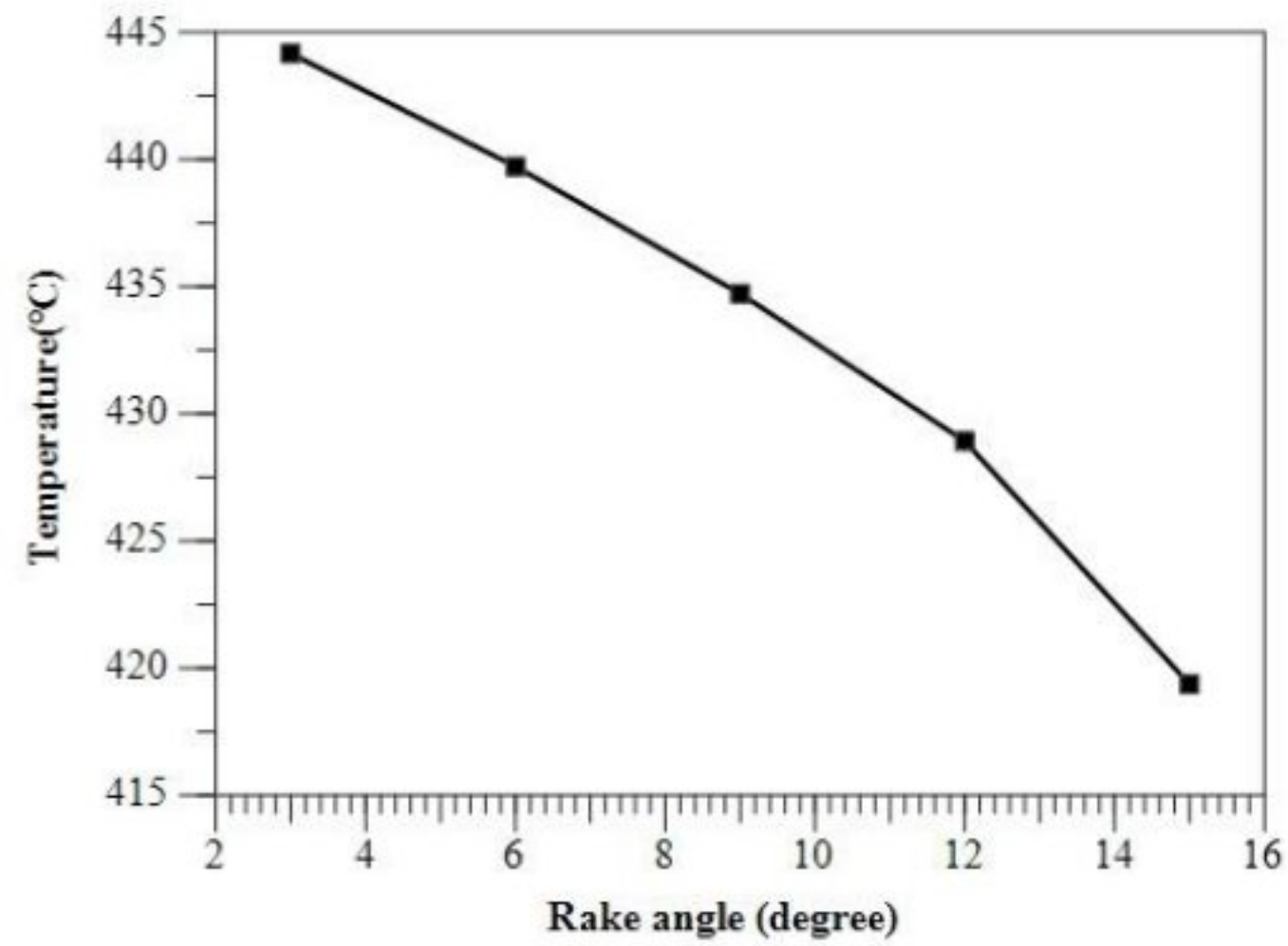


Figure 21 Distribution of temperature with the variation of rake angle for cemented carbide-General tool

In Fig. 22, a more detailed overview of the distribution of temperature in the tool, workpiece, chip and burr is showed. The temperature of the cemented carbide-General is 419.367°C , with a cutting speed of 150 m/min at rake angle of 15° . It is important to mention that the chip works well as a heat conductor, enabling the workpiece and the corner of the tool to have lower temperatures. With the depth of the cut, the maximum temperature increased. The chip is continuous and the main method of heat removal from the primary shear zone (this zone is the contact zone between the workpiece and the tool).

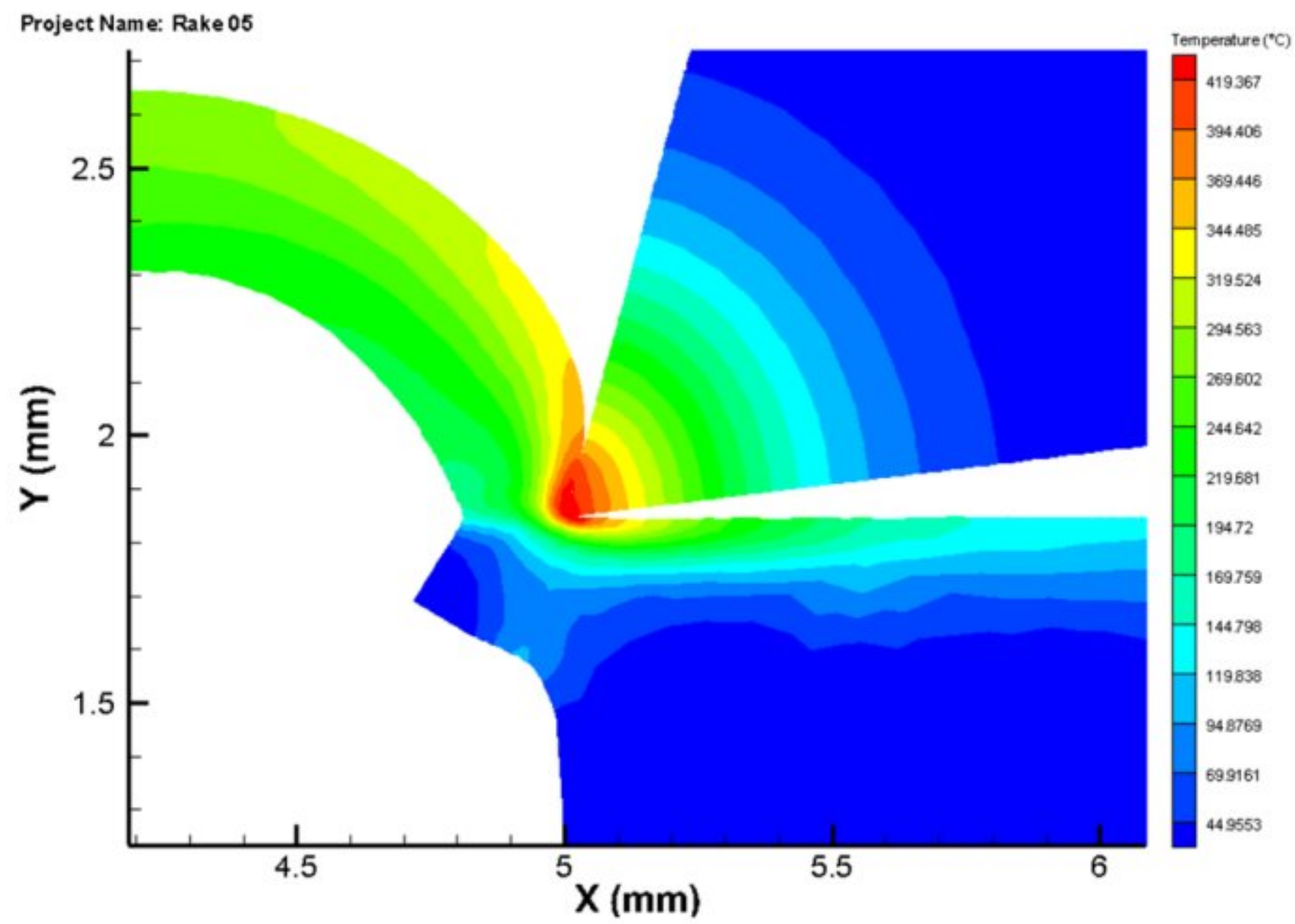


Figure 22 Distribution of temperature in the workpiece, tool(cemented carbide-General) and chip at the 150 m/min simulation when rake angle is 15° (image at 5 mm length of cut)

Taking the relief angle and cutting edge radius as constant, we have changed the rake angle for five times. So, we have got five different values of pressure. For rake angle of 3°, the value is 772.333 MPa. Pressure increases quite significantly after rake angle of 3°. At rake angle of 6°, the value is 877.667 MPa. The values are 918.684 MPa, 979.131 MPa and 993.32 MPa for rake angles of 9°, 12° and 15° respectively. Keeping other two parameters constant increasing the value of rake angles increases the pressure as well. In fig. 23, the change is shown.

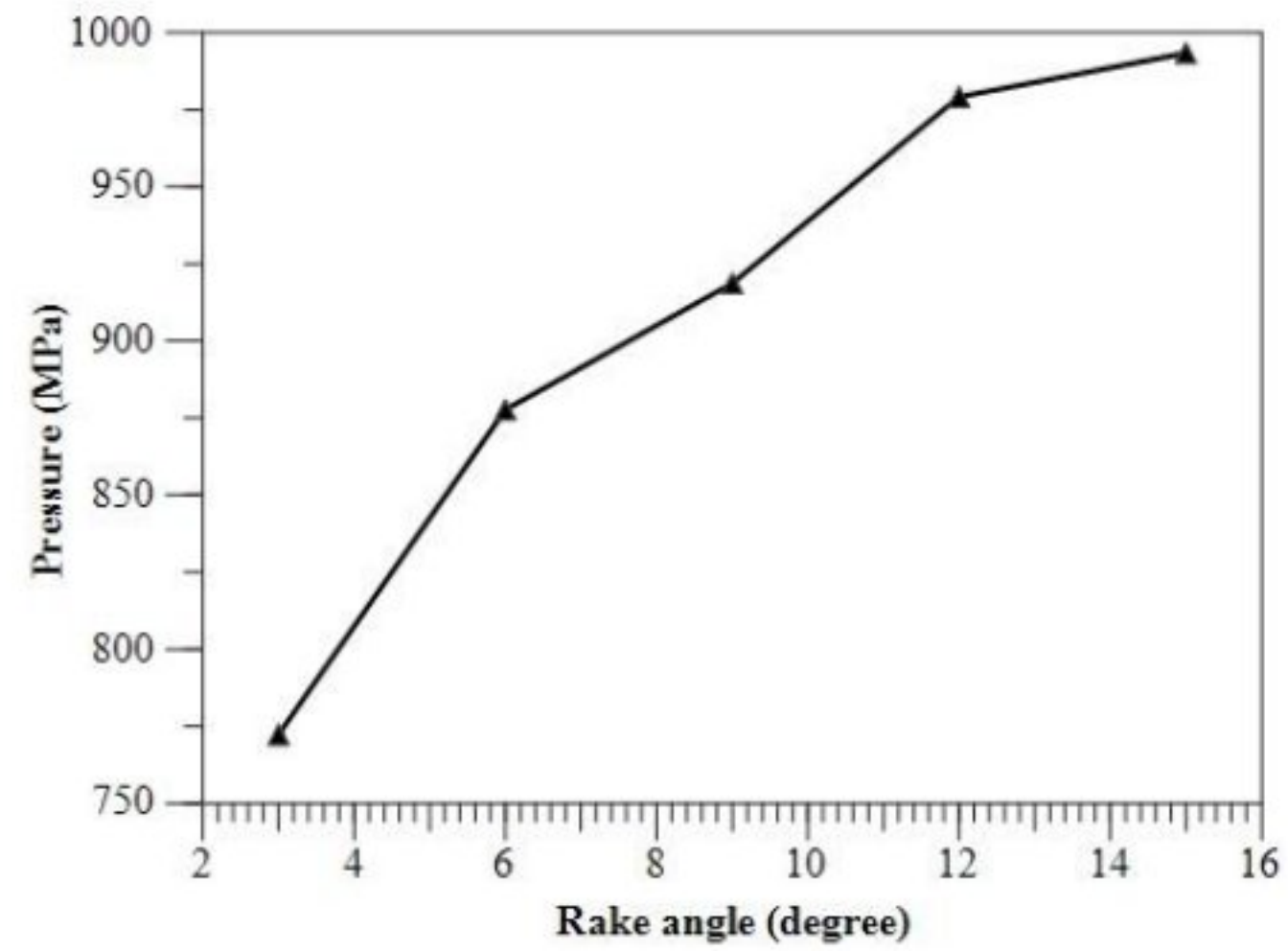


Figure 23 Distribution of pressure with the variation of rake angle for cemented carbide-General tool

In Fig. 24, a detailed overview of the distribution of pressure in the tool, workpiece, chip and burr is presented. The zone affected by the pressure is 877.667 MPa with a cutting speed of 150m/min indicating a high compression zone due to the force generated by the working tool.

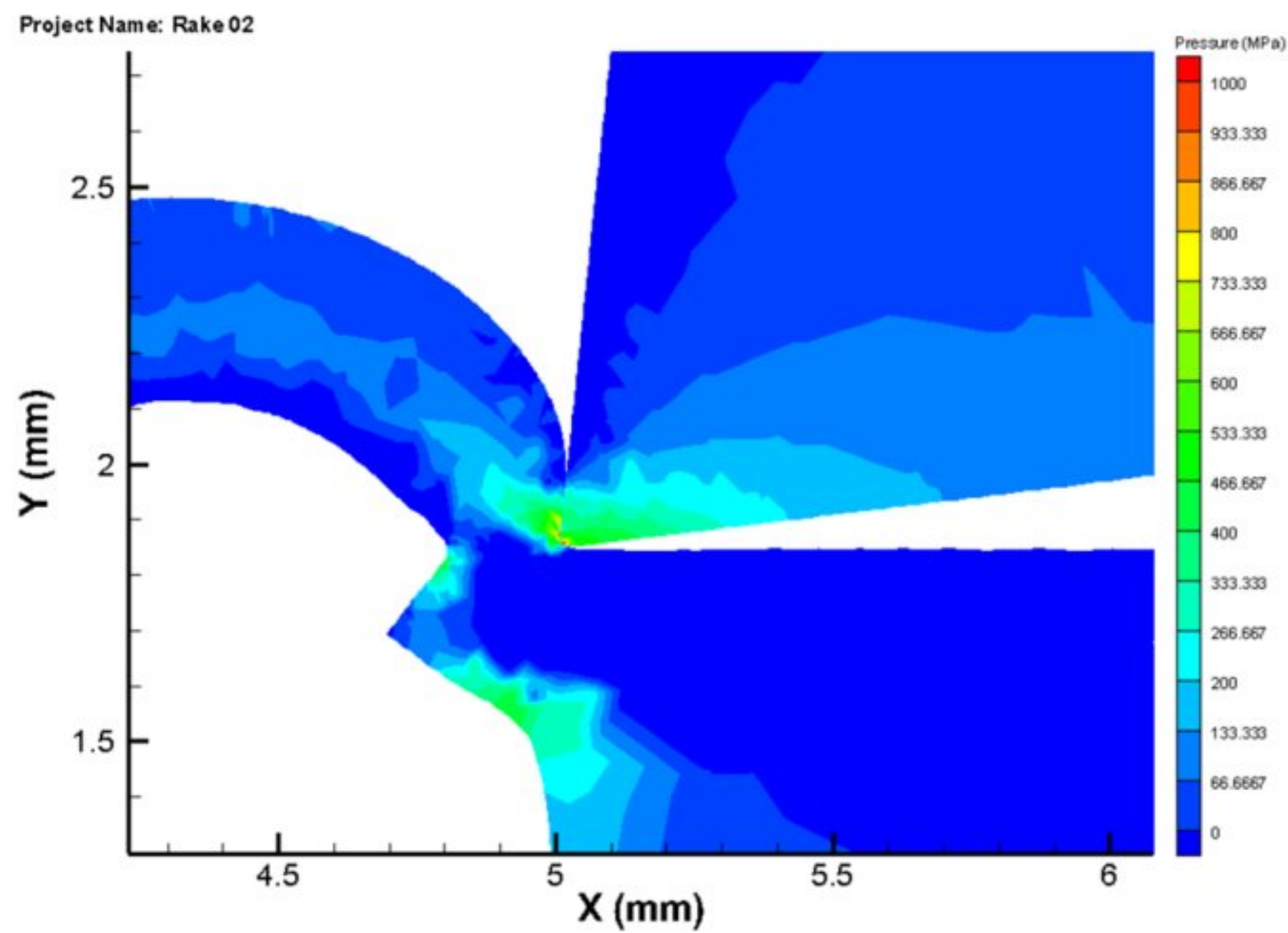


Figure 24 Distribution of pressure in the workpiece, tool(cemented carbide-General) and chip at the 150 m/min simulation when rake angle is 6° (image at 5 mm length of cut)

3.1.3 Maximum shear stress and von mises stress

In Fig. 25, the change of maximum shear stress along with the variation of rake angle is shown. For the rake angle of 3°, the maximum shear stress is 551.333 MPa. Maximum shear stress increases quite significantly after rake angle of 3°. From rake angle of 6° to rake angle of 9°, the changes are 713.587 MPa to 718.667 MPa which is quite less. After 9° to 12°, the change is massive. At 15°, we have got the maximum shear stress 868.298 MPa. So, increasing the rake angle gives higher shear stress.

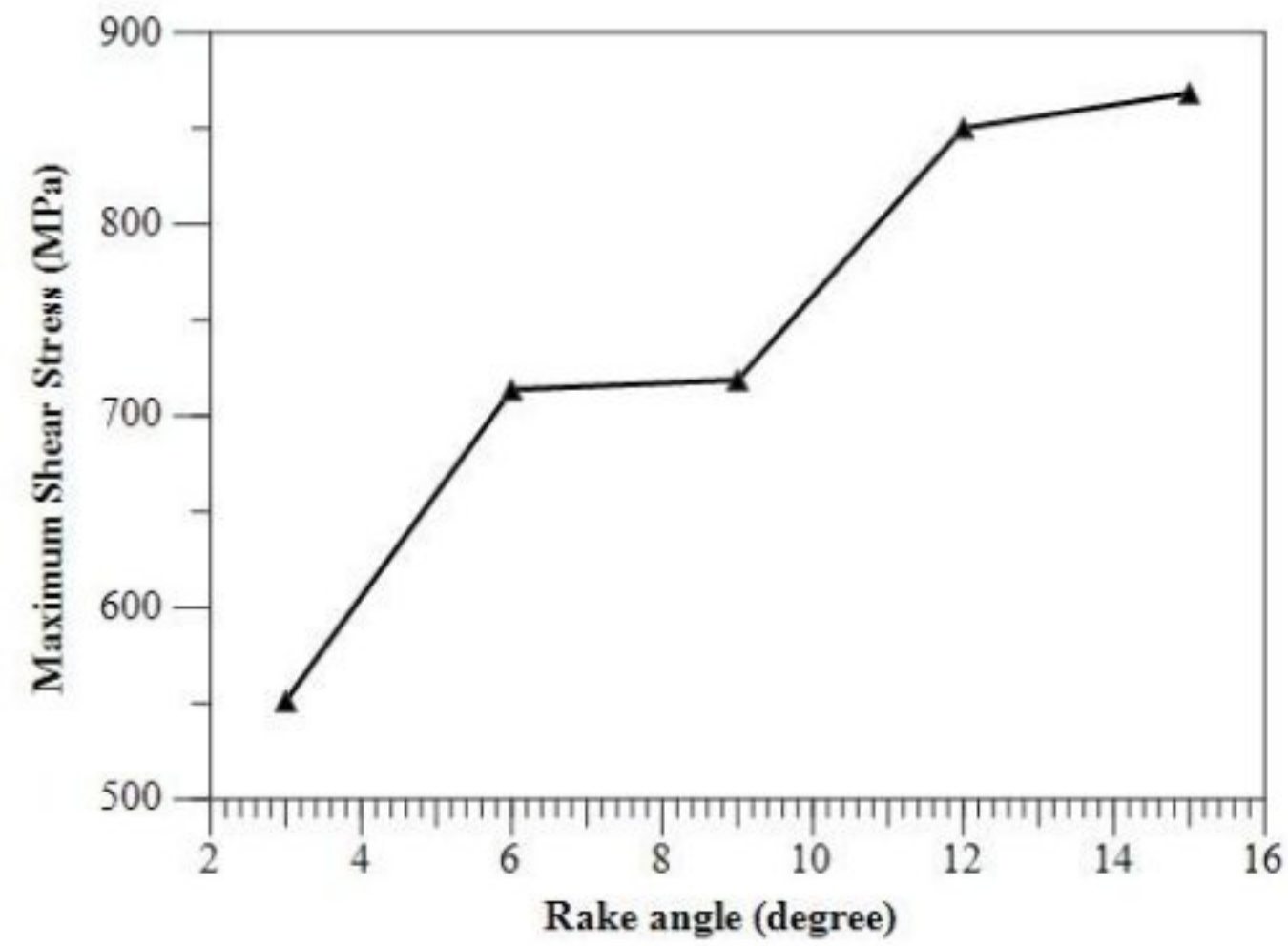


Figure 25 Distribution of maximum shear stress with the variation of rake angle for cemented carbide-General tool

In Fig. 26, the distribution of maximum shear pressure in the workpiece, tool, chip, and burr is presented. The stress reached 868.298 MPa and in the cemented carbide-General tool for a cutting speed of 150 m/min. Notice that when machined with the cemented carbide-General tool, the affected zone (in the workpiece) is much bigger at a rake angle of 15° than 3°. In general, when machining with cemented carbide-General tool, increasing the value of rake angle increases the maximum shear stress in the tool, chip, workpiece, and burr.

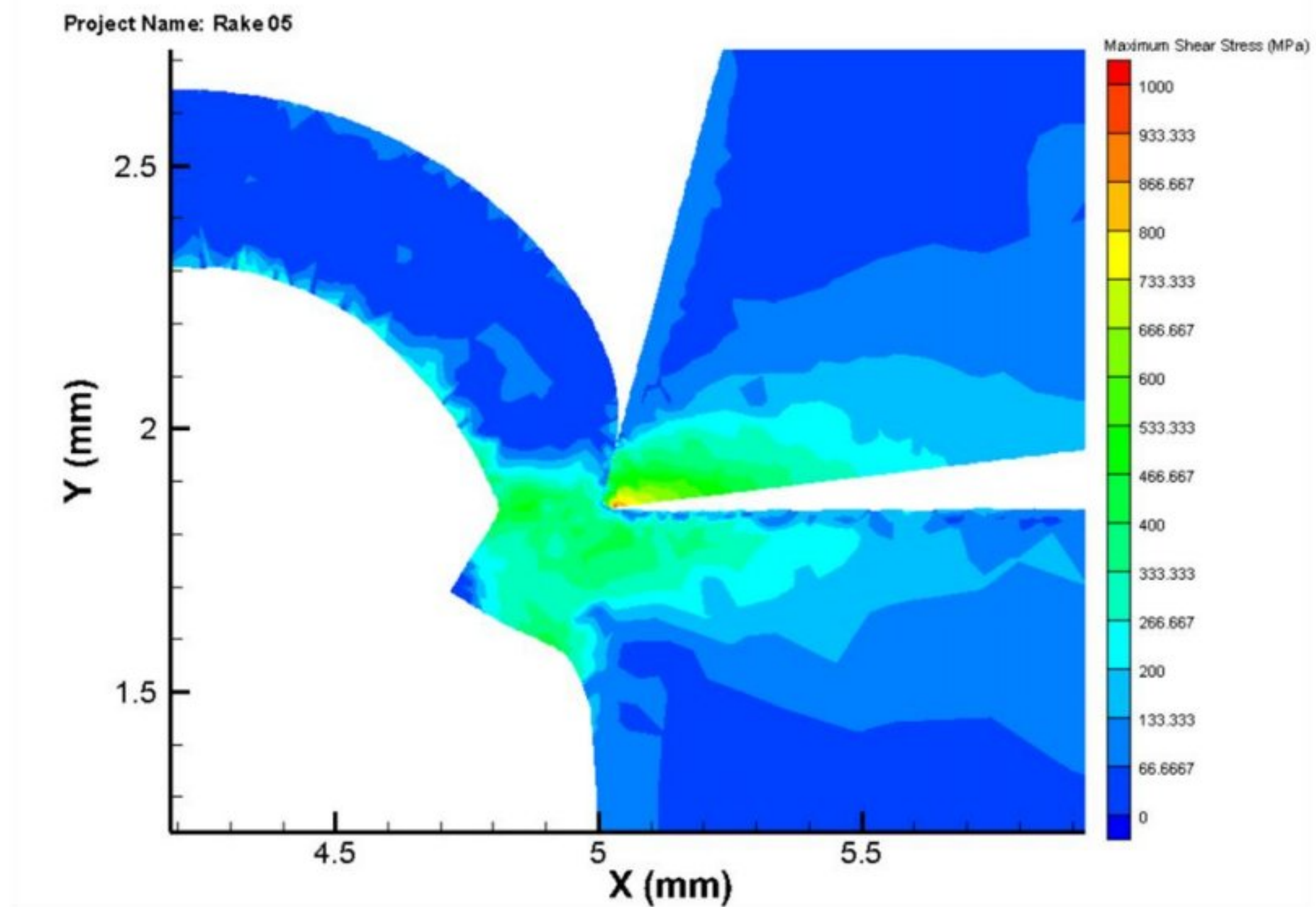


Figure 26 Distribution of maximum shear stress in the workpiece, tool(cemented carbide-General) and chip at the 150 m/min simulation when rake angle is 15° (image at 5 mm length of cut)

In Fig. 27, the simulation layouts for the distribution of von Mises stress is showed in detail, high speed machining at a cutting speed of 150 m/min for cemented carbide-General tool inserts. For cemented carbide-General tool, the value of rake angle of 3° is 962.333 MPa. Increasing the value of rake angle increases the value of the von mises stress. There has no massive change in von mises stress. The changes occur gradually. The significance of von Mises stress on the point of the tool and in the region of chip formation is noticeable. For von Mises stresses, the tool tip is strongly influenced. In the primary shear zone, the material being extracted is often subject to high values of Mises stress.

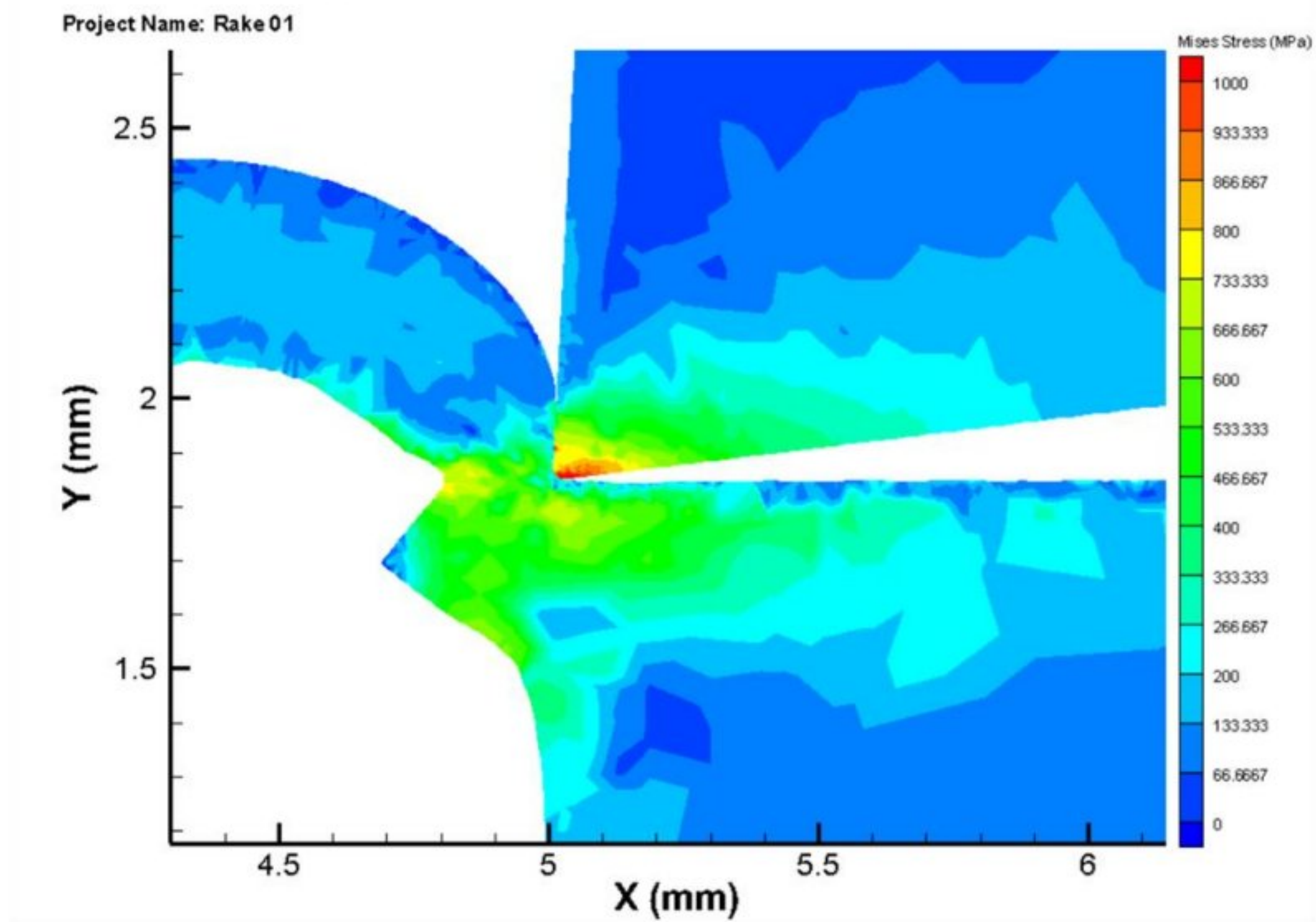


Figure 27 Distribution of von mises stress in the workpiece, tool(cemented carbide-General) and chip at the 150 m/min simulation when rake angle is 3° (image at 5 mm length of cut)

3.1.4 Heat rate

In Fig. 28, a more detailed overview of the distribution of heat rate in the tool, workpiece, chip and burr is showed. The heat rate of the cemented carbide-General is 16372.497 W/mm^3 , with a cutting speed of 150 m/min at rake angle of 12° . It is important to mention that the chip works well as a heat conductor. With the depth of the cut, the maximum heat rate increased. At rake angle of 3° , the value of the heat rate is 160566.7 W/mm^3 . Heat rate increases quite significantly after 6° where the value of the heat rate is 16155.6 W/mm^3 . This pattern is repeated throughout the progression of the rake angle. The heat rate is continued to high until the end of the length of cut and at 15° , the heat rate is 16484.01 W/mm^3 . It can be said that increasing the value of rake angle gives us higher amount of heat rate.

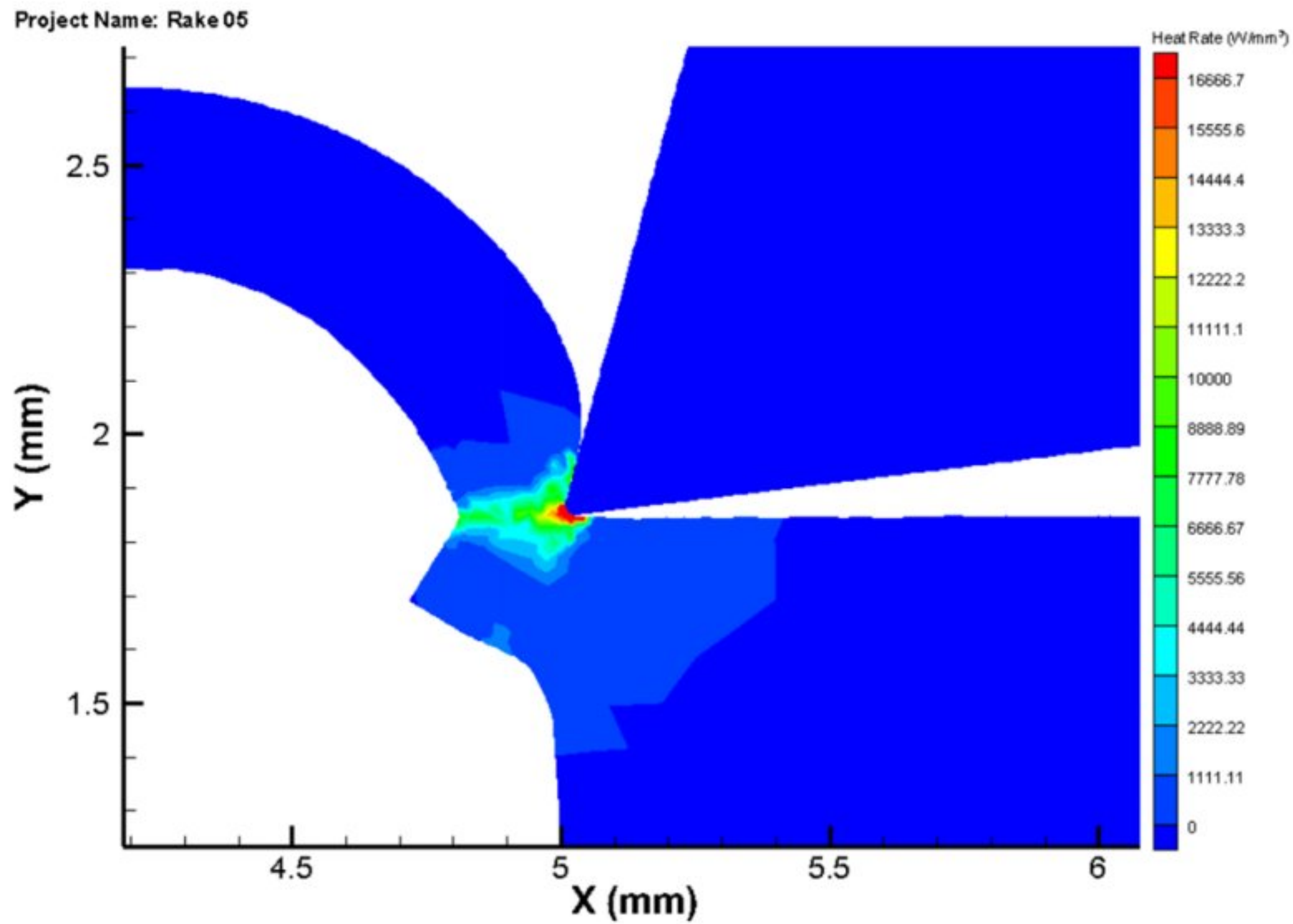


Figure 28 Distribution of heat rate in the workpiece, tool(cemented carbide-General) and chip at the 150 m/min simulation when rake angle is 15° (image at 5 mm length of cut)

3.1.5 Plastic strain and plastic strain rate

In Fig. 29, the plastic strain distribution in the workpiece, tool, chip, and burr is showed in detail where plastic strain of the cemented carbide-General is 3.89223, with a cutting speed of 150 m/min at rake angle of 9°. We have taken the variance of rake angle as 3°, 6°, 9°, 12° and 15°. The value of the plastic strain is 3.86203 when the rake angle is 3°. The value increases at 3.87893 when the rake angle is 6°. The value of plastic strain increases quite significantly after rake angle of 9° and the value is 3.89223. At rake angle of 12°, the value increases at 3.90563 and finally the value of plastic strain is 3.93193 at 15° and other two parameters are constant. It is clarified that increasing the rake angle, increases the plastic strain.

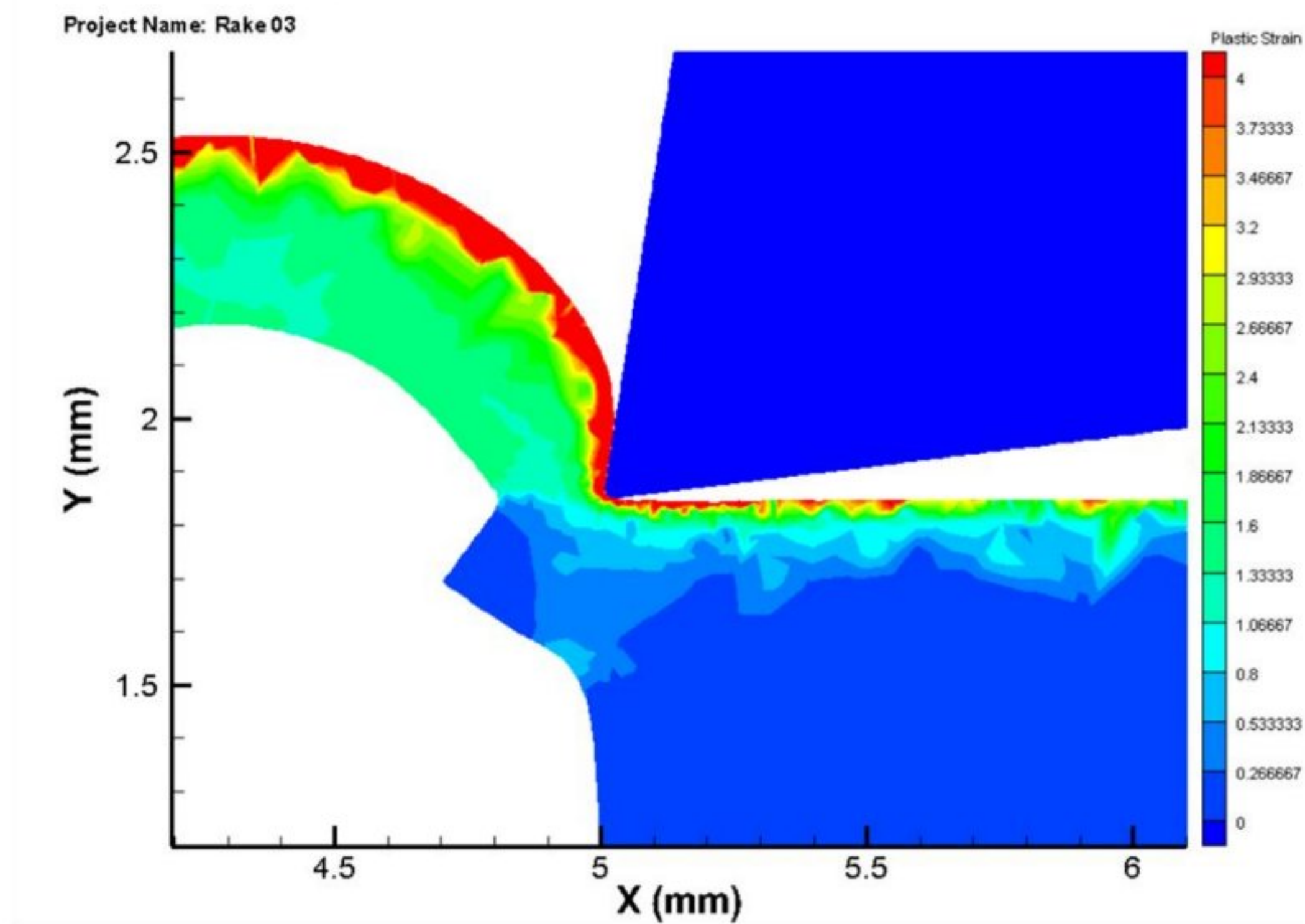


Figure 29 Distribution of plastic strain in the workpiece, tool(cemented carbide-General) and chip at the 150 m/min simulation when rake angle is 9° (image at 5 mm length of cut)

Additionally the plastic strain rate distribution in the workpiece, tool, chip, and burr is showed in detail in Fig. 30 where plastic strain rate of the cemented carbide-General is 16035.6 s^{-1} when the cutting speed is 150 m/min at rake angle of 3°. The value increases at 16155.6 s^{-1} when the rake angle is 6°. The value of plastic strain rate increases quite significantly after rake angle of 9° and the value is 16265.6 s^{-1} . At rake angle of 12° and 15°, the value increases at 16360.6 s^{-1} and 15617.96 s^{-1} respectively and other two parameters are constant. It is clarified that increasing the rake angle,

increases the plastic strain rate.

Third Wave AdvantEdge

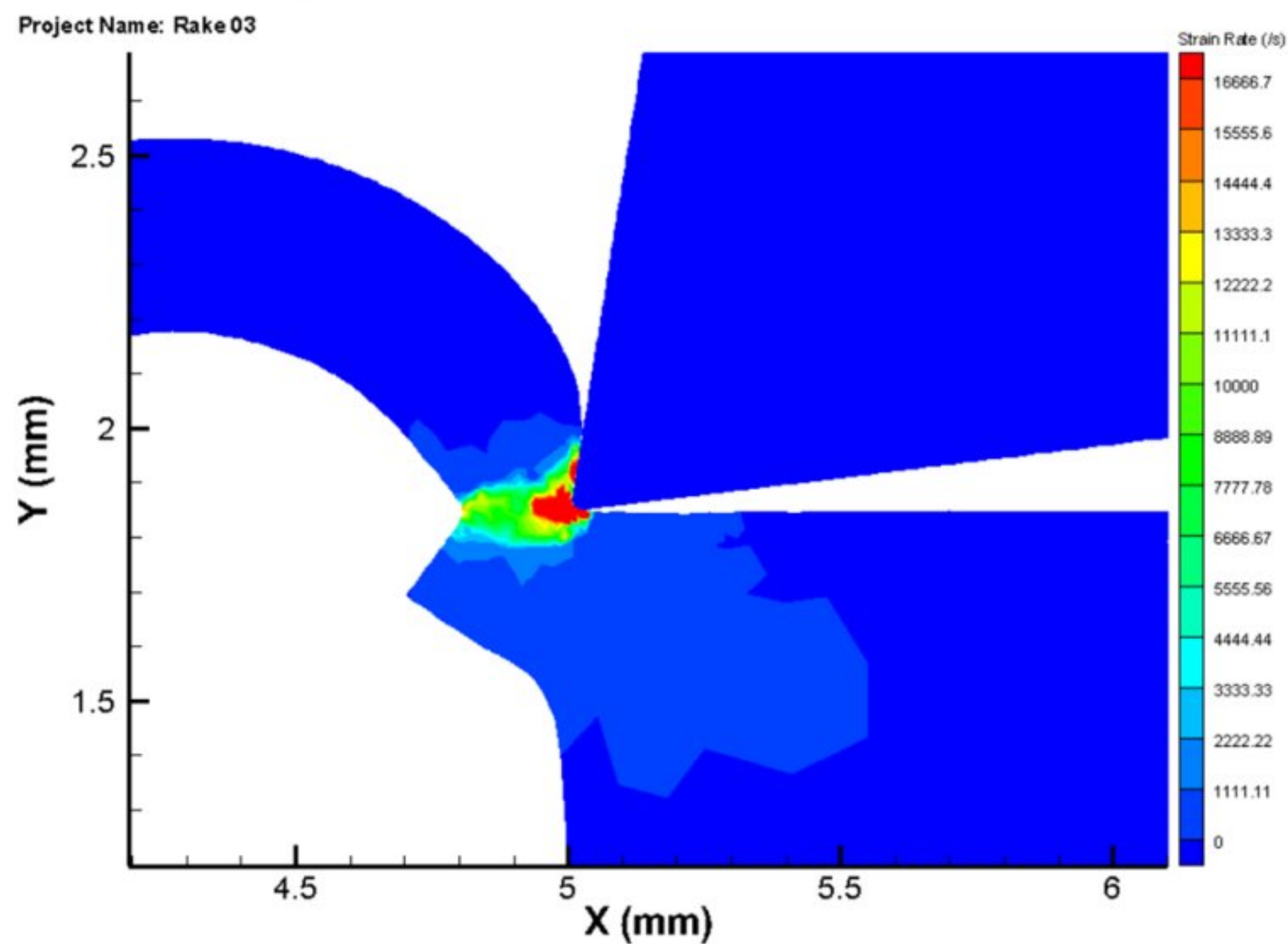


Figure 30 Distribution of plastic strain rate in the workpiece, tool(cemented carbide-General) and chip at the 150 m/min simulation when rake angle is 9° (image at 5 mm length of cut)

3.1.6 Cutting power and maximum cutting temperature

In Fig. 31, the evolution of the maximum cutting temperature and the cutting power over the cutting time is shown at the rake angle of 3° . In fig. 21, shows with the rise in the rake angle, the maximum cutting temperature (in the cutting tool) decreases. This can also be explained by the low thermal conductivity (tending to concentrate heat) of the stainless steel and the tool. And the chip is the key mechanism that extract heat from the shear zone. There has no change of power but for taking different rake angles give different cutting temperature. We have taken the rake angles as 3° , 6° , 9° , 12° , 15° and the maximum cutting temperature we have got are 1615°C , 1550°C , 1450°C ,

1375°C and 1320°C. Which means increasing the rake angle decreases the cutting temperature.

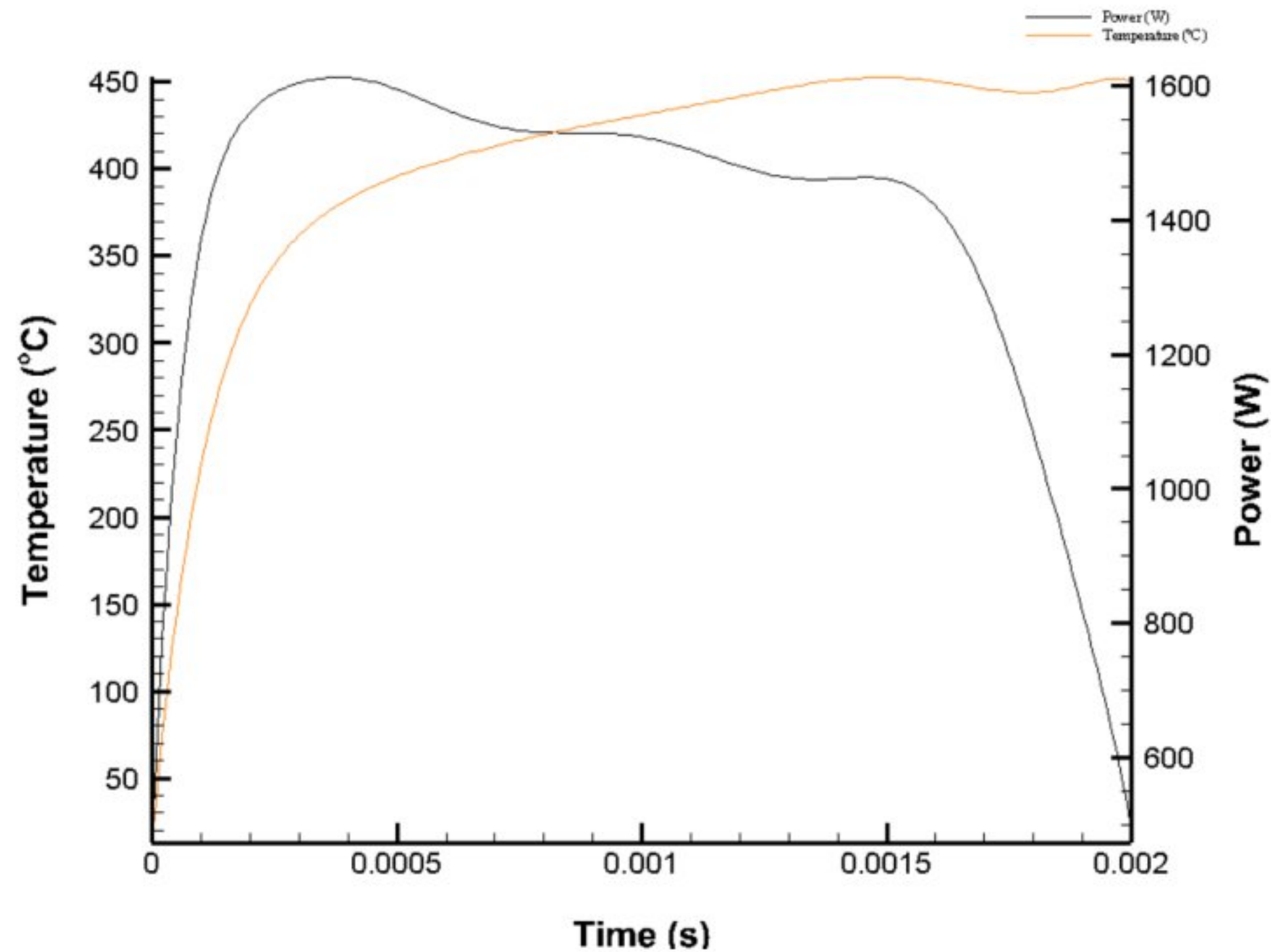


Figure 31 Cutting power and maximum cutting temperature along the time in the machining of the cemented carbide-General with a cutting speed of 150 m/min at the rake angle of 3° and a depth of cut of 2 mm

3.2 Effect of relief angle

Here, we have taken the rake angle and cutting edge radius as constant and changed the values of relief angle for five times like 7°, 10°, 13°, 16° and 19° where for different angles the heat rate, temperature, pressure, maximum shear stress, von mises stress, plastic strain and strain rate varies. Some of the changes are shown in graphs and a brief discussion is given below.

3.2.1 Cutting forces and feed forces

In Fig. 32, the evolution of the cutting forces and feed forces along with the variance in

relief angle for cemented carbide-General is showed. For example, at a cutting speed of 150 m/min, the cutting force for the cemented carbide-General is 648 N and the feed force is 310 N when relief angle is taken 7° and other two parameters are kept constant. For relief angle 10°, 13°, 16° and 19°, the cutting forces are 640 N, 632 N, 630 N and 623 N and feed forces are 307 N, 303 N, 294 N and 288 N respectively. After observing, it can be said that increasing the relief angle decreases the cutting force and feed force as well.

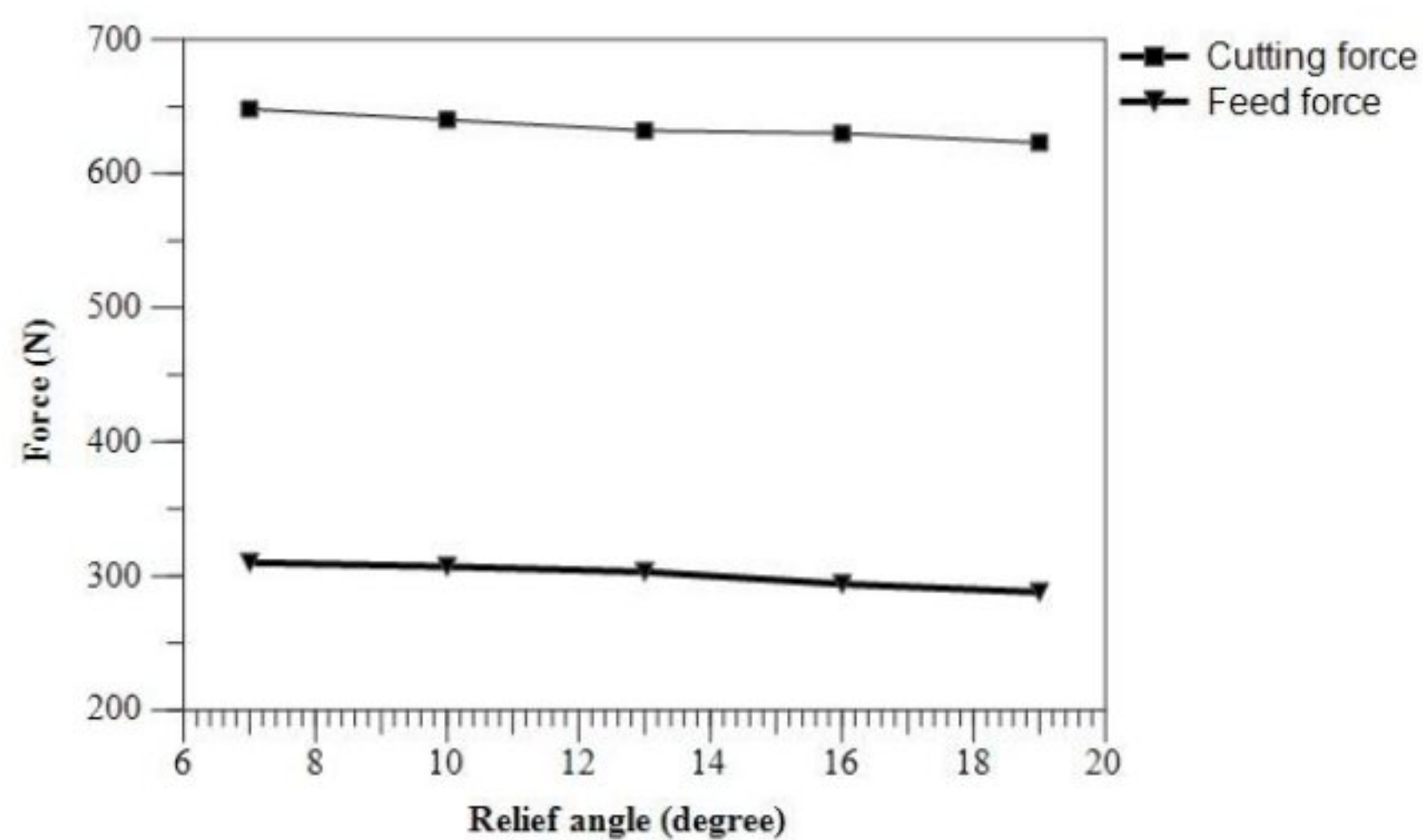


Figure 32 Distribution of cutting and feed forces with the variation of relief angle for Cemented carbide-General tool

3.2.2 Temperature and pressure

In Fig. 33, the evolution of the temperature with the varying relief angle for cemented carbide is presented. It can be seen that increasing the value of relief angle gives us decreasing of temperature. For example, at a cutting speed of 150 m/min, with the increment of relief angle by 3°, temperature decreases. Temperature decreases quite significantly after 16° where the value of the temperature is 439.892°C. This pattern is

repeated throughout the progression of the relief angle. The temperature continued to low until the end of the length of cut and at 19°, the temperature is 435.735°C.

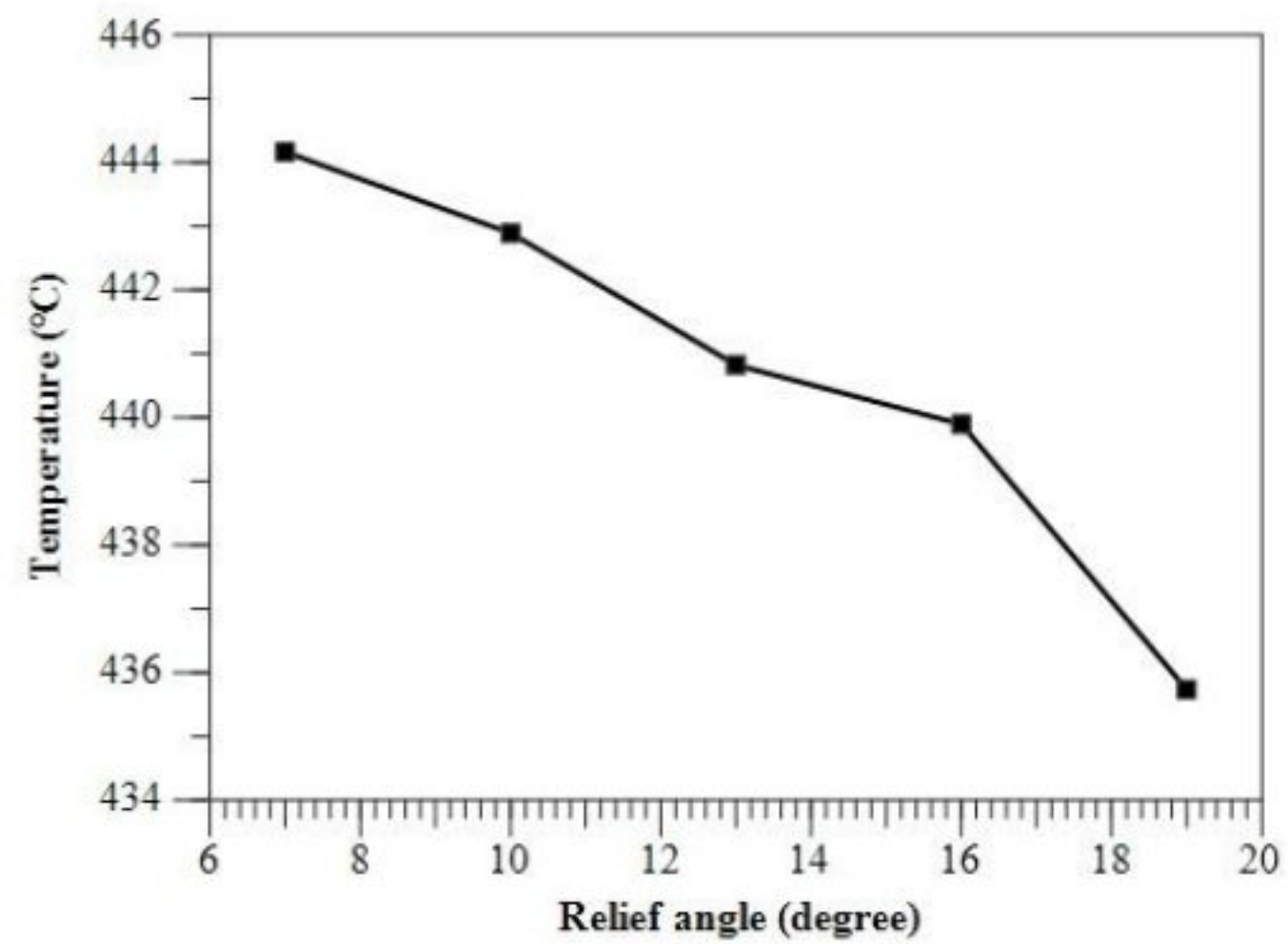


Figure 33 Distribution of temperature with the variation of relief angle for Cemented carbide-General tool

In Fig. 34, a more detailed overview of the distribution of temperature in the tool, workpiece, chip and burr is showed. The temperature of the cemented carbide-General is 435.735°C, with a cutting speed of 150 m/min at relief angle of 19°.

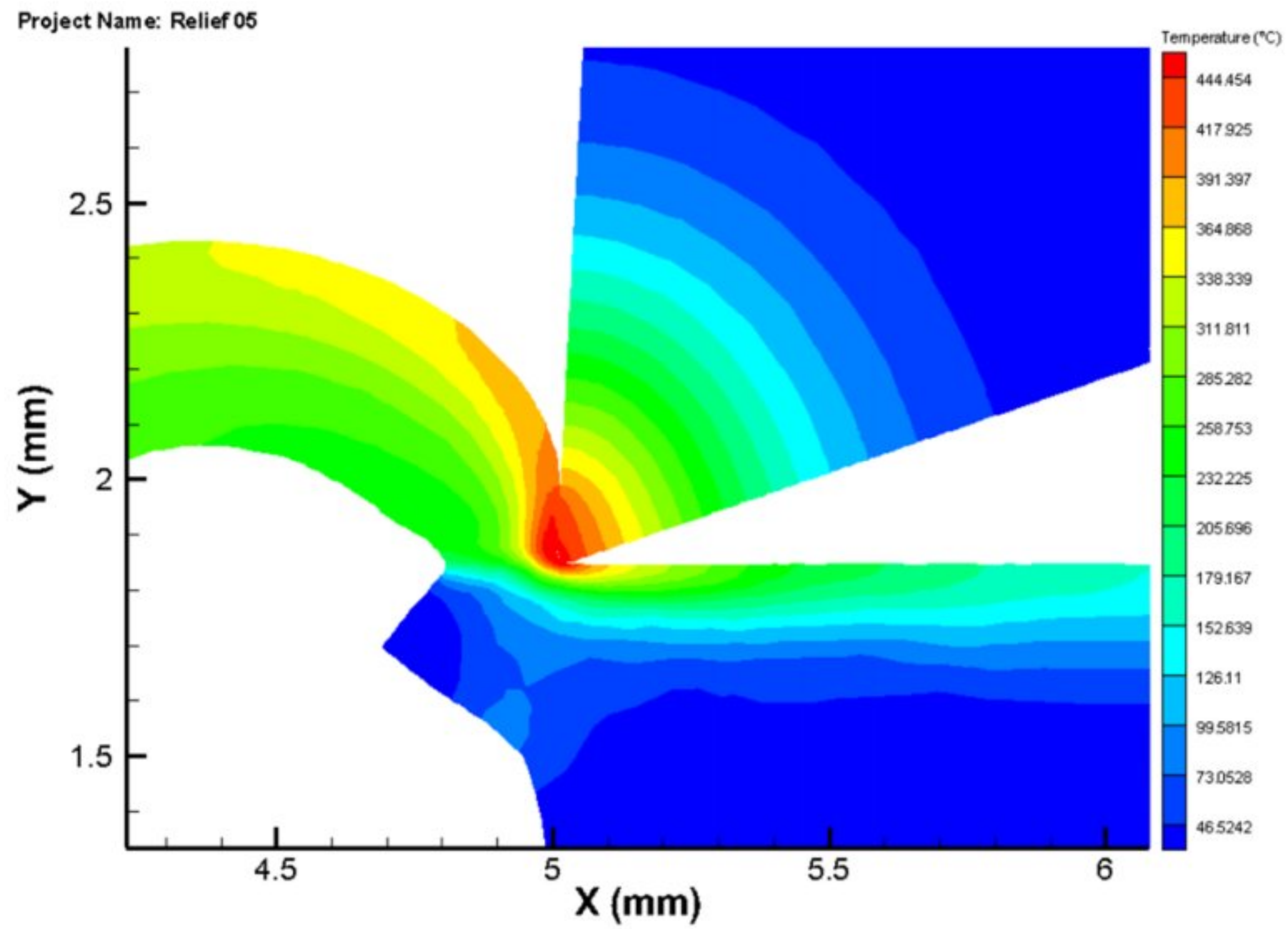


Figure 34 Distribution of temperature in the workpiece, tool(cemented carbide-General) and chip at the 150 m/min simulation when relief angle is 19° (image at 5 mm length of cut)

Taking the rake angle and cutting edge radius as constant, we have changed the relief angle for five times. So, we have got five different values of pressure. For relief angle of 7°, the value is 772.333 MPa. Pressure increases quite significantly after relief angle of 7°. At rake angle of 10°, the value is 884.564 MPa. The values are 905.654 MPa, 919.897 MPa and 932.875 MPa for relief angles of 13°, 16° and 19° respectively. Keeping other two parameters constant increasing the value of relief angles increases the pressure as well. In fig. 35, the change is shown.

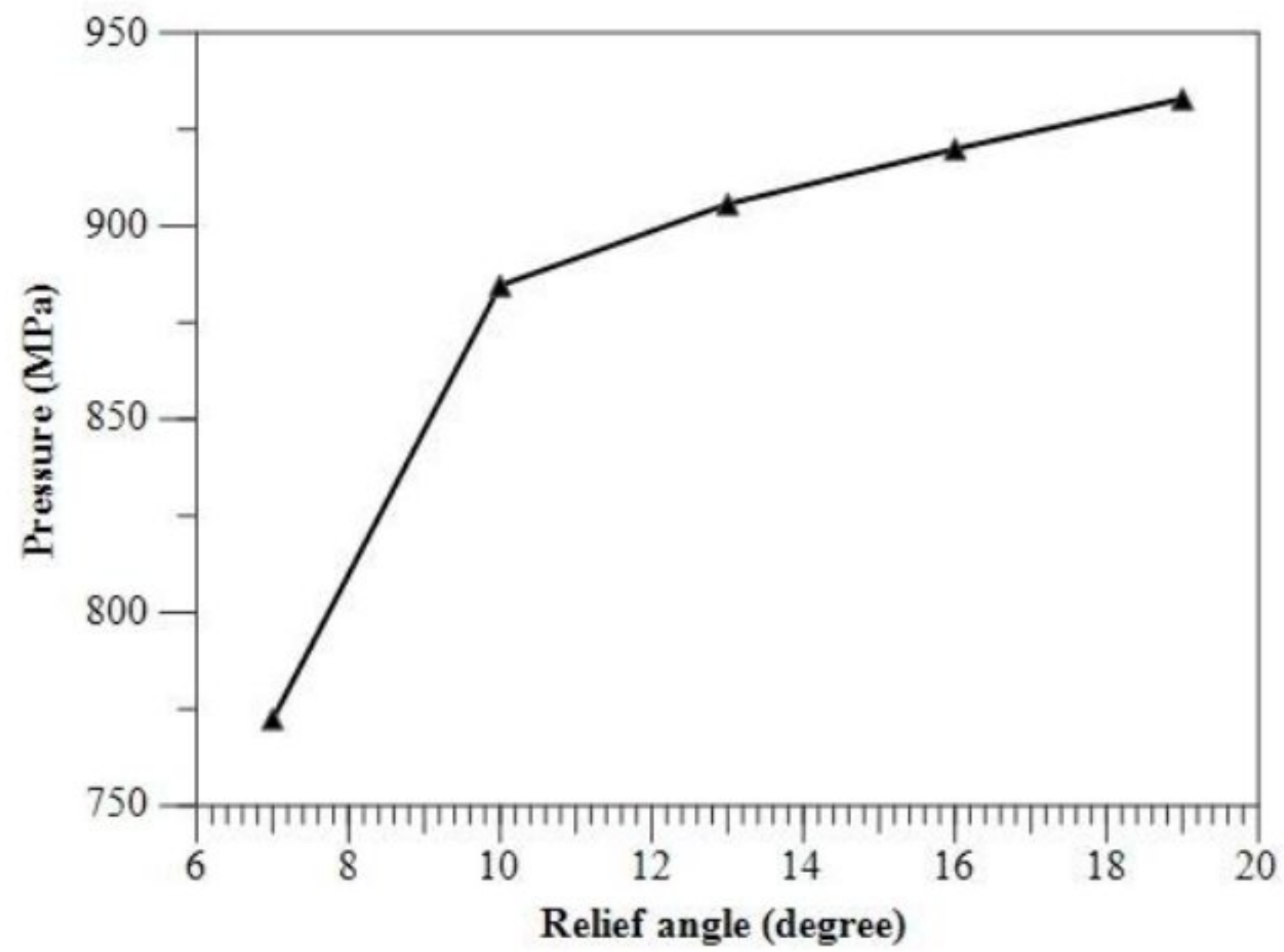


Figure 35 Distribution of pressure with the variation of relief angle for Cemented carbide-General tool

In Fig. 36, a detailed overview of the distribution of pressure in the tool, workpiece, chip and burr is presented. The zone affected by the pressure is 905.654 MPa with a cutting speed of 150m/min at relief angle of 13° indicating a high compression zone due to the force generated by the working tool.

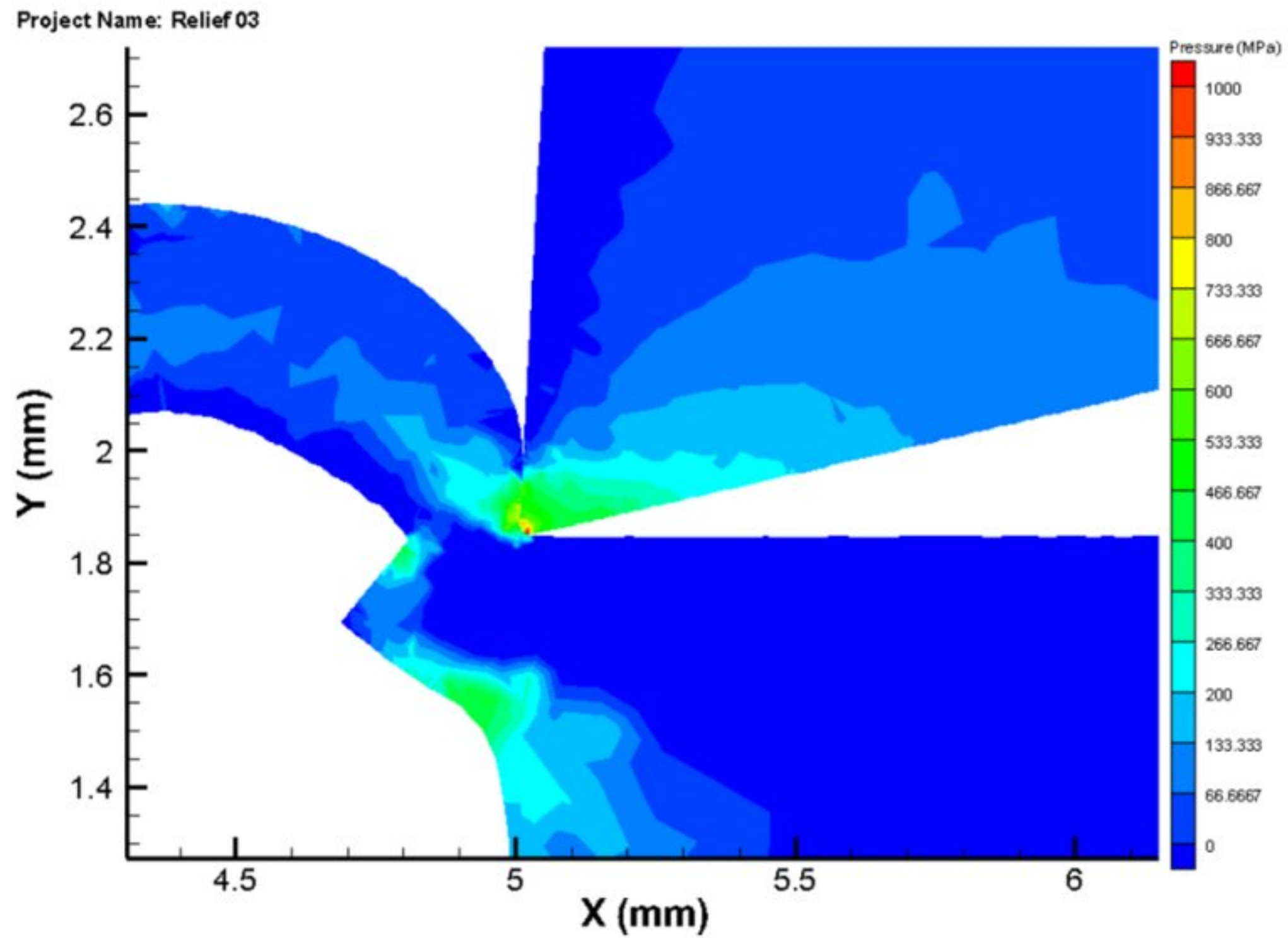


Figure 36 Distribution of pressure in the workpiece, tool(cemented carbide-General) and chip at the 150 m/min simulation when relief angle is 13° (image at 5 mm length of cut)

3.2.3 Maximum shear stress and von mises stress

In Fig. 37, the change of maximum shear stress along with the variation of relief angle is shown. For the relief angle of 3°, the maximum shear stress is 551.333 MPa. Maximum shear stress increases quite significantly after relief angle of 7°. From relief angle of 10° to relief angle of 13°, the changes are 665.641 MPa to 669.587 MPa which is quite less. After 13° to 16°, the change is not massive and the value at 16° is 705.893 MPa. At 15°, we have got the maximum shear stress 868.298 MPa. So, increasing the relief angle gives higher shear stress.

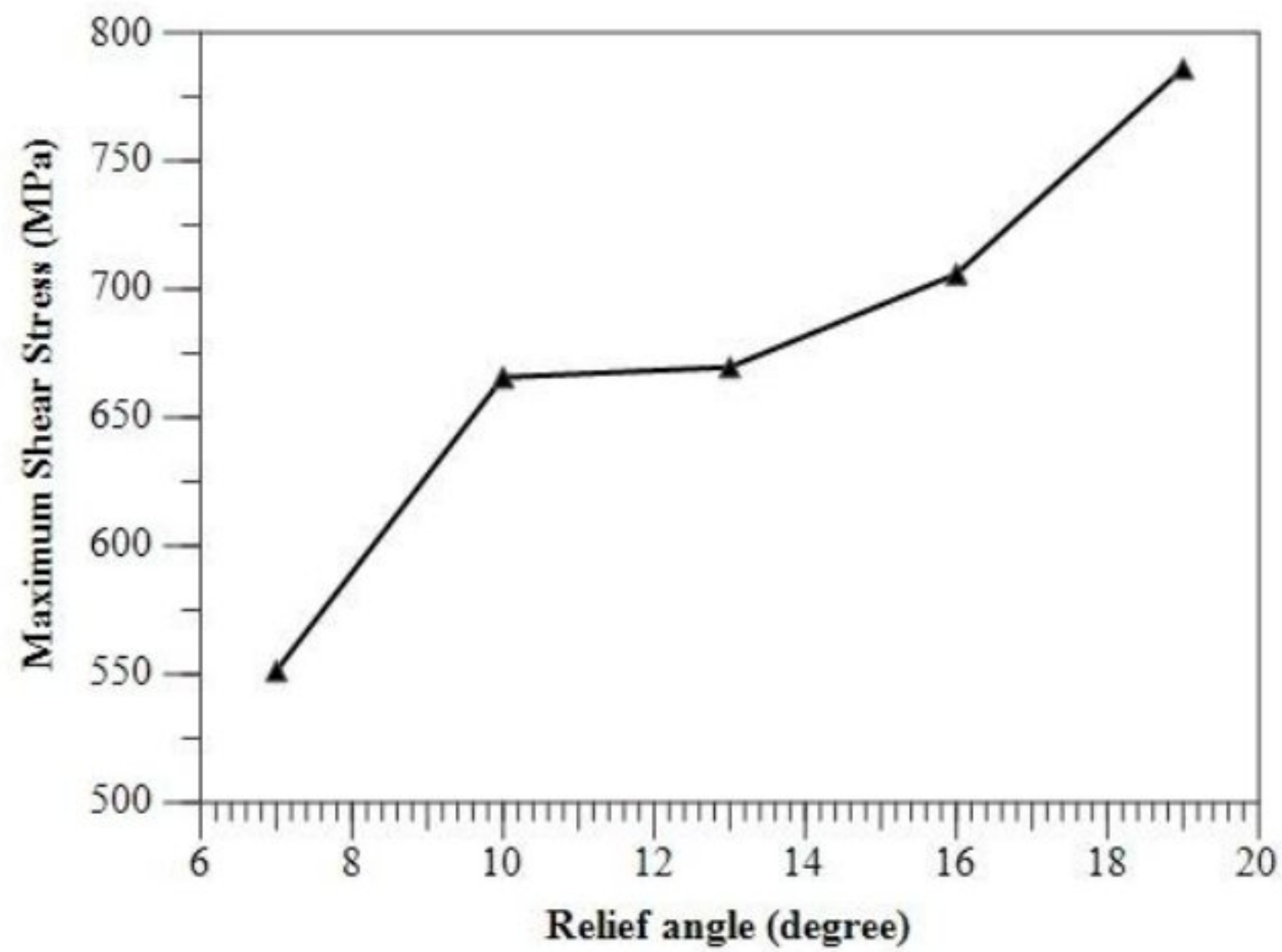


Figure 37 Distribution of maximum shear stress with the variation of relief angle for Cemented carbide-General tool

In Fig. 38, the distribution of maximum shear pressure in the workpiece, tool, chip, and burr is presented. The stress reached 785.908 MPa in the cemented carbide-General tool for a cutting speed of 150 m/min at the relief angle of 19°. Notice that when machined with the cemented carbide-General tool, the affected zone (in the workpiece) is much bigger at a relief angle of 19° than 7°. In general, when machining with cemented carbide-General tool, increasing the value of relief angle increases the maximum shear stress in the tool, chip, workpiece, and burr.

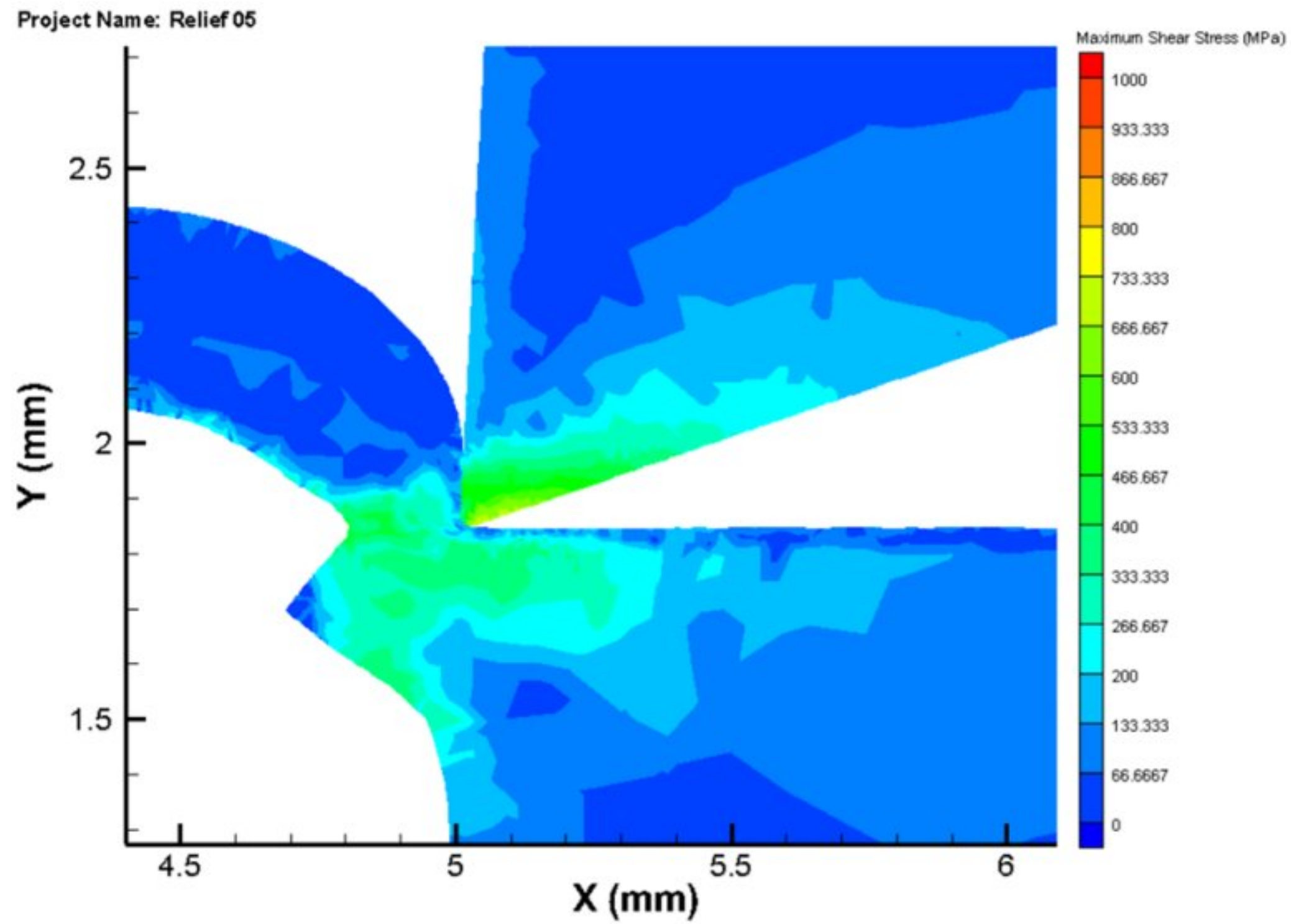


Figure 38 Distribution of maximum shear stress in the workpiece, tool(cemented carbide-General) and chip at the 150 m/min simulation when relief angle is 19° (image at 5 mm length of cut)

In Fig. 39, the simulation layouts for the distribution of von Mises stress is showed in detail where high speed machining at a cutting speed of 150 m/min for cemented carbide-General tool inserts. For cemented carbide-General tool, the value of relief angle of 7° is 962.333 MPa. Increasing the value of relief angle increases the value of the von mises stress. There has no massive change in von mises stress. Here, the changes occur gradually as like as rake angle where the other two parameters kept constant. The significance of von Mises stress on the point of the tool and in the region of chip formation is noticeable. For von Mises stresses, the tool tip is strongly influenced. In the primary shear zone, the material being extracted is often subject to high values of Mises stress.

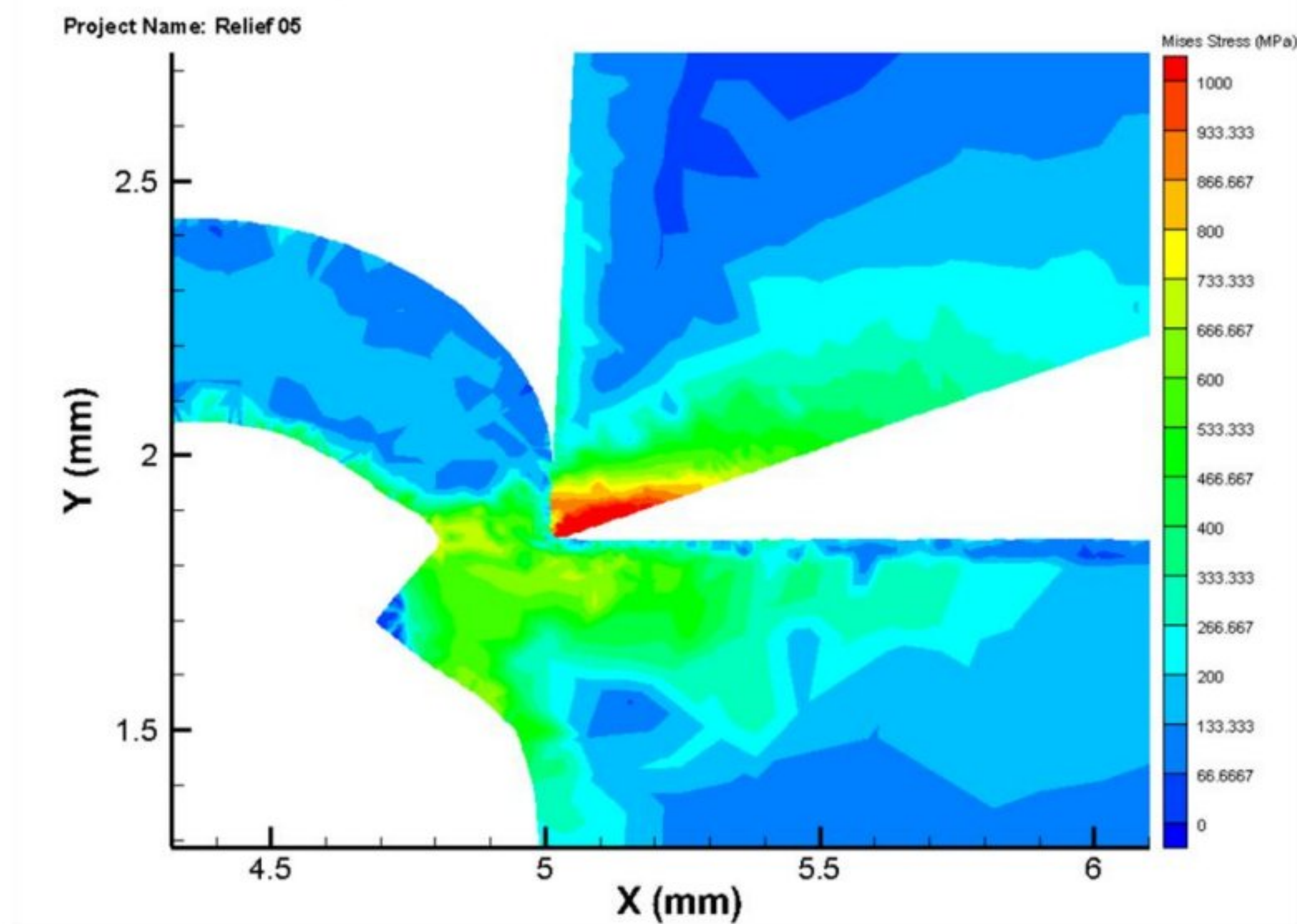


Figure 39 Distribution of von mises stress in the workpiece, tool(cemented carbide-General) and chip at the 150 m/min simulation when relief angle is 19° (image at 5 mm length of cut)

3.2.4 Heat rate

In Fig. 40, a more detailed overview of the distribution of heat rate in the tool, workpiece, chip and burr is showed. The heat rate of the cemented carbide-General is 16451.384 W/mm^3 , with a cutting speed of 150 m/min at relief angle of 16° . With the depth of the cut, the maximum heat rate increased. At relief angle of 7° , the value of the heat rate is 160566.7 W/mm^3 . Heat rate increases quite significantly after 10° where the value of the heat rate is 16154.354 W/mm^3 . This pattern is repeated throughout the progression of the relief angle. The heat rate is continued to high until the end of the length of cut and at 19° , the heat rate is 16542.83 W/mm^3 . Increasing the value of relief angle gives us higher amount of heat rate.

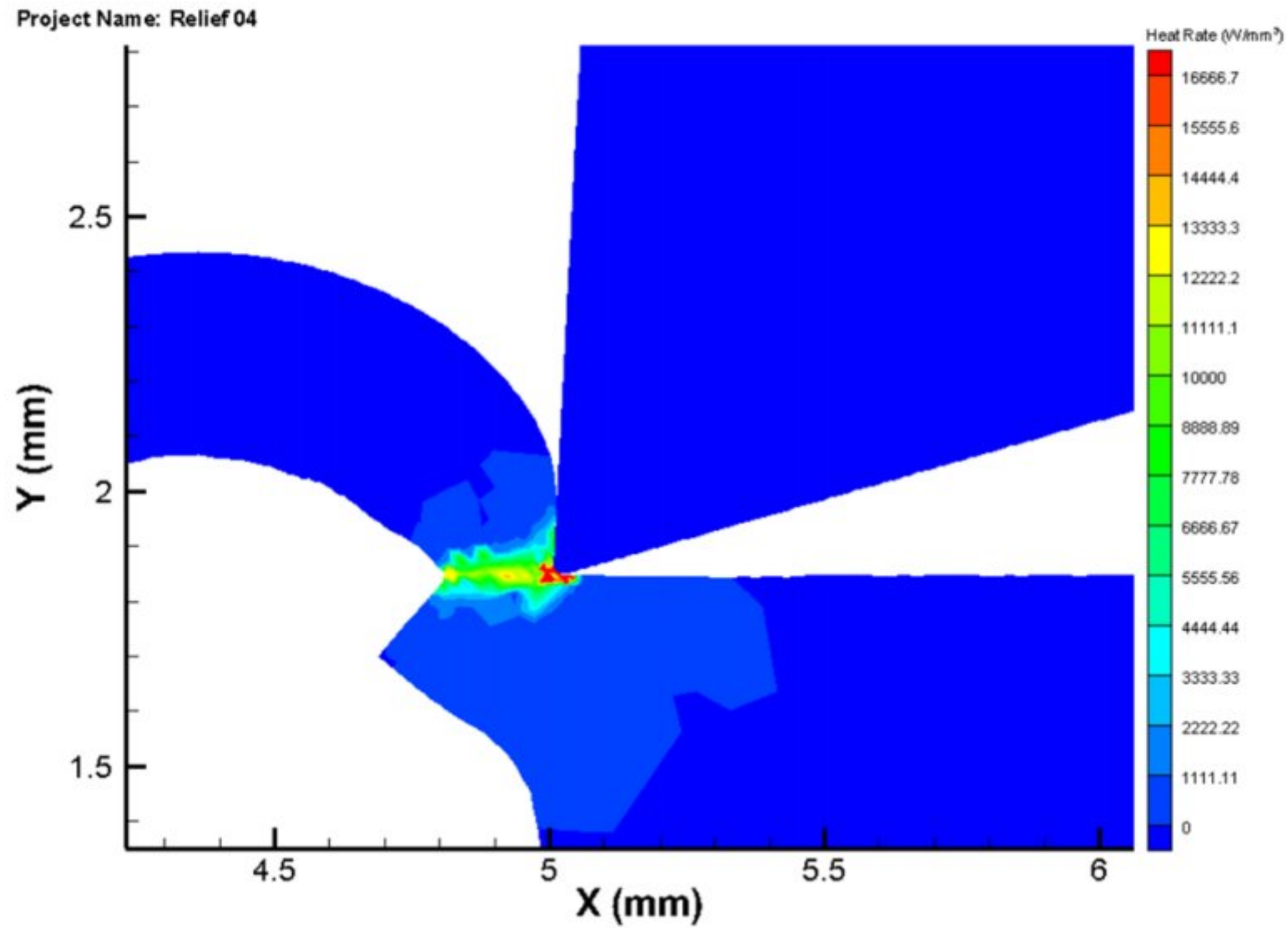


Figure 40 Distribution of heat rate in the workpiece, tool(cemented carbide-General) and chip at the 150 m/min simulation when relief angle is 16° (image at 5 mm length of cut)

3.2.5 Plastic strain and plastic strain rate

In Fig. 41, the plastic strain distribution in the workpiece, tool, chip, and burr is showed in detail where plastic strain of the cemented carbide-General is 3.87922, with a cutting speed of 150 m/min at relief angle of 10°. We have taken the variance of relief angle as 7°, 10°, 13°, 16° and 19°. The value of the plastic strain is 3.86203 when the relief angle is 7° and the other two parameters are constant. The value increases at 3.87922 when the relief angle is 10°. The value of plastic strain increases quite significantly after relief angle of 13° and value is 3.91313. At relief angle of 16°, the value increases 3.93203 and finally the value of plastic strain is 3.95223 at 15° and other two parameters are constant. It is clarified that increasing the relief angle, increases the plastic strain.

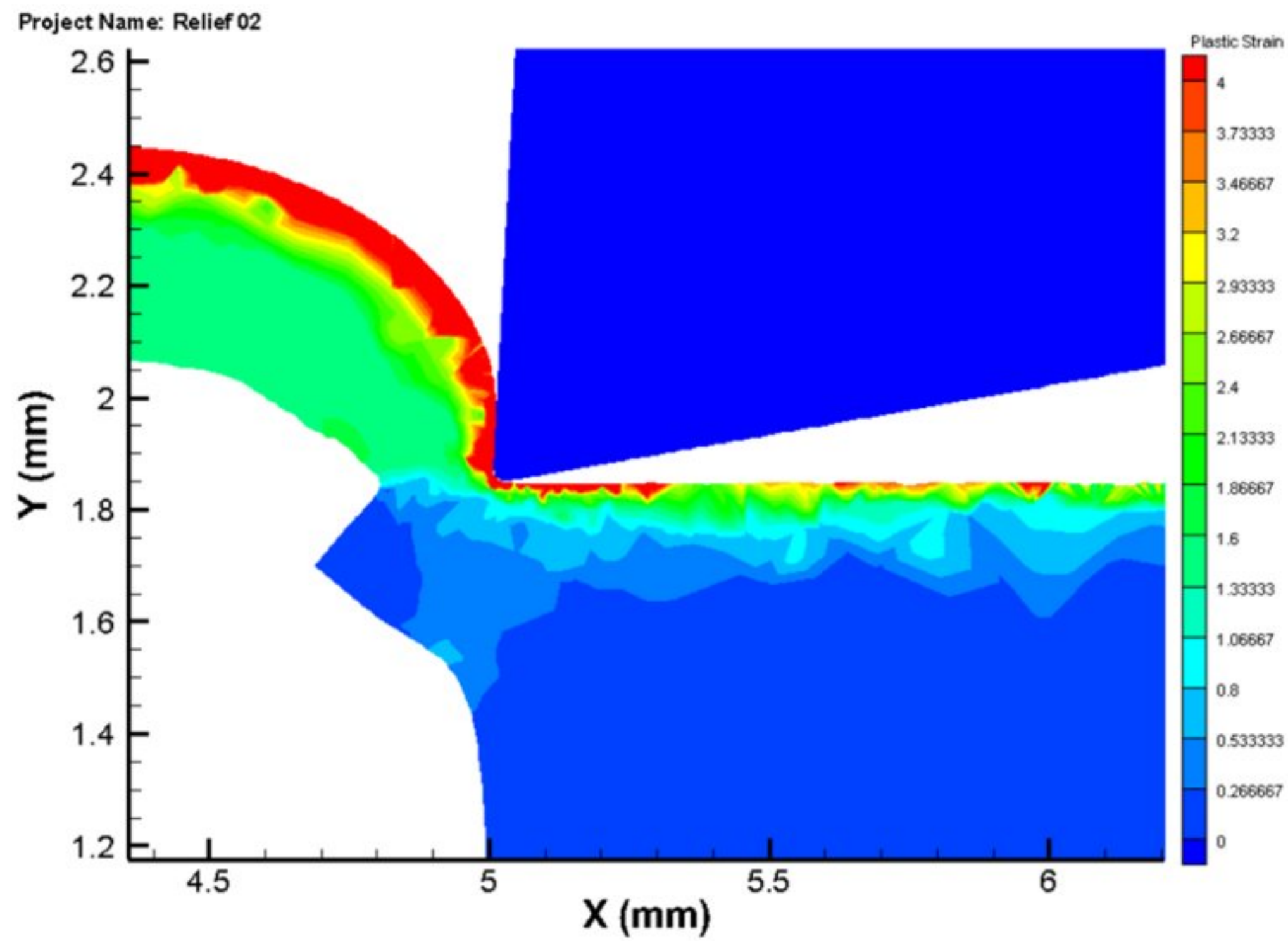


Figure 41 Distribution of plastic strain in the workpiece, tool(cemented carbide-General) and chip at the 150 m/min simulation when relief angle is 10° (image at 5 mm length of cut)

Additionally the plastic strain rate distribution in the workpiece, tool, chip, and burr is showed in detail in Fig. 42 where plastic strain rate of the cemented carbide-General is 16035.6 s^{-1} when the cutting speed is 150 m/min at relief angle of 7° and the other two parameters are constant. The value increases at 16145.587 s^{-1} when the relief angle is 10°. The value of plastic strain rate increases quite significantly after relief angle of 13° and the value is 16353.85 s^{-1} . At relief angles of 16° and 19°, the value increases at 16452.968 s^{-1} and 16542.856 s^{-1} respectively and other two parameters are constant. It is clarified that increasing the relief angle, increases the plastic strain rate.

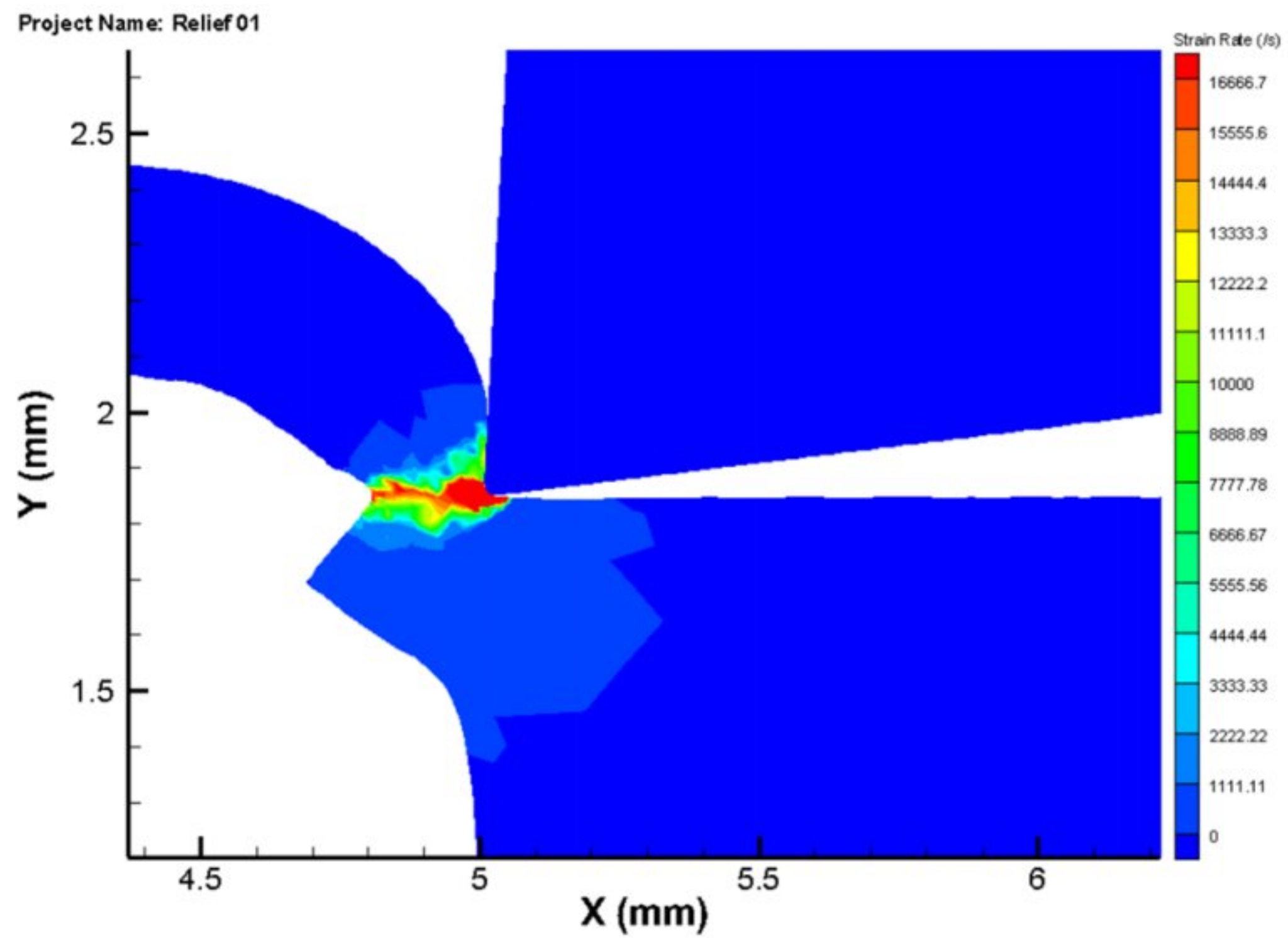


Figure 42 Distribution of plastic strain rate in the workpiece, tool(cemented carbide-General) and chip at the 150 m/min simulation when relief angle is 7° (image at 5 mm length of cut)

3.2.6 Cutting power and maximum cutting temperature

In Fig. 43, the evolution of the maximum cutting temperature and the cutting power over the cutting time is shown at the relief angle of 13°. In fig. 33, shows with the rise in the relief angle, the maximum cutting temperature (in the cutting tool) decreases. There has no change of power but for taking different relief angles give different cutting temperature. We have taken the rake angles as 7°, 10°, 13°, 16°, 19° and the maximum cutting temperature we have got are 1615°C, 1610°C, 1600°C, 1590°C and 1580°C. Which means increasing the relief angle decreases the cutting temperature. But the change in cutting temperature is not massive.

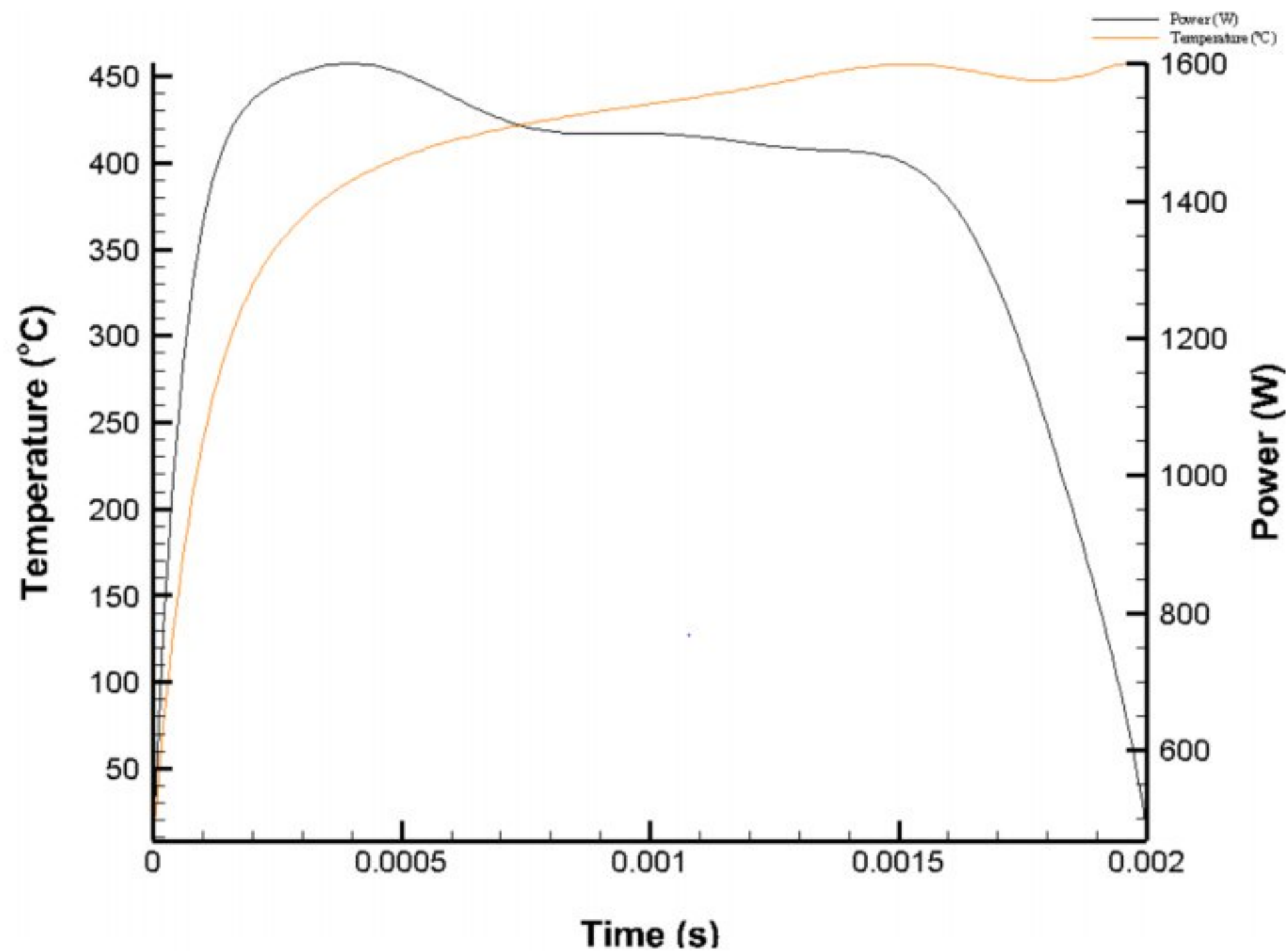


Figure 43 Cutting power and maximum cutting temperature along the time in the machining of the cemented carbide-General with a cutting speed of 150 m/min at the relief angle of 13° and a depth of cut of 2 mm

3.3 Effect of cutting edge radius

Here, we have taken the rake angle and relief angle as constant and changed the values of cutting edge radius for five times like 0.02 mm, 0.04 mm, 0.06 mm, 0.08 mm and 0.10 mm where for different radii the heat rate, temperature, pressure, maximum shear stress, mises stress, plastic strain and strain rate varies. Some of the changes are shown in graphs and a brief discussion is given below.

3.3.1 Cutting forces and feed forces

In Fig. 44, the evolution of the cutting forces and feed forces along with the variance in cutting edge radii for cemented carbide-General is showed. For example, at a cutting speed of 150 m/min, the cutting force for the cemented carbide-General is 648 N and the feed force is 310 N when cutting edge radius is taken 0.02 mm and others two

parameters keep constant. For cutting edge radii of 0.04 mm, 0.06 mm, 0.08mm and 0.10 mm, the cutting forces are 660 N, 675 N, 691 N and 716 N and feed forces are 330 N, 375 N, 412N and 429 N respectively. It can be said that increasing the cutting edge radius increases the cutting force and feed force as well.

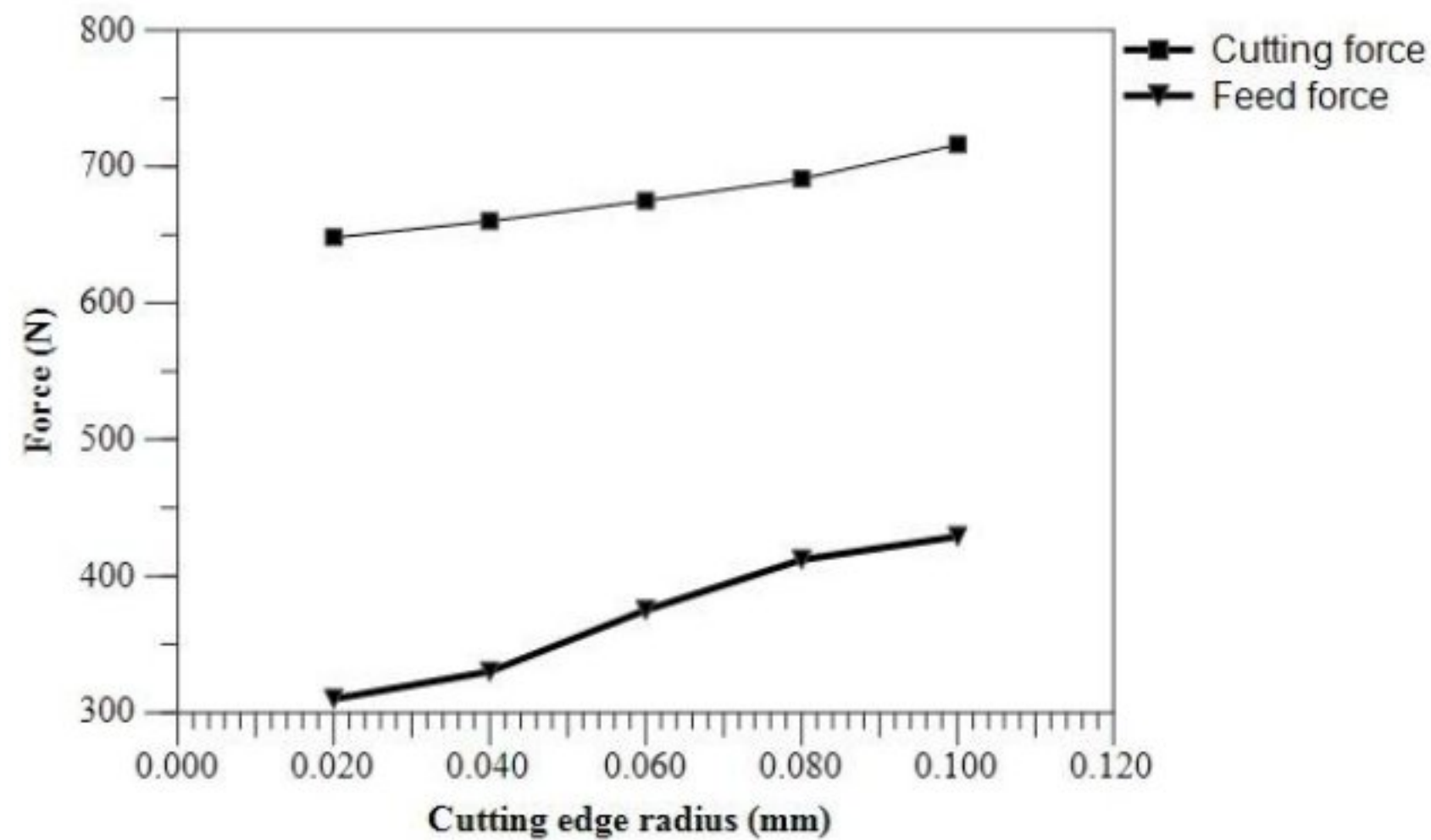


Figure 44 Distribution of cutting and feed forces with the variation of cutting edge radii for Cemented carbide-General tool

3.3.2 Temperature and pressure

In Fig. 45, the evolution of the temperature with the varying cutting edge radii for cemented carbide is presented. For example, at a cutting speed of 150 m/min, with the increment of cutting edge radius by 0.02 mm, temperature decreases. As we can see in this graph of Temperature vs Cutting edge radius, temperature decreases quite significantly after 0.040 mm where the value of the temperature is 443.45°C. This pattern is repeated throughout the progression of the cutting edge radii. The temperature continued to low until the end of the length of cut and at 0.10 mm, the

temperature is 425.168°C. It can be seen that increasing the value of cutting edge radii give us decreasing of temperature.

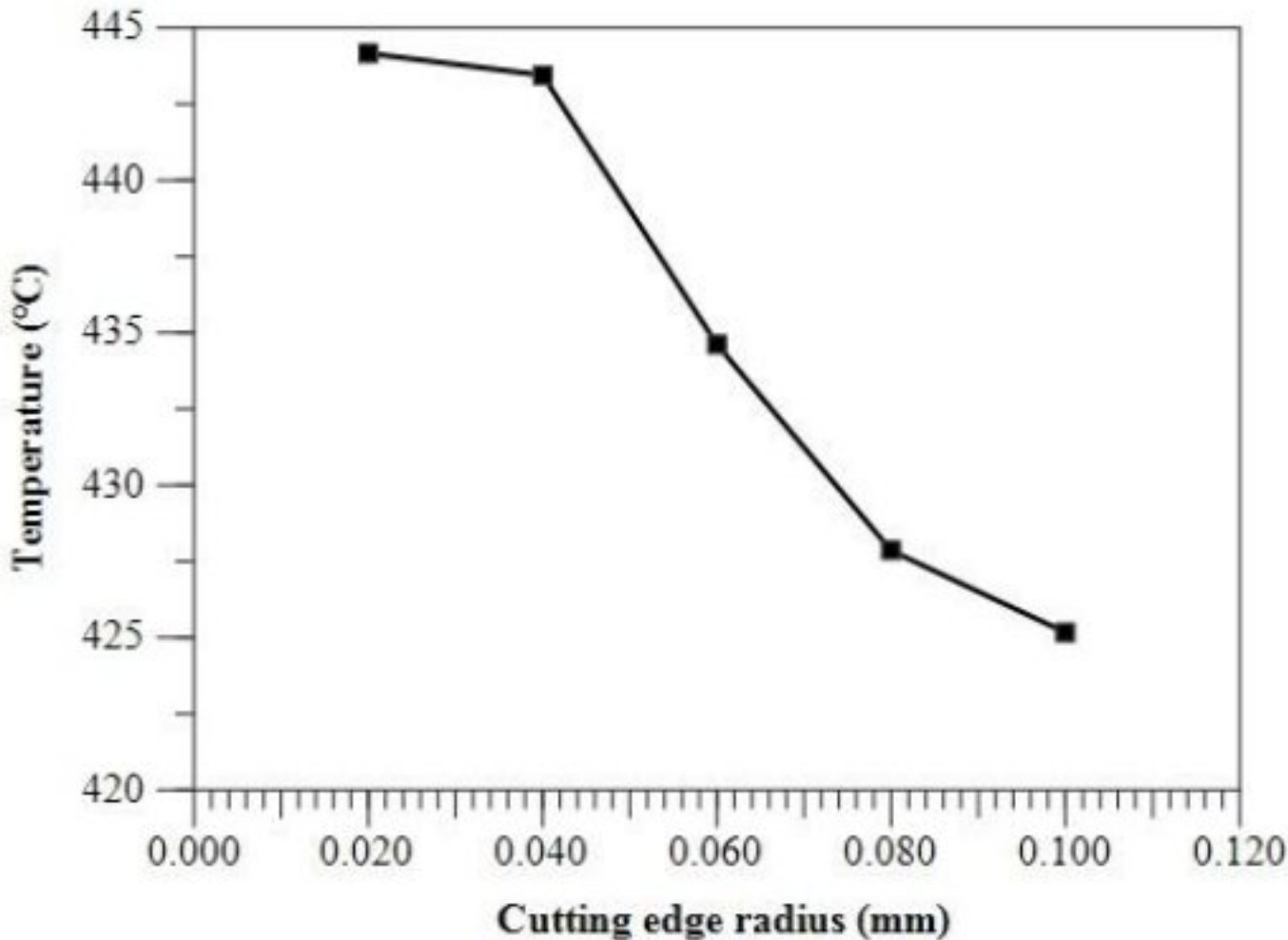


Figure 45 Distribution of temperature with the variation of cutting edge radii for Cemented carbide-General tool

In Fig. 46, a more detailed overview of the distribution of temperature in the tool, workpiece, chip and burr is showed. The temperature of the cemented carbide-General is 427.855°C, with a cutting speed of 150 m/min at cutting edge radius of 0.08 mm.

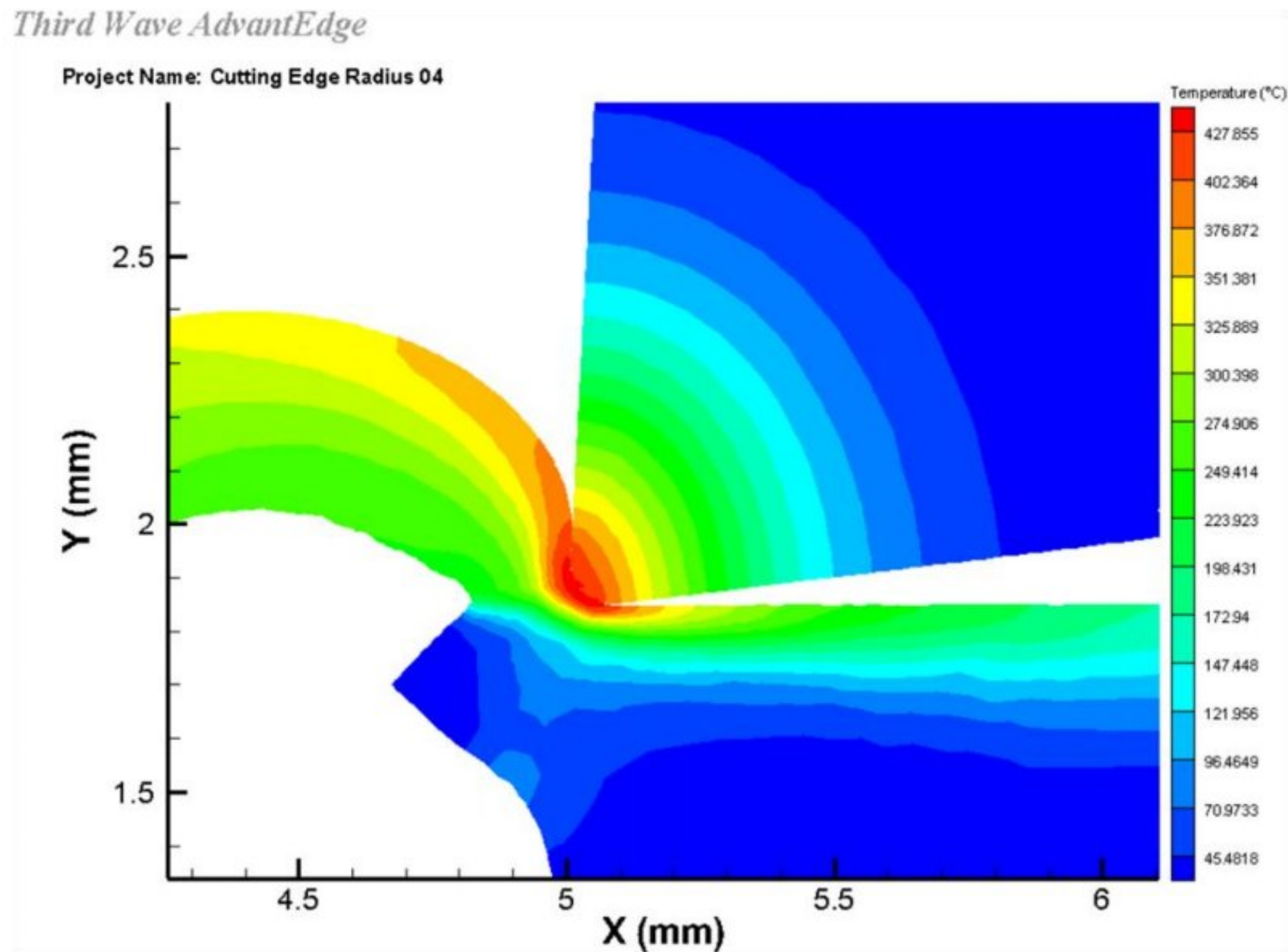


Figure 46 Distribution of temperature in the workpiece, tool(cemented carbide-General) and chip at the 150 m/min when cutting edge radius is 0.08 mm (image at 5 mm length of cut)

Taking the rake angle and relief angle as constant, we have changed the cutting edge radius for five times. So, we have got five different values of pressure. For cutting edge radius of 0.02 mm, the value is 772.333 MPa. Pressure increases quite significantly after cutting edge radius of 0.06 mm. At 0.06 mm, the value is 803.967 MPa. The values are 867.924 MPa and 898.716 MPa for cutting edge radii of 0.08 mm and 0.10 mm respectively. Keeping other two parameters constant increasing the value of cutting edge radius increases the pressure as well. In fig. 47, the change is shown.

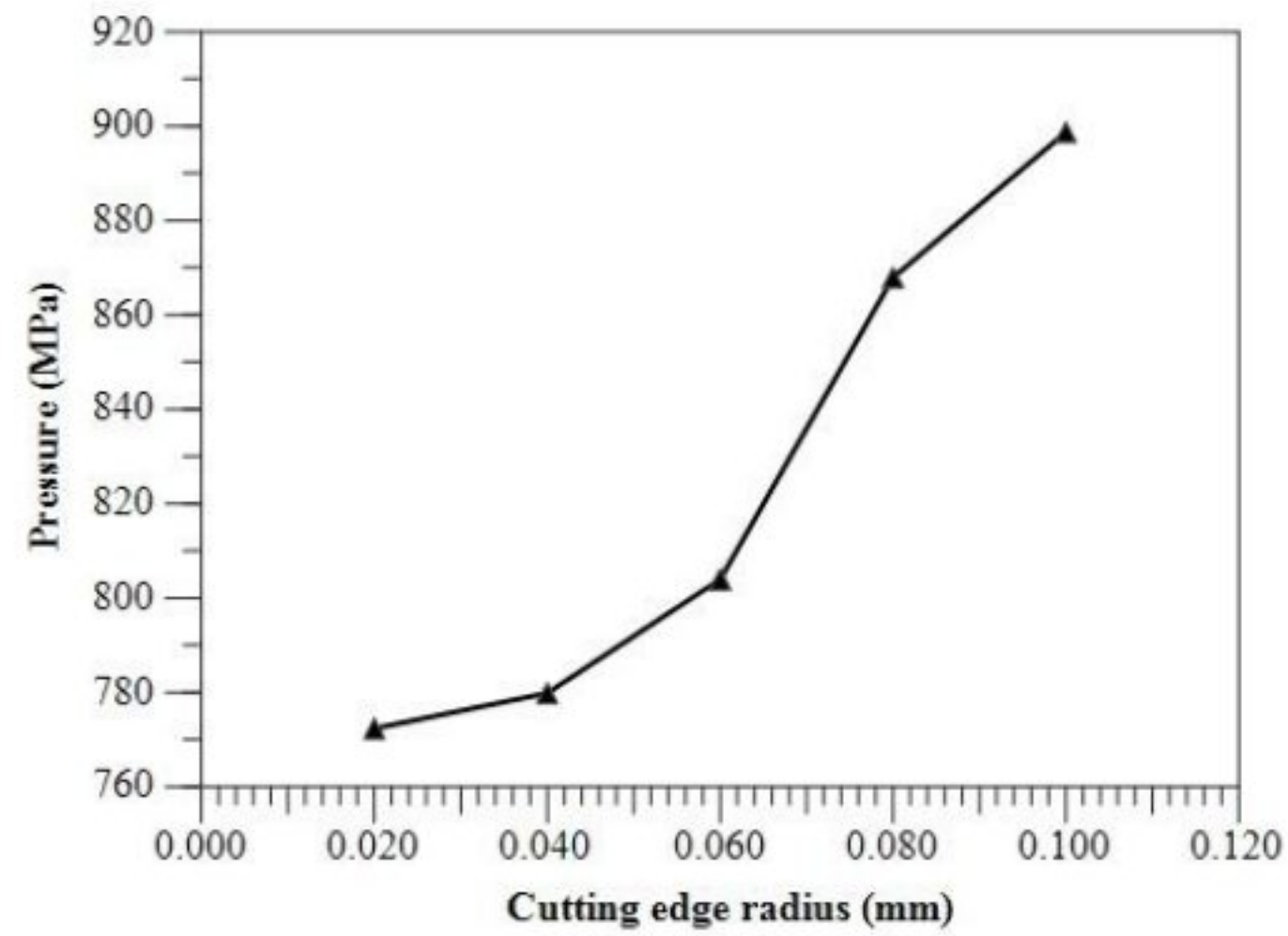


Figure 47 Distribution of pressure with the variation of cutting edge radii for Cemented carbide-General tool

In Fig. 48, a detailed overview of the distribution of pressure in the tool, workpiece, chip and burr is presented. The zone affected by the pressure is 898.716 MPa with a cutting speed of 150m/min indicating a high compression zone due to the force generated by the working tool.

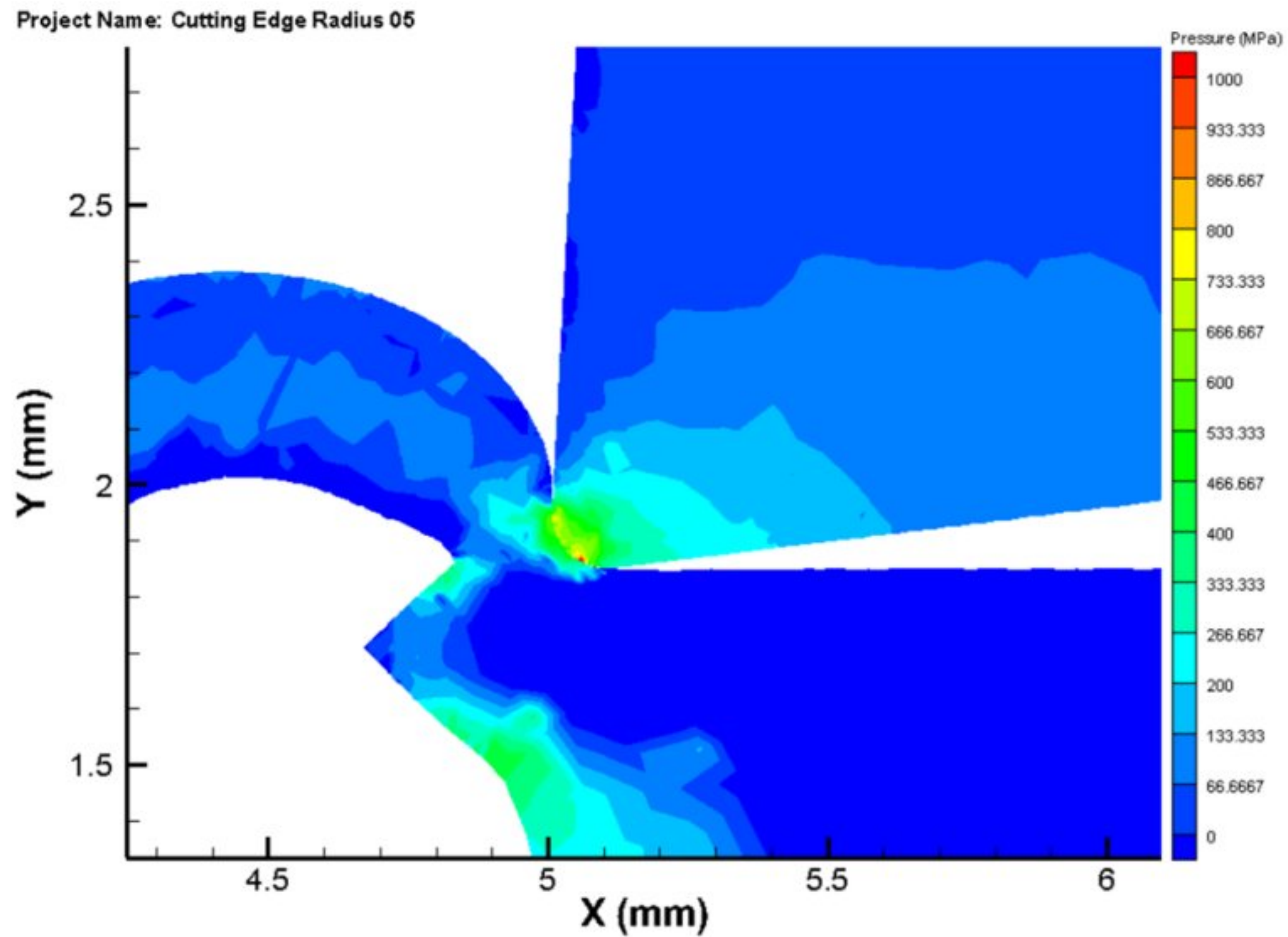


Figure 48 Distribution of pressure in the workpiece, tool(cemented carbide-General) and chip at the 150 m/min when cutting edge radius is 0.10 mm (image at 5 mm length of cut)

3.3.3 Maximum shear stress and von mises stress

In Fig. 49, the change of maximum shear stress along with the variation of cutting edge radius is shown. For the cutting edge radius of 0.02 mm, the maximum shear stress is 551.333 MPa. Maximum shear stress increases quite significantly after 0.02 mm. From cutting edge radius of 0.06 mm to cutting edge radius of 0.08 mm, the changes are 612.902 MPa to 658.215 MPa which is quite high. After 0.08 mm, the change is not massive. At 0.10 mm, we have got the maximum shear stress 664.902 MPa. So, increasing the value of cutting edge radius gives higher shear stress.

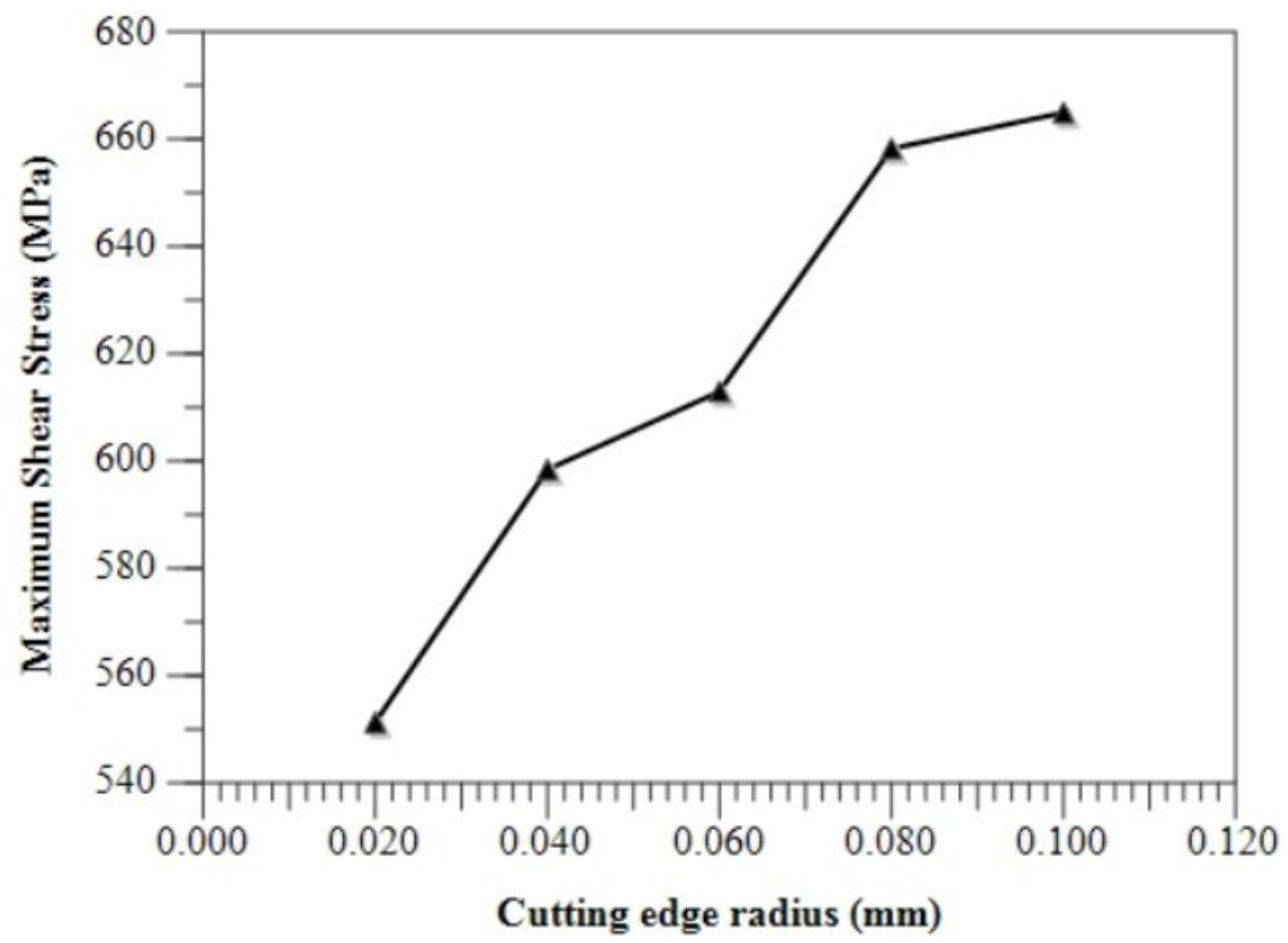


Figure 49 Distribution of maximum shear stress with the variation of cutting edge radii for Cemented carbide-General tool

In Fig. 50, the distribution of maximum shear pressure is presented. The stress reached 664.902 MPa. The affected zone is much bigger at 0.02 mm than 0.10 mm.

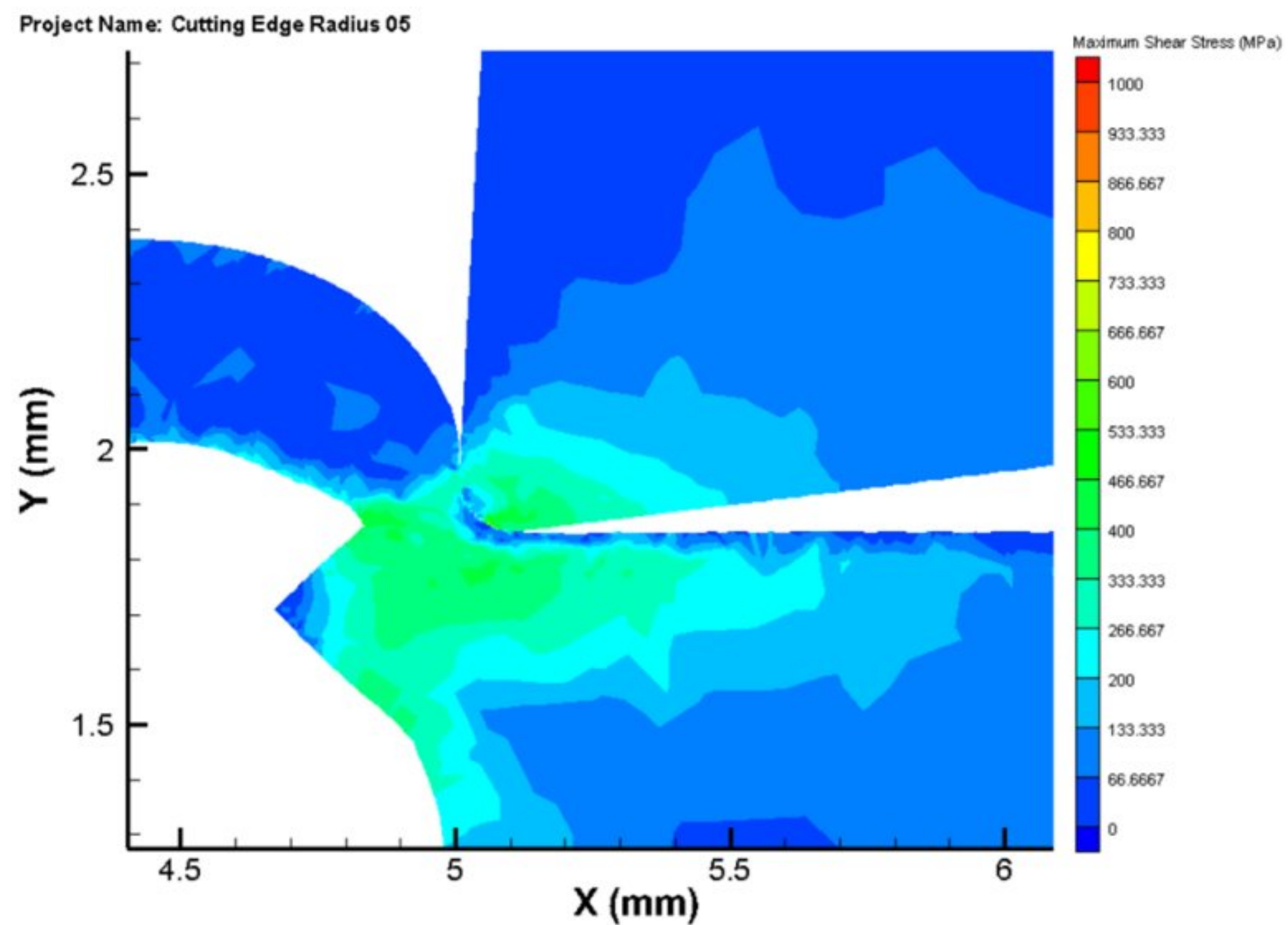


Figure 50 Distribution of maximum shear stress in the workpiece, tool(cemented carbide-General) and chip at the 150 m/min when cutting edge radius is 0.10 mm (image at 5 mm length of cut)

In Fig. 51, the simulation layout for the distribution of von Mises stress is showed in detail where high speed machining at a cutting speed of 150 m/min for cemented carbide-General tool inserts. For cemented carbide-General tool, the value of cutting edge radius of 0.02 mm is 962.333 MPa. Increasing the value of cutting edge radius increases the value of the von mises stress. There has no massive change in von mises stress. Here, the changes occur gradually as like as rake angle where the other two parameters kept constant. The significance of von Mises stress on the point of the tool and in the region of chip formation is noticeable. For von Mises stresses, the tool tip is strongly influenced. In the primary shear zone, the material being extracted is often subject to high values of Mises stress.

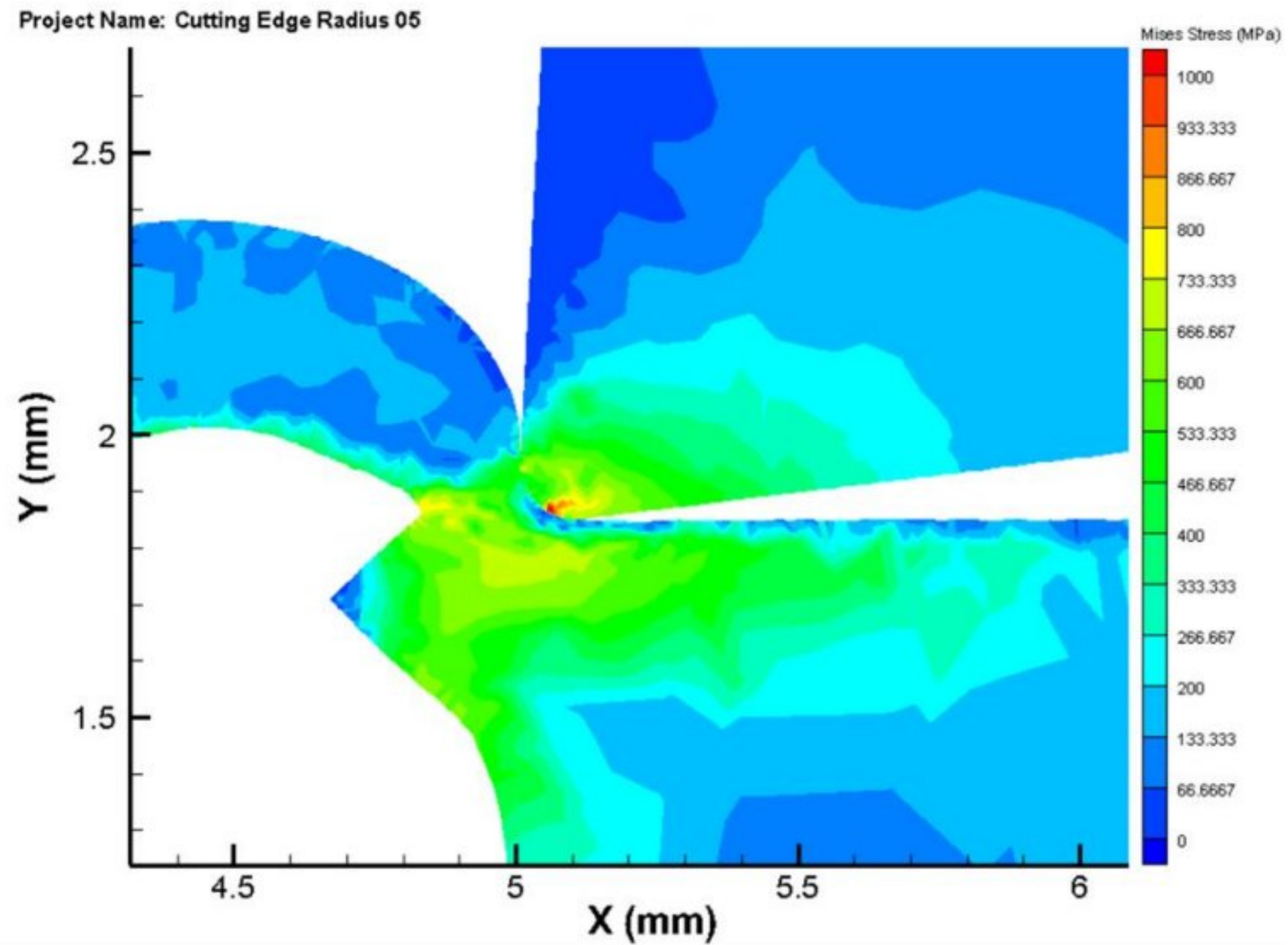


Figure 51 Distribution of von mises stress in the workpiece, tool(cemented carbide-General) and chip at the 150 m/min when cutting edge radius is 0.10 mm (image at 5 mm length of cut)

3.3.4 Heat rate

In Fig. 52, a more detailed overview of the distribution of heat rate in the tool, workpiece, chip and burr is showed. The heat rate of the cemented carbide-General is 15426.557 W/mm^3 , with a cutting speed of 150 m/min at cutting edge radius of 0.08 mm. With the depth of the cut, the maximum heat rate decreases. At cutting edge radius of 0.02 mm, the value of the heat rate is 160566.7 W/mm^3 . Heat rate decreases quite significantly after 0.04 mm where the value of the heat rate is $15497.8097 \text{ W/mm}^3$. This pattern is repeated throughout the progression of the cutting edge radius. The heat rate is continued to low until the end of the length of cut and at 0.10 mm, the heat rate is 14444.4 W/mm^3 . It can be said that increasing the value of cutting edge radii give lower amount of heat rate.

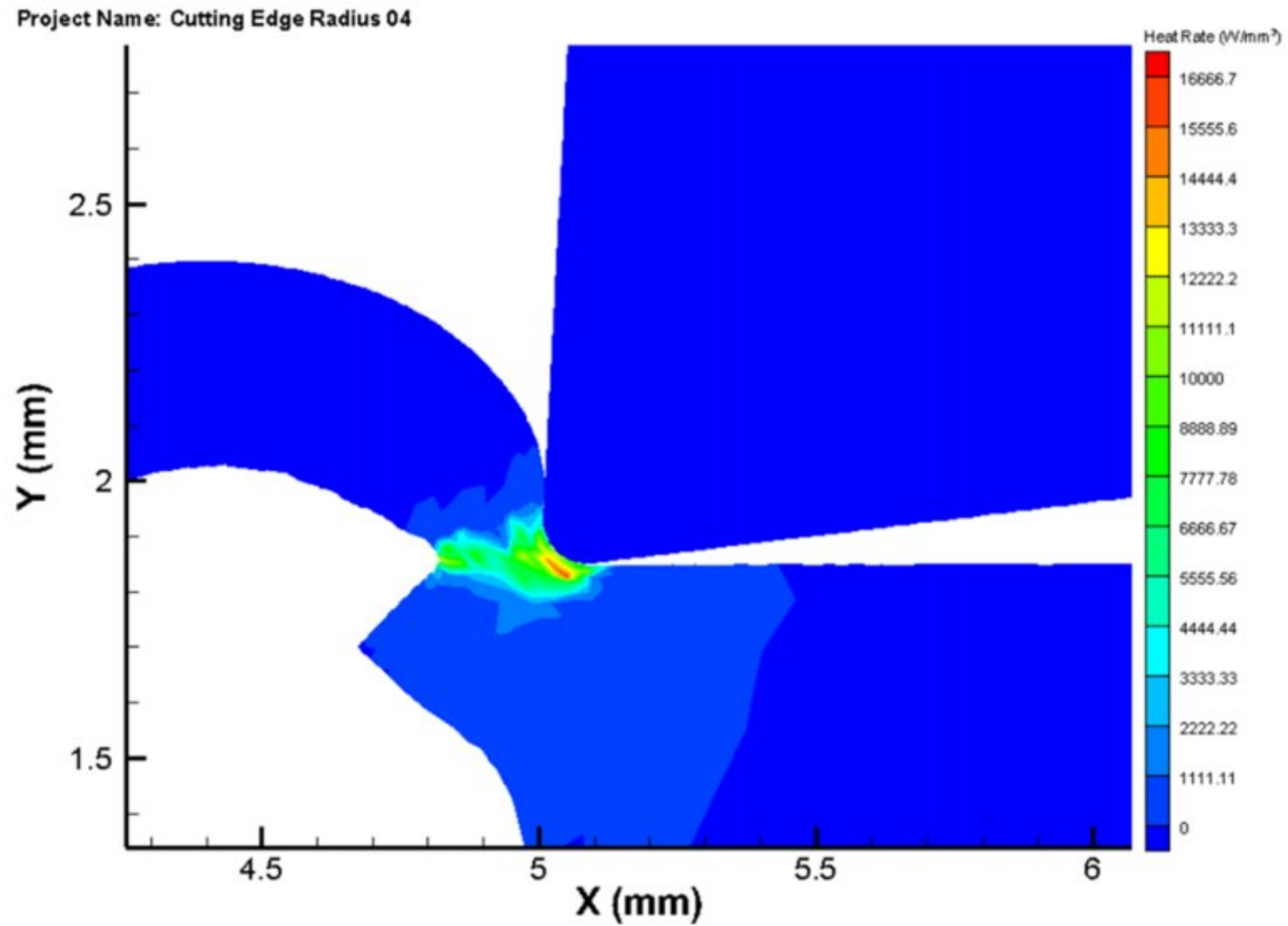


Figure 52 Distribution of heat rate in the workpiece, tool(cemented carbide-General) and chip at the 150 m/min when cutting edge radius is 0.08 mm (image at 5 mm length of cut)

3.3.5 Plastic strain and plastic strain rate

In Fig. 53, the plastic strain distribution in the workpiece, tool, chip, and burr is showed in detail where plastic strain of the cemented carbide-General is 3.90251, with a cutting speed of 150 m/min at cutting edge radius of 0.06 mm. We have taken the variance of the cutting edge radii as 0.02 mm, 0.04 mm, 0.06mm, 0.08mm and 0.10 mm. The value of the plastic strain is 3.86203 when the cutting edge radius is 0.02 mm. The value increases at 3.88313 when the edge radius is 0.04 mm. The value of plastic strain increases quite significantly after edge radius of 0.08 mm and value is 3.92571. Finally the value of plastic strain is 3.94610 at cutting edge radius of 0.10 mm and other two parameters are constant. It is clarified that increasing the cutting edge radius increases the plastic strain.

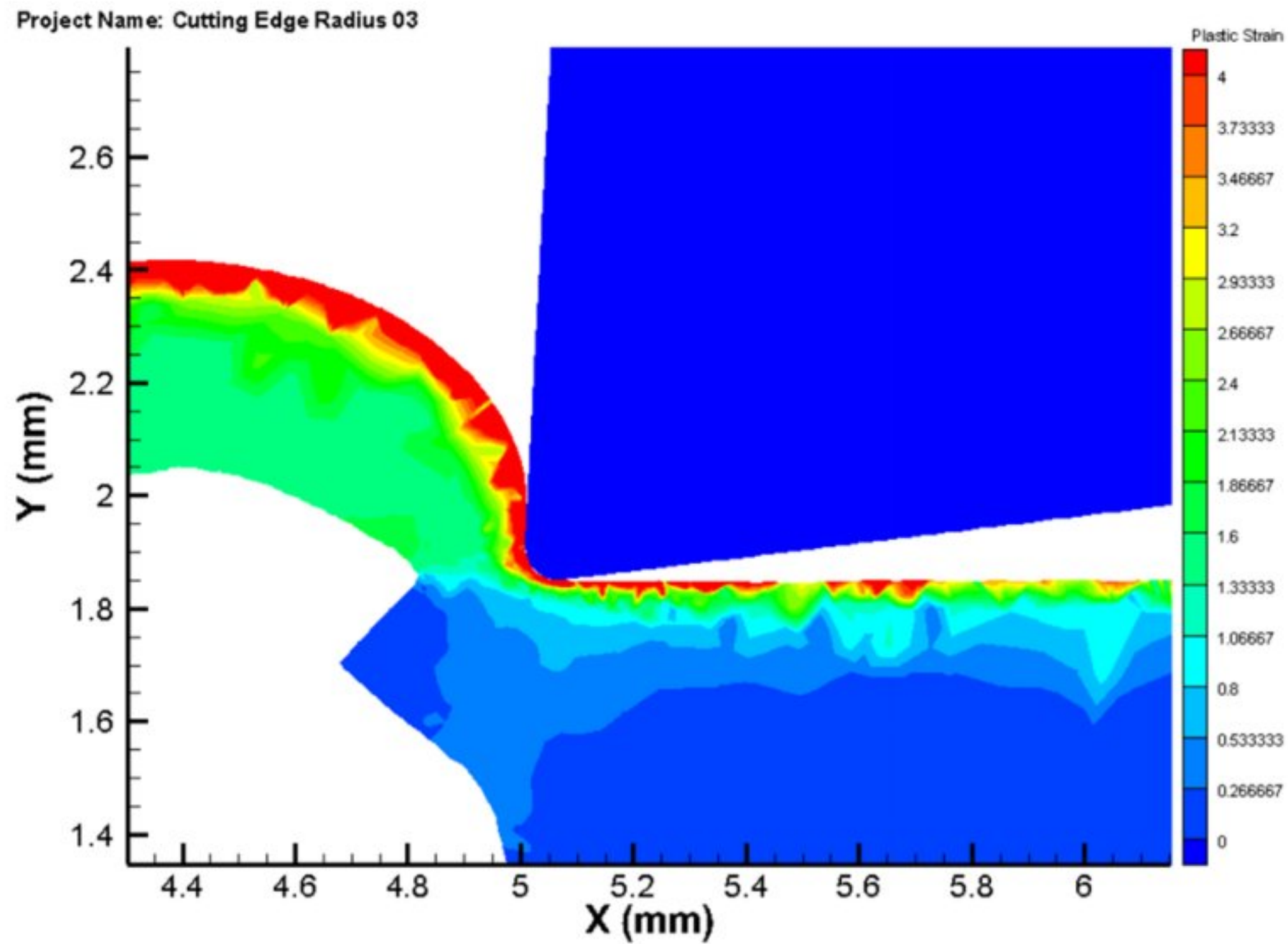


Figure 53 Distribution of heat rate in the workpiece, tool(cemented carbide-General) and chip at the 150 m/min when cutting edge radius is 0.08 mm (image at 5 mm length of cut)

The plastic strain rate distribution in the workpiece, tool, chip, and burr is showed in detail in Fig. 54 where plastic strain rate of the cemented carbide-General is 16035.6 s^{-1} when the cutting speed is 150 m/min at cutting edge radius of 0.02 mm. The value increases at 16144.867 s^{-1} when the cutting edge radius of 0.04 mm. The value of plastic strain rate increases quite significantly after edge radius of 0.06 mm and the value is 16254.358 s^{-1} . At cutting edge radii of 0.08 mm and 0.10 mm, the values increase to 16452.85 s^{-1} and 16538.475 s^{-1} respectively and other two parameters are constant. It is clarified that increasing the cutting edge radius increases the plastic strain rate.

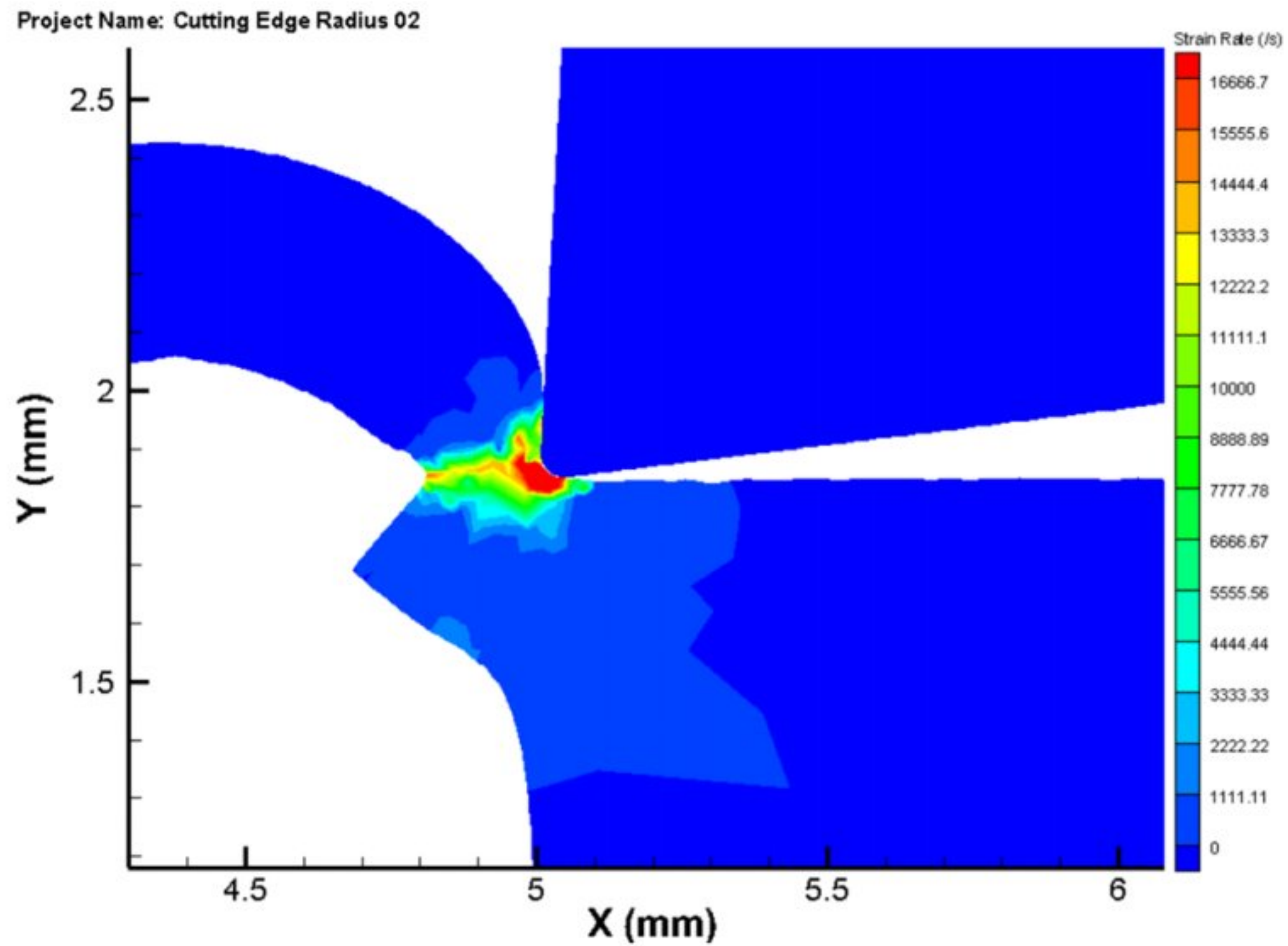


Figure 54 Distribution of plastic strain rate in the workpiece, tool(cemented carbide-General) and chip at the 150 m/min when cutting edge radius is 0.04 mm (image at 5 mm length of cut)

3.3.6 Cutting power and maximum cutting temperature

In Fig. 55, the evolution of the maximum cutting temperature and the cutting power over the cutting time is shown at the cutting edge radius of 0.02 mm. In fig. 45, shows with the rise in the cutting edge radii, the maximum cutting temperature (in the cutting tool) decreases. There has no change of power but for taking different rake angles give different cutting temperature. We have taken the cutting edge radii as 0.02 mm, 0.04 mm, 0.06 mm, 0.08mm and 0.10 mm and the maximum cutting temperature we have got are 1610°C, 1650°C, 1670°C, 1690°C and 1740°C. Which means increasing the cutting edge radius increases the cutting temperature.

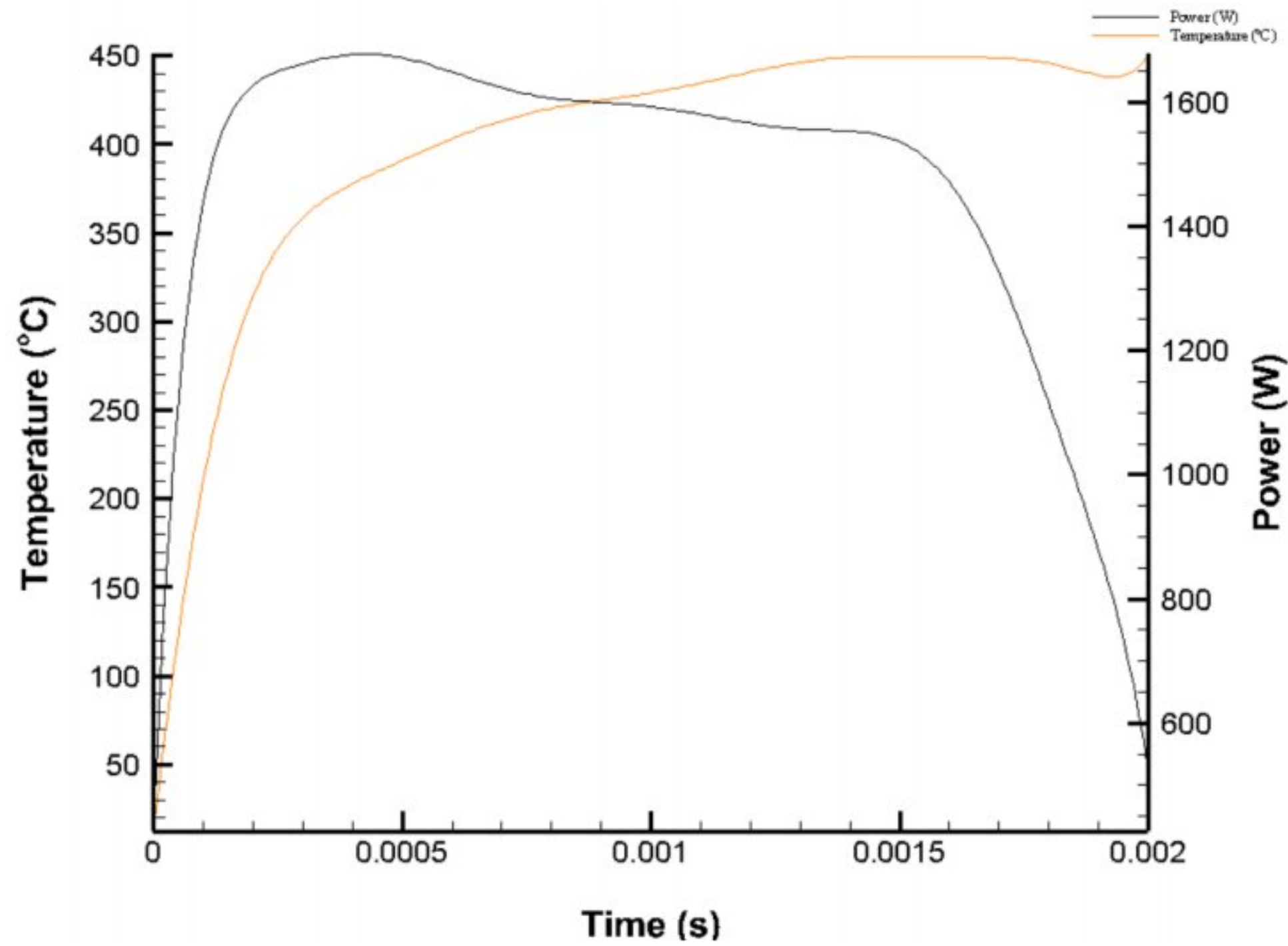


Figure 55 Cutting power and maximum cutting temperature along the time in the machining of the cemented carbide-General with a cutting speed of 150 m/min at the cutting edge radius of 0.06 mm and a depth of cut of 2 mm

3.4 Chip formation on three different parameters

3.4.1 Effect of chip thickness on variation of rake angle

It can be observed clearly from fig. 56 that whenever we are increasing the value of rake angle, the chip thickness decreases. At rake angle of 3° , the chip thickness is almost 0.376 mm. There has no change in between rake angle of 6° and rake angle of 9° . After that, there has a massive change when the rake angle is 12° . At this angle, the value is 0.350 mm. The change at 15° from the rake angle of 12° is almost the similar range as the change of 12° from the rake angle of 9° . The value at rake angle of 15° is 0.332mm.

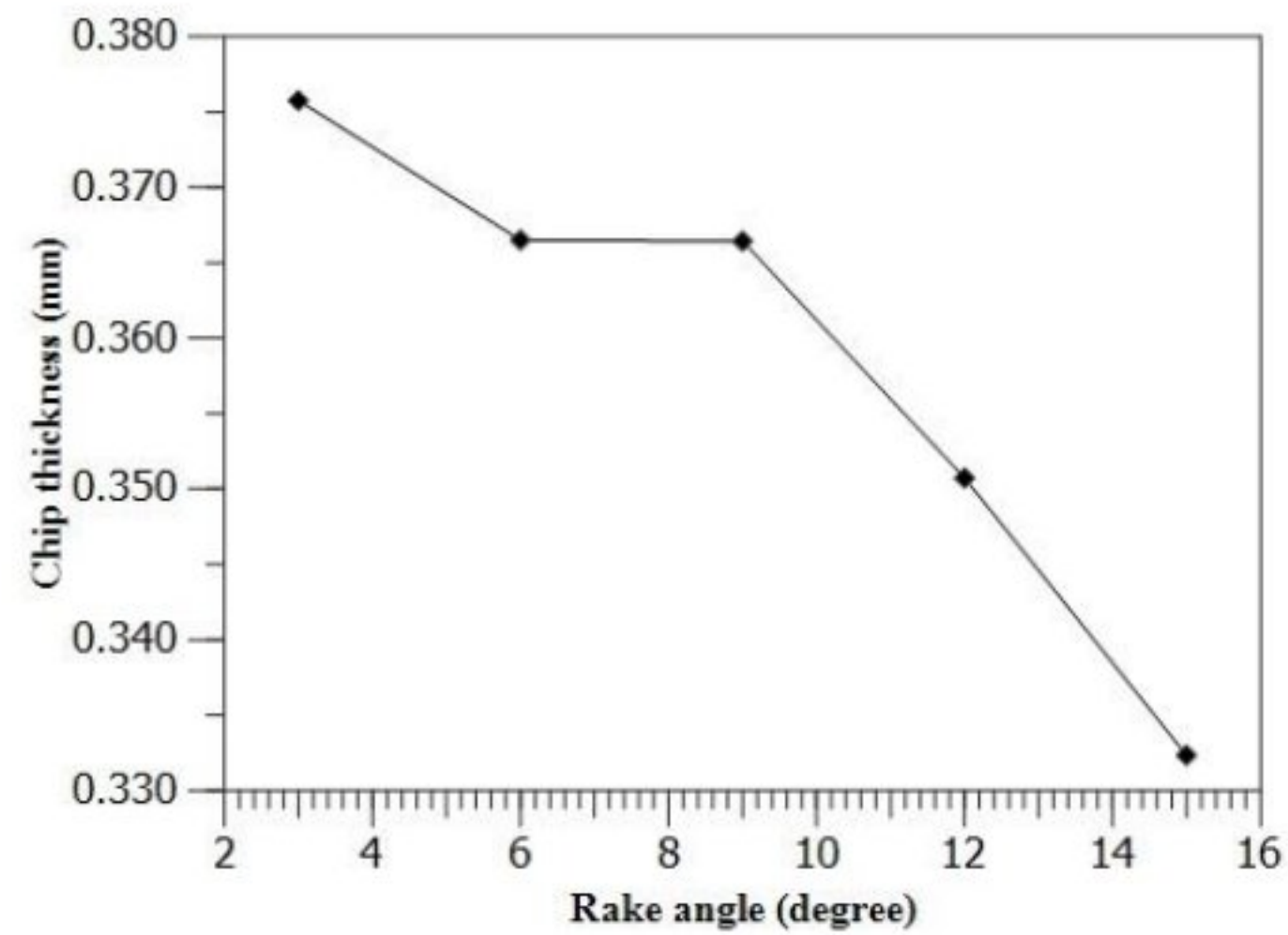


Figure 56 Distribution of chip thickness with the variation of rake angles for Cemented carbide-General tool

3.4.2 Effect of chip thickness on variation of relief angle

In fig. 57, distribution of chip thickness with the variation of relief angle is shown. At relief angle of 7° , the chip thickness is almost 0.388 mm. There has a massive change between relief angle of 10° and 13° . The value at rake angle of 13° is 0.365 mm. The change at 19° from the rake angle of 16° is almost the similar range as the change of 16° from the rake angle of 13° . The value at rake angle of 19° is 0.354 mm.

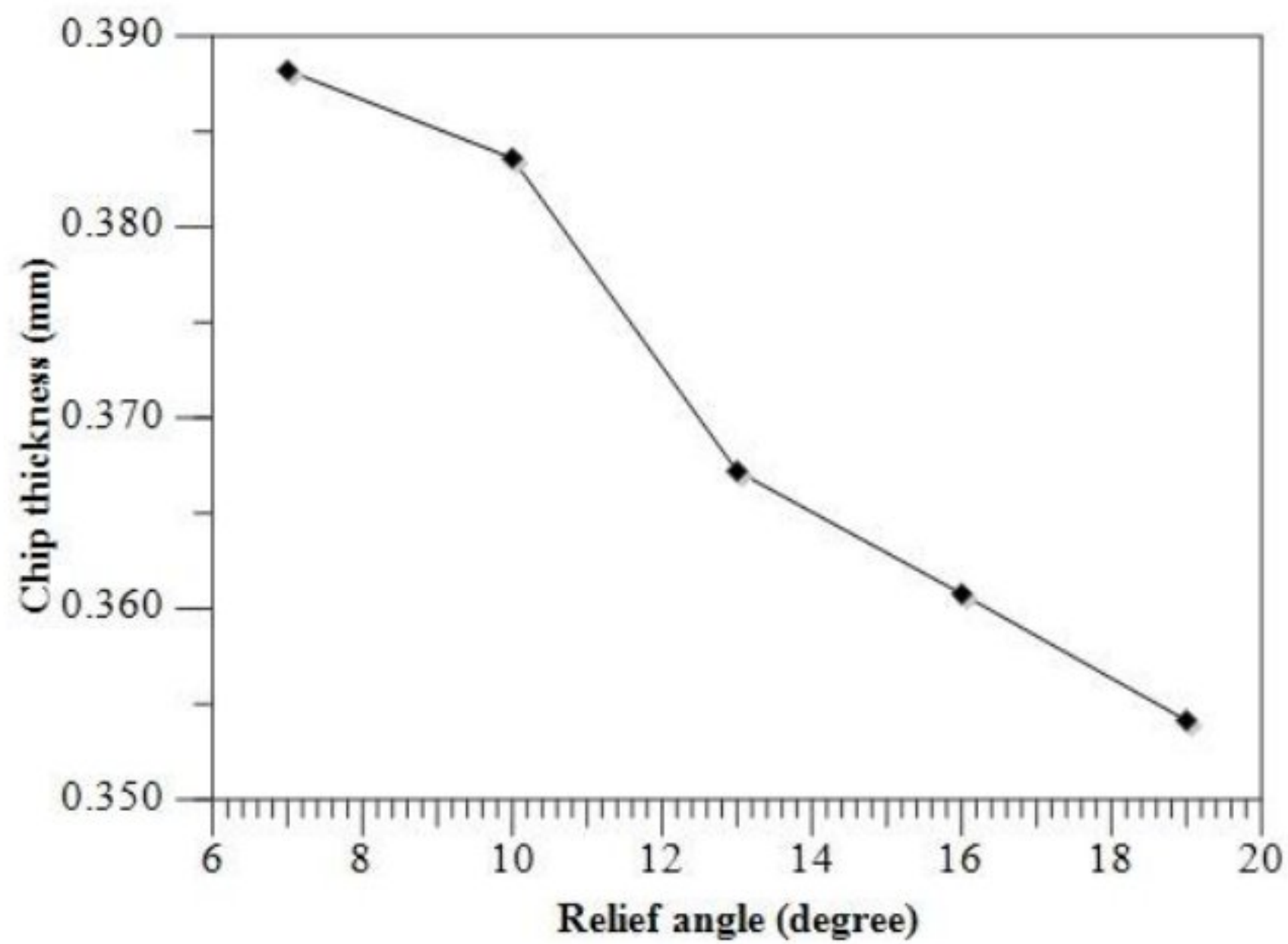


Figure 57 Distribution of chip thickness with the variation of rake angles for Cemented carbide-General tool

So, it can be said that increasing the value of relief angle, decreases the chip thickness.

3.4.3 Effect of chip thickness on variation of cutting edge radius

In fig. 58, distribution of chip thickness with the variation of cutting edge radii is shown. At cutting edge radius of 0.02 mm, the chip thickness is almost 0.3748 mm. There has a massive change between 0.02 mm and 0.04 mm. The value at cutting edge radius of 0.04 mm is 0.3677 mm. There has no change in between edge radius of 0.04 mm and 0.06 mm. There has a little change from 0.06 mm to 0.08 mm. At 0.08 mm, the value of chip thickness is 0.3670 mm. A massive change occurs at 0.10 mm from 0.08 mm. At edge radius of 0.10 mm, the chip thickness is 0.3575 mm. So, it can be said that, increasing the value of cutting edge radius also decreases the chip thickness.

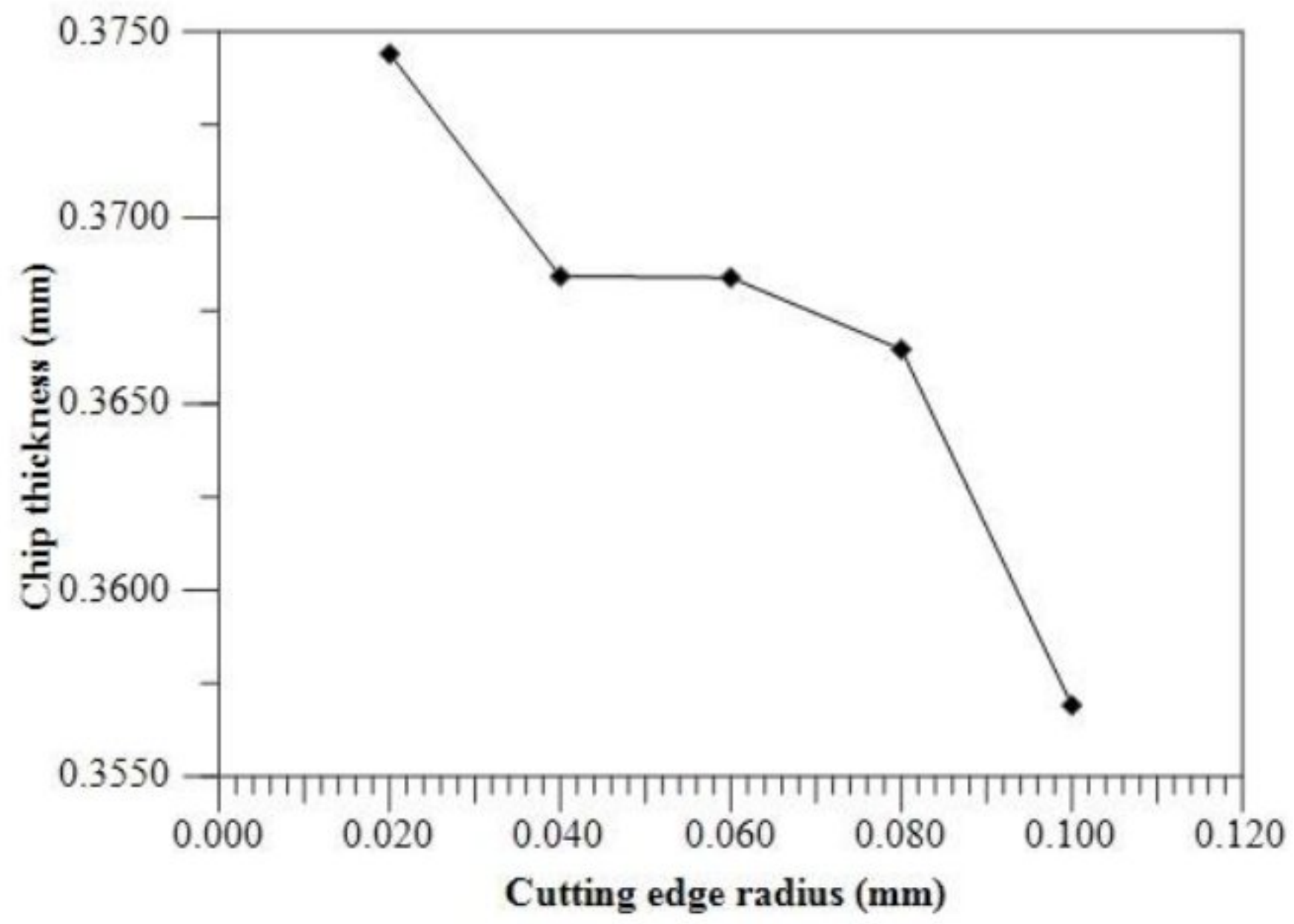


Figure 58 Distribution of chip thickness with the variation of cutting edge radii for Cemented carbide-General tool

CHAPTER 5

CONCLUSION

In case of effect of rake angle, temperature decreases, pressure increases and the maximum shear stress increases. Heat rate, plastic strain and strain rate increases as well. We also observed that increasing the rake angle decreases the cutting force and feed force as well when the others two parameters were kept constant.

In case of effect relief angle on temperature decreases and pressure and max shear stress increase at the same time. Here the cutting force and feed force also decreases. Heat rate, plastic strain and strain rate increases as well when the relief angle is increased and rake angle and cutting edge radius were kept constant.

In case of effect of cutting edge radius on temperature, it decreases. On pressure, we observe that with the increment of cutting edge radius, pressure increases. In case of effect on cutting edge radius, shear stress increases. Cutting force and feed force increases when others two parameters were constant. Here the heat rate decreases when we increasing the cutting edge radius. On the other hand, plastic strain and strain rate increases.

In all three cases like the variation of chip thickness with varying cutting edge radius, rake angles and relief angles, the chip thickness decreases with the increase of the other parameters. The change in thickness is sharper on relief angle compared to cutting edge radius and rake angle.

REFERENCES

- [1] H. Bil, S. E. Kiliç, and A. E. Tekkaya, "A comparison of orthogonal cutting data from experiments with three different finite element models," *Int. J. Mach. Tools Manuf.*, vol. 44, no. 9, pp. 933–944, 2004, doi: 10.1016/j.ijmachtools.2004.01.016.
- [2] J. P. Davim, P. Reis, C. Maranhão, M. J. Jackson, G. Cabral, and J. Grácio, "Finite element simulation and experimental analysis of orthogonal cutting of an aluminium alloy using polycrystalline diamond tools," *Int. J. Mater. Prod. Technol.*, vol. 37, no. 1–2, pp. 46–59, 2010, doi: 10.1504/ijmpt.2010.029458.
- [3] P. Sartkulvanich, T. Altan, and A. Göcmen, "Effects of flow stress and friction models in finite element simulation of orthogonal cutting - A sensitivity analysis," *Mach. Sci. Technol.*, vol. 9, no. 1, pp. 1–26, 2005, doi: 10.1081/MST-200051211.
- [4] J. Mackerle, "Finite-element analysis and simulation of machining: A bibliography (1976-1996)," *J. Mater. Process. Technol.*, vol. 86, no. 1–3, pp. 17–44, 1998, doi: 10.1016/S0924-0136(98)00227-1.
- [5] J. Mackerle, "Finite element analysis and simulation of polymers - An addendum: A bibliography (1996-2002)," *Model. Simul. Mater. Sci. Eng.*, vol. 11, no. 2, pp. 195–231, 2003, doi: 10.1088/0965-0393/11/2/307.
- [6] L. Li, N. He, M. Wang, and Z. G. Wang, "High speed cutting of Inconel 718 with coated carbide and ceramic inserts," *J. Mater. Process. Technol.*, vol. 129, no. 1–3, pp. 127–130, 2002, doi: 10.1016/S0924-0136(02)00590-3.

- [7] I. J. Munch and T. Manufact, “~ P e r g a m o n,” 1997.
- [8] W. B. Sai, “An investigation of tool wear in high-speed turning of AISI 4340 steel,” *Int. J. Adv. Manuf. Technol.*, vol. 26, no. 4, pp. 330–334, 2005, doi: 10.1007/s00170-003-1991-5.
- [9] D. Joel, A. David, and J. D. Gardner, “Consortium on Deburring and Edge Finishing,” 2005.
- [10] T. Özel, “The influence of friction models on finite element simulations of machining,” *Int. J. Mach. Tools Manuf.*, vol. 46, no. 5, pp. 518–530, 2006, doi: 10.1016/j.ijmachtools.2005.07.001.
- [11] O. Access, “Finite Element Modelling of the effect of tool rake angle on tool temperature and cutting force during high speed machining of AISI 4340 steel Finite Element Modeling of the effect of tool rake angle on tool temperature and cutting force during high speed,” 2013, doi: 10.1088/1757-899X/50/1/012040.
- [12] W. Bouzid, “Cutting parameter optimization to minimize production time in high speed turning,” *J. Mater. Process. Technol.*, vol. 161, no. 3, pp. 388–395, 2005, doi: 10.1016/j.jmatprotec.2004.07.062.
- [13] M. D. Agrahari and T. V. K. Gupta, “Materials Today : Proceedings FE based simulation and experimental validation of forces in dry turning of aluminium 7075,” *Mater. Today Proc.*, no. xxxx, 2019, doi: 10.1016/j.matpr.2019.09.120.
- [14] K. Gok, “Development of three-dimensional finite element model to calculate the turning processing parameters in turning operations,” *MEASUREMENT*, vol. 75, pp. 57–68, 2015, doi: 10.1016/j.measurement.2015.07.034.

- [15] Y. Yen, A. Jain, and T. Altan, "A finite element analysis of orthogonal machining using different tool edge geometries," vol. 146, pp. 72–81, 2004, doi: 10.1016/S0924-0136(03)00846-X.
- [16] J. S. Strenkowski and K. J. Moon, "Finite element prediction of chip geometry and tool/workpiece temperature distributions in orthogonal metal cutting," *J. Manuf. Sci. Eng. Trans. ASME*, vol. 112, no. 4, pp. 313–318, 1990, doi: 10.1115/1.2899593.
- [17] K. Li, X. L. Gao, and J. W. Sutherland, "Finite element simulation of the orthogonal metal cutting process for qualitative understanding of the effects of crater wear on the chip formation process," *J. Mater. Process. Technol.*, vol. 127, no. 3, pp. 309–324, 2002, doi: 10.1016/S0924-0136(02)00281-9.
- [18] J. S. Strenkowski and J. T. Carroll, "A finite element model of orthogonal metal cutting," *J. Manuf. Sci. Eng. Trans. ASME*, vol. 107, no. 4, pp. 349–354, Nov. 1985, doi: 10.1115/1.3186008.
- [19] J. P. Davim, C. Maranhão, M. J. Jackson, G. Cabral, and J. Grácio, "FEM analysis in high speed machining of aluminium alloy (Al7075-0) using polycrystalline diamond (PCD) and cemented carbide (K10) cutting tools," *Int. J. Adv. Manuf. Technol.*, vol. 39, no. 11–12, pp. 1093–1100, 2008, doi: 10.1007/s00170-007-1299-y.
- [20] K. D. Bouzakis *et al.*, "Micro-blasting of PVD films, an effective way to increase the cutting performance of coated cemented carbide tools," *CIRP Ann. - Manuf. Technol.*, vol. 54, no. 1, pp. 95–98, 2005, doi: 10.1016/S0007-

8506(07)60058-4.

- [21] T. Özel, “Computational modelling of 3D turning: Influence of edge micro-geometry on forces, stresses, friction and tool wear in PcBN tooling,” *J. Mater. Process. Technol.*, vol. 209, no. 11, pp. 5167–5177, 2009, doi: 10.1016/j.jmatprotec.2009.03.002.
- [22] I. J. Mech, S. Vol, and A. J. Shih, “Pergamon FINITE ELEMENT ANALYSIS OF THE RAKE ANGLE EFFECTS IN ORTHOGONAL METAL CUTTING F ϕ F ~ The plane-strain orthogonal metal cutting process , with the direction of relative movement of the wedge-shaped cutting tool perpendicular to its straight cutti,” vol. 38, no. 1, 1996.
- [23] J. C. Outeiro, D. Umbrello, and R. M’Saoubi, “Experimental and numerical modelling of the residual stresses induced in orthogonal cutting of AISI 316L steel,” *Int. J. Mach. Tools Manuf.*, vol. 46, no. 14, pp. 1786–1794, 2006, doi: 10.1016/j.ijmachtools.2005.11.013.
- [24] W. Grzesik, M. Bartoszuk, and P. Nieslony, “Finite element modelling of temperature distribution in the cutting zone in turning processes with differently coated tools,” vol. 165, pp. 1204–1211, 2005, doi: 10.1016/j.jmatprotec.2005.02.136.
- [25] ThirdWaveSystems, “Third Wave AdvantEdge™ User’s Manual Version 7.0,” p. 378, 2015.